
# A Corrosion Resistance Enhancing Potential via Oil-Water Separation Strategy

## Ph.D. Dissertation

By

**Mohanad Khairi Fadhil**

MSc in Metallurgical Engineering

**Antal Kerpely Doctoral School of Materials Science and Technology**

**Hungary, Miskolc, 2026**

**Antal Kerpely Doctoral School of Materials Science and Technology**

# A Corrosion Resistance Enhancing Potential via Oil-Water Separation Strategy

A PhD dissertation submitted to Antal Kerpely Doctoral School of Materials Science and Technology for the degree of Doctor of Philosophy in the subject of Materials Science and Technology


By

**Mohanad Khairi Fadhil**

MSc in Metallurgical Engineering

Supervisor

**Prof. Dr Peter Baumli,** Full Professor

Head of the Doctoral School

**Prof. Dr Valéria Mertinger,** Full Professor

Institute of Physical Metallurgy, Metalforming and Nanotechnology
Faculty of Materials and Chemical Engineering



Miskolc, 2026

بسم الله الرحمن الرحيم

ٱقۡرَأۡ بِٱسۡمِ رَبِّكَ ٱلَّذِي خَلَقَ (١)

Recite in the name of your Lord who created(1)

خَلَقَ ٱلۡإِنسَـٰنَ مِنۡ عَلَقٍ (٢)

Created man from a clinging substance(2)

ٱقۡرَأۡ وَرَبُّكَ ٱلۡأَكۡرَمُ (٣)

Recite, and your Lord is the most Generous(3)

ٱلَّذِي عَلَّمَ بِٱلۡقَلَمِ (٤)

Who taught by the pen(4)

عَلَّمَ ٱلۡإِنسَـٰنَ مَا لَمۡ يَعۡلَمۡ (٥)

Taught man that which he knew not(5)

صدق الله العلي العظيم

من سورة العلق رقم 96 ، القرآن الكريم

From Sura Al AlAQ No.96, Quran Karim

# Table of Contents

# Supervisor recommendation

## Acknowledgement

The thanks and gratitude first should be directed to Allah, the Exalted, the Majestic. Secondly, the success of my PhD dissertation is a collective effort by people and organisations alike. I extend my appreciation to myself for my efforts, my challenging days, my strength, my mindset, my persistence, my determination, my plans, my tears, my moments of struggle, my days of solitude, my goals, and my faith in Allah (the Exalted, the Majestic) and in myself. Special thanks to my family and their support throughout my studies, who have been a constant support system in my life, especially my mother, for her unwavering support, her belief in me, and her continuous prayers.

I am sincerely grateful to my supervisor, **Prof. Dr Peter Baumli**, who was more than just a supervisor in my journey. His continuous guidance has laid the foundation for my research direction and everyday experimentation. My sincere gratitude to my reviewer, **Prof. Dr Tamas Torok**, whose eminent research revision and visionary guidance made my study more structured and refined through seminar reports and the dissertation structure. Their warmth and affectionate conversations made me feel right at home in a place that felt like home.

I want to express my appreciation to the Iraqi Ministry of Oil, represented by the Midland Oil Company, which allowed me to complete my doctoral studies, and to the Tempus Public Foundation and the Stipendium Hungaricum scholarship program for selecting me and providing financial assistance for my incredible journey in Hungary and Europe. I want to thank the "Antal Kerpely Doctoral School of Material Science and Technology" for accepting me as a PhD student and for the opportunity to conduct research at the University of Miskolc. My gratitude extends to the Institute of Physical Metallurgy, Metal Forming and Nanotechnology and to **Prof. Dr Valeria Mertinger** for providing me with all the necessary equipment and an ambient work environment to carry out my research.

I want to thank **Dr Arpad Kovacs (unfortunately, he passed away) and Dr Daniel Koncz-Horvath for their kind cooperation and for** scheduling the SEM microstructural examination. I would also like to express my gratitude to Tamás László Koós and the Institute of Energy and Quality Laboratories for providing the elements analyser used to analyse the samples. A special thanks to **Mrs Aniko Markus and Mrs Bodnar Napsugar** for helping with both pre- and post-experimental sample preparation throughout my PhD. I express my appreciation to Dr Mate Czagany in the PVD laboratory for support with coating

applications and to the nanotechnology laboratory for wettability investigations. I would like to sincerely thank **Mrs Judit Szabo, Mrs Agnes Solczi, Dr Maria Sveda, and Mrs Eva Stumpf** for their continued and valuable support in the administrative work at the university. Finally, I would like to thank my colleagues, both Hungarian and International students, for their help, interaction, and support throughout the study period.

**Mohanad Khairi Fadhil**

**Hungary, Miskolc, 2026**

## List of Abbreviations and Notations

| | |
|---|---|
| API | Degree of density of the oil foundation |
| MIC | Microbiologically induced corrosion |
| CUI | Corrosion under insulation |
| SCC | Stress corrosion cracking |
| HDPE | High-Density polyethene |
| CA | Contact angle |
| θ | Theta (The contact angle of the liquid phase with the solid surface in the air) |
| $\sigma_{sg}$ | Surface energy of the solid phase in air |
| $\sigma_{lg}$ | Surface tension of the liquid phase in air |
| $\sigma_{sl}$ | adhesion energy Interfacial energy of the solid/liquid phase |
| $W_a$ | The adhesion energy |
| ρ | Intrusion pressure |
| $\theta_A$ | The advancing contact angle of one phase submerged in the other |
| φ | The size (length) of the square pore |
| $\gamma_L$ | Liquid–air interfacial tension |
| $\gamma_S$ | Surface free energy of the solid |
| EOS | Equation-of-State |
| CTAB | Cetyltrimethylammonium bromide |
| Ra | The average surface roughness of the pure metal substrates |
| wt. % | Weight Percentage |
| vol. % | Volume Percentage |
| PVD | Physical vapour deposition |
| CVD | Chemical vapour deposition |
| EG | Ethylene glycol |
| ChCl | Coline chloride |
| DES | Deep eutectic solvent |
| LDH | Layered double hydroxide |
| SEM | Scanning Electron Microscope |
| XRD | X-Ray Diffraction |
| XRF | X-Ray Fluorescence spectrometer |
| $\alpha$ and $\beta$ | Are semi-empirical parameters |
| $r_a$ | Atomic radius |

## List of Units

| | |
|---|---|
| $g/cm^3$ | Gram per cubic centimetre |
| mg/L | Milligrams per litre |
| MPa | Megapascal ($10^6$ pascal) |
| rpm | Revolutions per minute |
| $J/m^2$ | Joles per square metre |
| Pa·s | Pascal-second |
| µL | Microlitre ($10^6$ L) |
| mm | Millimetre ($10^{-3}$ m) |
| min | Minute |
| µm | Micrometre ($10^{-6}$ m) |
| mbar | Millibar (100 Pa) |
| sscm | Standard cubic centimetre per minute |
| V | Volt |
| mA | Milliampere ($10^{-3}$ A) |
| mN/m | Millinewton per meter |
| pm | Picometre ($10^{-12}$ m) |
| nm | Nanometre ($10^{-9}$ m) |
| m/m | Mass per mass |

# List of Figures

# List of Tables

## Ethical Use of Artificial Intelligence in Dissertation Preparation

"I declare that during the preparation of the dissertation, I did not use the services of artificial intelligence, except for grammatical and stylistic corrections".

Mohanad Khairi Fadhil

# 1. Introduction

The oil and gas industry has thousands of kilometres of pipelines and plays an essential role in the global energy supply by transporting oil and gas. Internal corrosion is one of the most critical challenges for their long-term operation. It is primarily caused by the presence of water, corrosive ions, dissolved gases, and flow conditions in the transported medium. Even a small amount of water can trigger localised corrosion, leading to material loss, reduced structural rigidity, and, in extreme cases, pipeline leakage or catastrophic failure.

Conventional corrosion protection methods are based almost exclusively on internal/external coatings, or lining with high-density polyethene (HDPE), which acts as a physical barrier between the metal surface and the corrosive environment, or by electrochemical control of electron transfer in the soil surrounding the pipes. However, for already-built large-scale pipeline networks, especially underground ones, applying or renewing such technologies is often technically, logistically, or financially challenging. As a result, alternative solutions are needed that limit corrosion not by insulating the pipeline surface, but by regulating the liquid environment itself, specifically by reducing the water phase that causes corrosion by transferring it to other phases.

One promising strategy is phase separation using a selective method, in which a stainless steel mesh with a porous geometry and a surface treated with a coating that exhibits selective wetting properties is used to separate oil-water mixtures, allowing only the oil phase to pass while preventing water from passing. The separation process is based on differences in interfacial interactions between the mesh surface and the liquid phases, which depend on adhesion and interfacial energy properties.

The key to effective separation is to design a surface with modified wetting properties that result in highly hydrophobic and oleophilic behaviour. If the contact angle between the mesh surface and water is sufficiently large, this phase is depleted and cannot pass through the mesh openings. In contrast, the oil phase wets the entire mesh surface and can flow through it. So, understanding and controlling wetting and interfacial phenomena are essential for ensuring the separation process. To design an effective separation method, it is necessary to investigate how surface energy, hole size, and surface coating affect oil-water contact angles and how these factors influence changes in separation performance. By continuously (non-accumulating) removal of water during transport, the corrosive environment is fundamentally altered, significantly reducing internal corrosion rates without changing the pipeline itself or relying on conventional methods.

In my work, I sought answers to the following questions:

1. What types of internal corrosion affect oil pipelines caused by water? What current solutions are used to reduce it?
2. What is the phenomenon of surface wettability? How do the surface roughness, surface chemistry or material structures influence the desired selective wetting behaviour?
3. Do wetting and interfacial properties of different materials allow us to separate oil from water selectively?
4. What is the effect of adhesion energy and free surface energy on the separation process?
5. Does stainless steel mesh are used to separate oil from water, and what are the mesh sizes used in the process?
6. Can surface coatings enhance oil-water separation? What types of coatings are used, and what is the best technology performed?

Based on these questions, the main objectives of my research were the following:

1. To highlight the types of internal corrosion that affect oil pipelines caused by water, and the most common solutions currently used.
2. To investigate the wetting behaviour of oil and water on various surfaces of the material and to identify the key interfacial parameters governing the behaviour.
3. To identify the parameters that affect the mechanism and efficiency of the separation.
4. To determine how surface energy, adhesion energy and roughness influence the contact angles of oil and water and thus the effectiveness of separation.
5. To identify stainless steel mesh pore sizes and coating compositions capable of separating oil and water based solely on their wetting properties.
6. To evaluate stainless steel mesh performance under Ni coating for oil-water separation.
7. To highlight the Physical Vapour Deposition (PVD) coating technology and its importance in the mesh coatings without other technologies.

# 2. Theoretical background and Literature review

In the following chapter, and in light of the previous scientific questions, I will discuss the importance of this work in the oil industry, starting from corrosion problems and current solutions, and how can I utilize the wettability phenomena to enhance corrosion resistance using stainless steel meshes, and oil-water separation possibilities as demonstrated through previous studies and the effect of adhesion and surface free energy on the process. The knowledge gaps will be outlined in Chapter Three.

## 2.1. Oil pipeline corrosion problems set

In the oil and gas industry, corrosive media (soil and water) pose a significant scientific and technical challenge, affecting the mechanical properties of steel [1]. Water, which is extracted with crude oil during the extraction process, is considered one of the most corrosive media for pipes due to its constant contact with the inner metal surfaces used in the production, refining, and transportation of crude oil. The continuity of metallic abrasion and probable growth from its detected damages [2, 3] will lead to a lessening in the wall of the pipe thickness, followed by cracks, then an oil spill and remarkable economic losses resulting from the stoppage of production and needed for maintenance, in addition to extreme ecological consequences [4, 5], this has been affirmed through the day statistical data, namely, that nearly 80% of all oil pipeline disasters are due to the number one corrosion harm, and through progressing bases fissuring problems in locations of corrosive caverns and welding joints [6].

On the other hand, the expansion of oil and gas production from unconventional resources was highly dependent on technologies that utilise large amounts of water for oil and gas extraction from shale regions, such as hydraulic fracturing, which pumps water and sand under high pressure to crack deep rocks. In terms of produced water production volumes, about three to four barrels of water are used with each barrel of regular oil extracted. Many factors (type, geological properties, and the lifetime of a formation) affect the number of barrels, which may increase the number of water barrels by more than four barrels [7, 8].

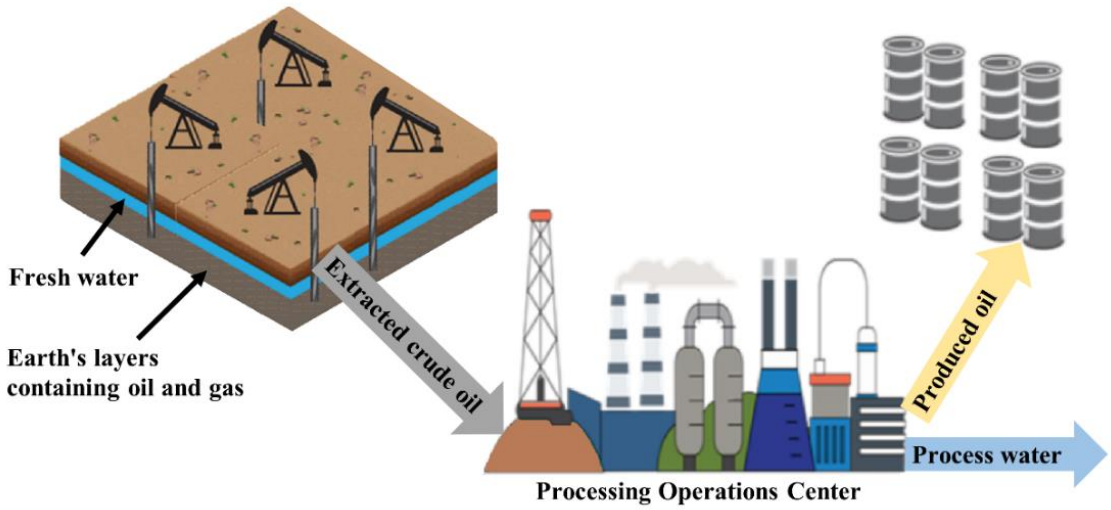


***Figure 1.*** *Schematic diagram of the extraction and processing operations of crude oil [7].*

Generally, oil-water mixtures may be classified as immiscible or emulsions, which consist of oil-water emulsions [9]. The petroleum enterprise typically classifies crude oil by the geographic region it's produced in (Brent, Oman, West Texas) and its oil density (API gravity), as well as its sulfur content. Crude oil can be considered mild if it has low density, heavy if it has high density, or medium if it has a density between those of mild and heavy [10]. Additionally, it may be described as sweet if it contains little sulfur, less than 1 wt.% or sour if it contains a lot of sulfur, more than 1 wt.% [11]. Produced water from crude oil typically contains various additives and varying concentrations of carbon, hydrogen, nitrogen, oxygen, sulfur, various metals, and stones and pebbles (Table 1 [12]), which could increase corrosion.

***Table 1.*** *Typical chemical analysis of crude oil [12].*

| Element | Carbon | Hydrogen | Nitrogen | Oxygen | Sulphur | Metals |
|---|---|---|---|---|---|---|
| wt.% | 82.2-87.1 | 11.7-14.7 | 0.1-1.5 | 0.1-4.5 | 0.1-5.5 | < 0.1 |

The literature review [13-18] provides an overview of the different types of internal corrosion that can occur in oil pipelines:

a. General corrosion: As a result of electrochemical reactions between the metal and the crude oil compounds, there is a uniform loss of metal from the internal surface of the pipeline.
b. Pitting corrosion: The formation of small pits or holes in the internal surface of the oil pipeline as a result of the localised corrosion.

c. Erosion corrosion: Bends and joints affected by high fluid flow velocity are disrupted, causing a combined effect with corrosion and erosion
d. Galvanic corrosion: When two dissimilar metals are in contact, the less noble metal corrodes, which can occur in pipelines that have different metals or alloys in contact, such as copper and steel.
e. Microbiologically induced corrosion (MIC): Acids or other corrosive agents produced by microorganisms living on the internal surface of the pipeline can cause MIC.
f. Corrosion under insulation (CUI): Trapped moisture in areas where the internal surface of the pipeline is insulated can lead to CUI.
g. Stress corrosion cracking (SCC): When tensile stress, a corrosive environment, and susceptible material are combined, cracks form and grow, leading to SCC. It is a failure mechanism in the pipeline metals.

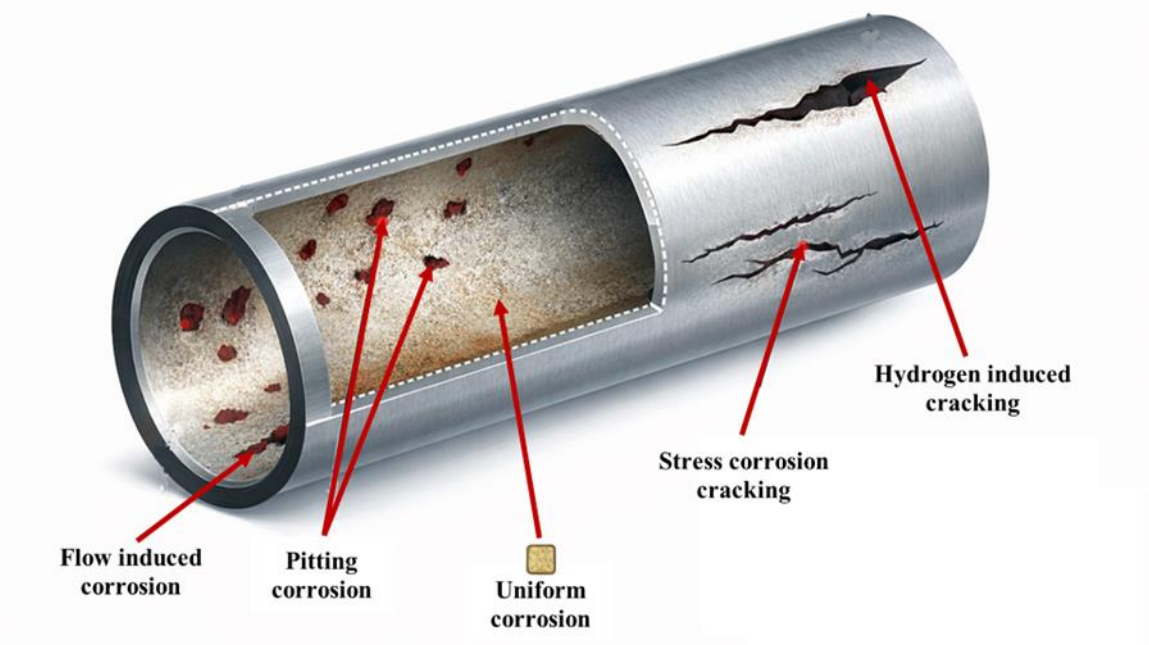


***Figure 2.*** *Schematic diagram of the oil pipe corrosion types [15].*

## 2.2. Oil-Pipelines corrosion protection methods

There are many methods used to protect oil pipelines from corrosion caused by oil contents during operations. Currently, the following methods are used to avoid pipeline corrosion.

### 2.2.1. Lining with high-density polyethene (HDPE) method

High-density polyethene (HDPE) is a flexible plastic pipe used to transport various fluids, especially crude oil and gas. It is made from the thermoplastic HDPE; it has high impermeability and strong molecular bonds, making it useful for high-pressure pipelines. Now, HDPE pipe is used to line some of the oil pipeline network parts in fields containing highly corrosive media, such as high-sulfur and salty fields, to prevent crude oil from contacting the inner pipe surface. It is a complex, costly process [19].

### 2.2.2. Anticorrosion coatings method

A coating is a metallic covering (layer of a liquid mixture containing fundamental metal particles) that is applied on the surface of the substrate, which is made of (epoxy and polyurethane) by using different techniques with the help of spraying, brushing, or rolling for protection and change the mechanical properties of the substrate surface for instance adhesion, wettability, corrosion resistance, and wear resistance and thus increasing the age of the alloys resulting. The main goal of applying the coating is to protect the metals against corrosion by isolating the metal surface from the effects of the external environment, it is one of the perfect effective solutions for many types of equipment, but it is challenging to apply to the inner surface for small diameters pipes and long distances so increasing the cost and losing the time [20].

### 2.2.3. Electrochemical method

The protection provided by the electrochemical method depends on the cathodic protection system used to protect steel pipelines, tanks, and other steel structures exposed to aggressive soil and varying climatic conditions that increase corrosion. This method employs cathodic polarization to regulate the kinetics of electrode processes at the metal/electrolyte interface, and depends on preventing the erosion current from flowing from the body to be protected (pipe) by converting a metal to a cathode via an impressed current or coupling to a sacrificial anode to reduce or eliminate corrosion, it mean is two ways of cathodic protection are Sacrificial Anodes and Impressed Current [21, 22]. Magnesium and zinc are the most commonly used materials as a galvanic anode for pipeline cathodic protection, but

economic considerations have led to the use of aluminium and its alloys. Between any point on the surface of the pipe and the soil, the voltage difference should not exceed 2.5 volts [23].

### 2.2.4. The oil separation from the water

Many oil companies use a single vessel as a three-phase separator to separate water from oil within engineered internals and controls based on density differences [24, 25]. When Influent enters, the deflectors reduce the kinetic energy of the flow and spread it. Gas rises rapidly and exits after foam/slug control using a foam breaker/baffle plate. In contrast, oil droplets coalesce on plates and form a stable oil layer in the middle. At the same time, heavier water settles to the bottom; the level controller maintains the set point, while vortex breakers and foam baffles prevent mixing during discharge. Finally, each phase leaves through its dedicated outlet according to control settings. The benefits of efficient single-vessel separation save space. Improves the quality of oil and gas sent downstream. Disadvantages include the need to monitor water level closely to avoid oil-in-water or vice versa, the need to clean coalescing plates periodically to prevent blockages that reduce separation efficiency, and the importance of verifying the foam breaker condition, as excess foam can carry oil into the gas outlet.

In the following sub-chapters of my research, to enhance the corrosion resistance of the oil pipe, I will focus on the oil-water separation method using stainless steel mesh, based on the wettability behaviour of the liquids on the steel and metal surfaces.

## 2.3. The oil wettability and the wetted surface types

It is the ability of liquids to maintain contact with a solid surface; it arises from intermolecular interactions as molecules come into contact with the surface. It is described as a solid selection for contact with one liquid rather than another. If the solid does not prefer one liquid over the other, it is called intermediate-wetting or neutral-wetting [26, 27]. The degree of wettability is determined by the balance between adhesive and cohesive forces at the interface. The equilibrium contact angle could describe it (θ), which is the angle formed by the tangent drawn to the plane solid surface and the liquid/gas interface at a point on the gas/liquid/solid triple line in the direction of the liquid phase (Fig. 3). When a liquid droplet on a solid surface forms a bead, a contact angle θ is 180° means nonwetting, while a contact angle is zero means perfect wetting, and what is between them is the gradation of wettability from weak (greater than 90°, less than 180°) to normal (greater than 0°, less than 90°) [28].

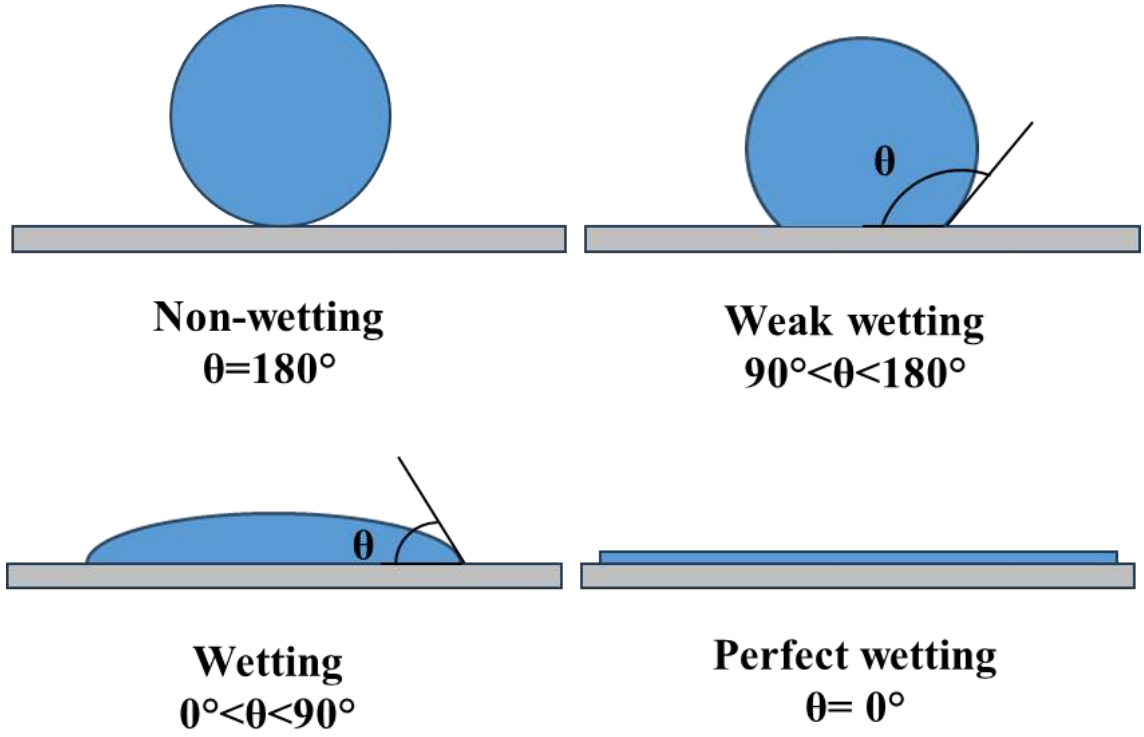


***Figure 3.*** *Schematic diagram representing the description of different wettability states for the liquid droplet.*

The contact angle establishes a relationship between the three interface energies characterising the system. This relationship can be expressed by Young's equation [29, 30], which actually describes the mechanical balance of the interfacial forces derived from the three interfacial energies:

$$\sigma_{sg} = \cos\theta \,.\, \sigma_{lg} + \sigma_{sl} \tag{1}$$

where: $\sigma_{sg}$ is the surface energy of the solid/air phase, $\sigma_{lg}$ is the surface tension of the liquid/air phase, and $\sigma_{sl}$ it is the interfacial energy of the solid/liquid phase.

On the other hand, the resulting contact angle value is fundamentally influenced by chemical interactions occurring at the molecular level. For that, Dupré described the degree of wetting depending on thermodynamic adhesion energy ($W_a$, in J/m$^2$) according to the following equation:

$$W_a = \sigma_{sg} + \sigma_{lg} - \sigma_{sl} \tag{2}$$

Substituting Eq. (1) into Eq. (2) will yield Eq. (3), which is the Young-Dupré equation:

$$W_a = \sigma_{lg}(1 + \cos\theta) \tag{3}$$

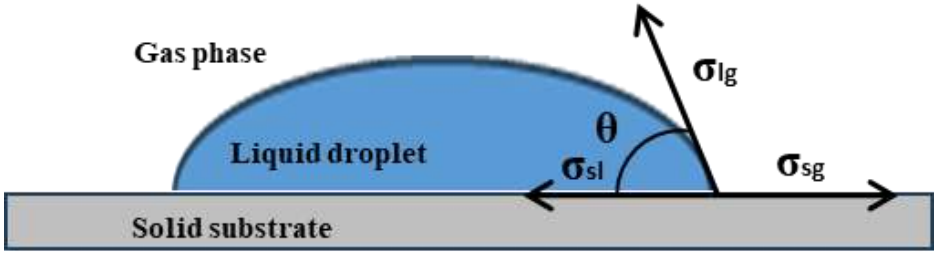


***Figure 4.*** *Schematic diagram representing the interfacial energies of a liquid droplet resting on a solid surface.*

The wetting of a substrate surface by a liquid is a vital part of many industrial and natural processes, significantly influencing the performance and durability of metallic components across diverse industries, especially when the liquid is oil, water, or both, as in the oil industry. Hence, obtaining a comprehensive grasp of the factors that steer oil wetting on metal surfaces is imperative for refining industrial procedures [31, 32]. When metal surfaces come into contact with oil, a complex interplay of intermolecular forces determines how the oil spreads on the surface, and this interplay describes how a liquid adheres to and spreads across a solid surface [33, 34].

Numerous investigations [35-37] have shown that the surface energies of both the oil and the metal surfaces determine the extent of oil wetting. The equilibrium between adhesive and cohesive forces significantly affects the contact angle and the spreading behaviour of the oil on the metal surface. The spreading parameters (SPs) depicted in Fig. 5 reveal a notable contrast in surface wetting behaviour compared to the conclusions drawn from contact-angle measurements by Kalin and Polajnar [37]. Even with positive values, lower spreading parameter values suggest that the liquid will spread more slowly over the surface, indicating inferior wetting.

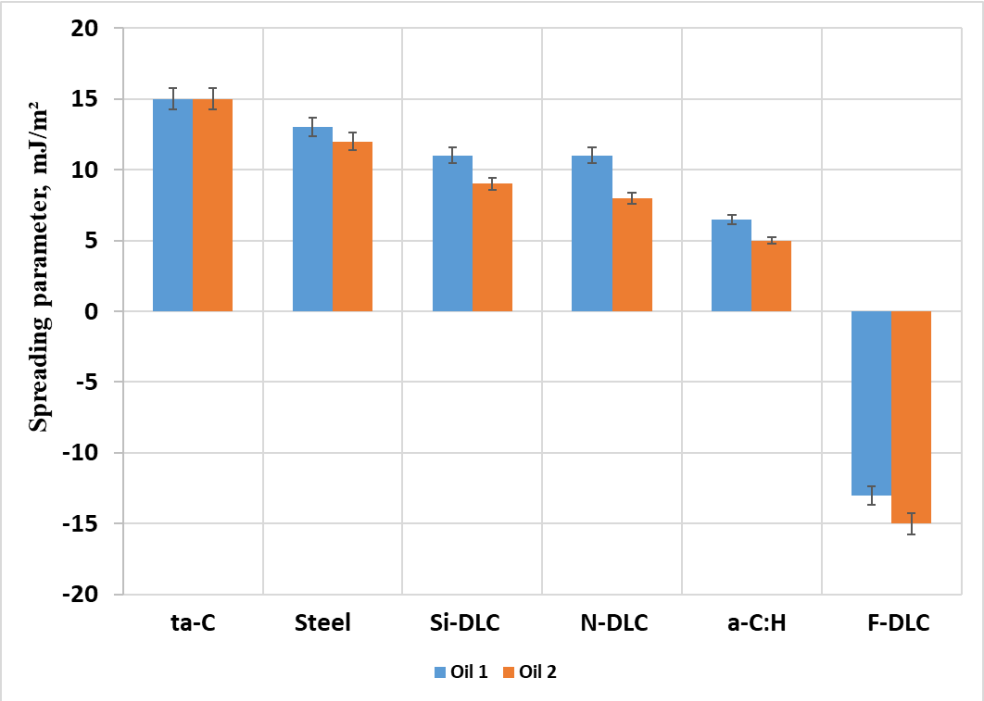


***Figure 5.*** *Spreading parameter for two oil types over steel and DLC coatings [37].*

Beyond this, David Quéré [38] and Junchao Wang et al. [39] have also affirmed another variable, the roughness of the metal surface, which influences the effective contact area between the oil and the metal and, in turn, wetting behaviour. Surface roughness modifies the observed contact angle and can lead to either enhanced or reduced oil wetting. Meanwhile, Huan Zhu et al. [40] investigated surface chemistry, demonstrating that the chemical composition and functional groups on the metal surface can influence oil wetting behaviour. Alterations in surface chemistry through treatments and modifications can subsequently impact the contact angle and spreading behaviour of the oil [41, 42]. It aids in predictive modelling for industrial applications such as investigating lubricant behaviour, fluid flow dynamics [43-46], and oil-water separation [47, 48], where divergent wetting behaviours can lead to effective oil-water separation. This knowledge is indispensable in industries and chemical technologies, especially in metal corrosion processes, oil sector water-oil separation [49-52], and other applications, such as preparing metallic nanoparticles or studying corrosion behaviour [53-55].

Furthermore, surface wetting can affect cavitation formation: enhanced wetting reduces cavitation. Additionally, the flow, whether turbulent or laminar, is influenced by surface wetting behaviour [56, 57]. This concise overview reveals a spectrum of outcomes for the contact angles of various oil types on metal surfaces, compared with the behaviour

of water wetting in prior studies. In several research papers [58-61], contradictions arise regarding wettability behaviour within oil-water systems. These inconsistencies can be attributed to the creation of an oxide layer with uncertain composition and thickness during cleaning procedures. This layer facilitates ideal wetting between metals and water, a phenomenon supported by Zaera's research [62].

In addition to distinct disparities in spreading behaviour, oils exhibited a more rapid spreading force than water. According to Jiang et al. explanation [63], this phenomenon is attributed to a persistent condition in which the spreading force remains below the maximum adhesion force. This maximum adhesion force corresponds to the droplet that is the most stable interfacial contact with either the solid or the liquid substrate. The distinction between spreading force and maximum adhesion force is influenced by solid surface imperfections, even in cases of perfectly smooth liquid surfaces. This empirical insight implies that factors beyond roughness and heterogeneity contribute to contact angle hysteresis. The most stable arrangement for a liquid droplet on a solid surface occurs when the droplet base is axisymmetric. While it is still possible to deform the contact line in this situation, the driving force is the attempt of the droplet to increase adhesion. This is achieved by increasing contact with a surface component that exhibits a higher affinity for the liquid [64].

Understanding the wettability behaviour of both water and oil helps in classifying solid surfaces as hydrophobic and oleophilic, or hydrophilic and oleophobic. This knowledge has received considerable attention in biology, chemistry, physics, and materials science [65], with numerous practical applications in daily life, industry, and agriculture [66], and especially in oil-water separation [67]. It is inspired by the excellent hydrophobic properties of natural elements, such as lotus leaves, rose petals, taro leaves, rice leaves [68], water strider legs, cicada wings, butterfly wings, and penguin body feathers [69, 70].

Recent studies in this field primarily focus on the wettability of superwetting surfaces, including superhydrophobicity, superoleophilicity, superhydrophilicity, and superoleophobicity properties [71]. Surface wettability is an inherent property of a solid surface and determines the final wetting/dewetting characteristics when a liquid contacts the material. The surface chemistry and geometric morphology of solid surfaces directly impact the wetting/dewetting behaviours of liquids on them [72]. Wettability can be controlled/designed by adjusting these two factors to achieve extreme water repellency and oil affinity or vice versa [73, 74]. Superhydrophobic materials with extremely high contact angles (more than 150) that allow a small water droplet to move with low sliding angles (less than 5-10) have been widely studied [75, 76], it is much easier to prepare superhydrophobic

materials than superoleophobic materials [77, 78] because oils with low surface tensions tend to wet and spread across most solid surfaces easily.

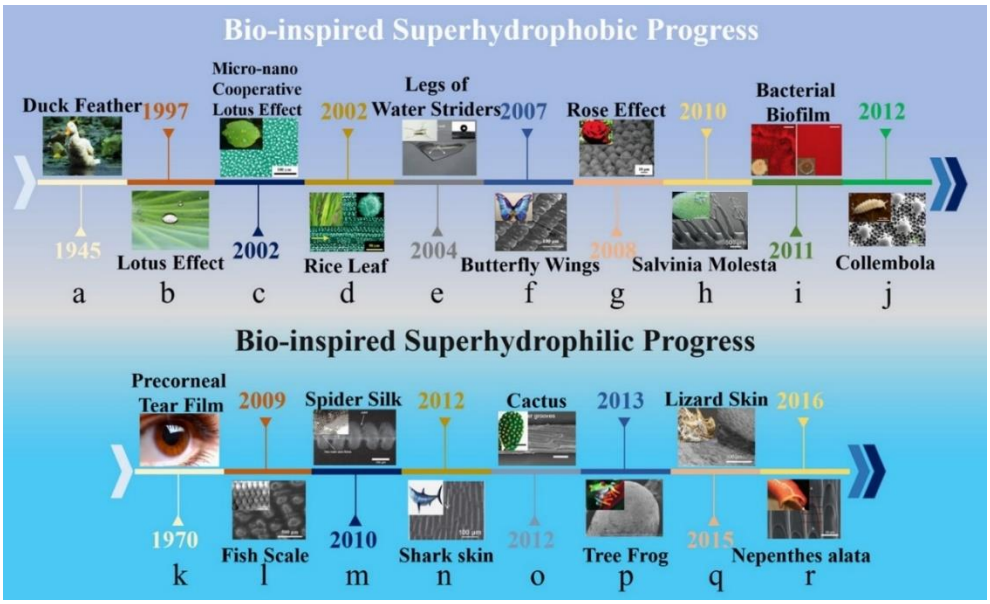


***Figure 6.*** *Timeline of bioinspired superhydrophobic and superhydrophilic process of development till 2018 (a: Duck feather, b: Lotus effect, c: Micro–nano cooperative lotus effect, d: Rice leaf, e: Legs of water striders, f: Butterfly wings, g: Rose effect, h: Salvinia molesta, i: Bacterial biofilm, j: Collembola, k: Precorneal tear film, l: Fish scale, m: Spider Silk, n: Shark skin, o: Cactus, p: Tree frog, q: Lizard skin, r: Nepenthes alata) [79].*

## 2.4. Oil-water separation

In subchapter 2.2.4, I discussed separating oil from water in oil facilities using a three-phase separator as one method to protect pipelines against internal corrosion caused by water accompanying the oil. Here, I will discuss the process of oil-water separation using materials with specialised properties for purposes other than corrosion control and then employ this separation for corrosion control. Therefore, the development of functional materials for handling oil-water mixtures is crucial, with direct practical implications [80].

These oil-water separation techniques are classified based on filtration methods (including membrane, filter, film, and mesh) or absorbent materials (including porous media, powder/particle, gel, and nanocomposite) [81]. These methods have been utilized in various applications, including cleaning oil spills in offshore or on-shore oil production sites (e.g., rivers and seas), for liquid filtration / solid-liquid separation in oil fields and refinery equipment [82]; in treating the produced water and oily wastewater spill from drilling/production/refining or refineries [83]; in chemical and petrochemical facilities associated with oil and gas activities; chemical/ petrochemical plants (including those tied

to oil/gas operations); and purifying water from oils for industrial, medical, and human uses, like sponges [84], foams [85], and textiles [86], which were commonly used to absorb oils from water.

Many researchers [87] also demonstrated oil-water separation using a highly hydrophobic/oleophilic stainless steel mesh, which prevented water from preferentially permeating the mesh while allowing oil to pass through. In turn, offers a promising opportunity for easy oil-water separation, and could employs it in the oil industry to separate oil from water when crude oil passes through the oil pipelines, this decreases of water passing enhance pipe protect from corrosion type that caused by water, while considering potential surface effects during the separation process or improving the separation process after making surface modifications, such as coating. To that end, in my research, I will focus on stainless steel mesh filtration and on potentially improving its separation properties.

### 2.5. Oil-water separation with stainless steel mesh

Based on a research survey of the Scopus database (a multidisciplinary abstract and citation database), there has been a noticeable increase in the number of research papers describing oil-water separation using stainless steel meshes over the last seven years, as illustrated in Fig. 7. It highlights the importance of the topic and its impactful, beneficial outcomes in applications across the oil industry.

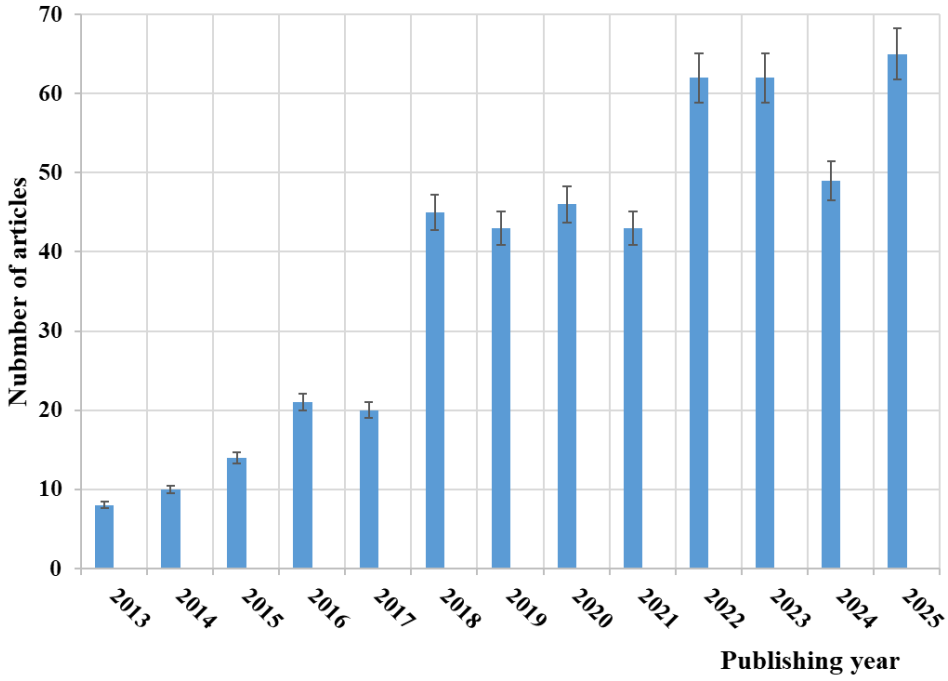


***Figure 7.*** *Number of articles by the title "oil-water separation with stainless steel meshes" indexed in the Scopus website till December 11, 2025.*

The main principle of the separation by stainless steel mesh depends on the difference in wetting phenomena behaviour of both oil and water on the mesh surfaces, which are classified as oleophilic and hydrophobic [77] consequently the stainless steel meshes were used to separate oil from water when the stainless steel mesh allowed oil to pass through them while preventing water from penetrating [88].

There are many challenges [89-93] that have been faced in the separation process by meshes during the initial use of metal meshes for oil-water separation without any coatings, which suffered from low corrosion resistance, especially when exposed to the harsh environments typically encountered in oil-water separation processes (salty water, acidic, or basic conditions); this limited their longevity and performance. Achieving the correct balance of hydrophobicity and oleophilicity, or vice versa, was challenging. Early designs did not incorporate self-cleaning features or materials resistant to the adhesion of contaminants (which reduced their effectiveness and required frequent cleaning or replacement), or not durable enough to withstand the high pressures or mechanical stresses of industrial applications (leading to deformation or failure during use), additionally the costly production and rough structures, hence limitation use in a different applications, due to lower lifetime use and performance limitations.

The use of metal meshes with tailored properties has gained significant attention due to their simplicity, cost-effectiveness, and scalability. The mesh size, which directly affects pore dimensions [94, 95], plays a vital role in determining separation efficiency, throughput, and selectivity. Meshes with varying sizes, such as 200, 300, 400, and 500 mesh, provide different pore structures, which influence their ability to separate oil from water. Larger meshes (e.g., 200 mesh) offer higher permeability and are suitable for separating large oil droplets but may struggle with smaller droplets or emulsified oil. Conversely, finer meshes (e.g., 500 mesh) provide better retention of smaller droplets, improving the separation of emulsified mixtures but potentially reducing throughput due to increased fluid resistance. The interplay between mesh size and wettability is also critical. Surface modifications, such as hydrophilic or oleophilic coatings, are often employed to enhance selectivity and efficiency [96].

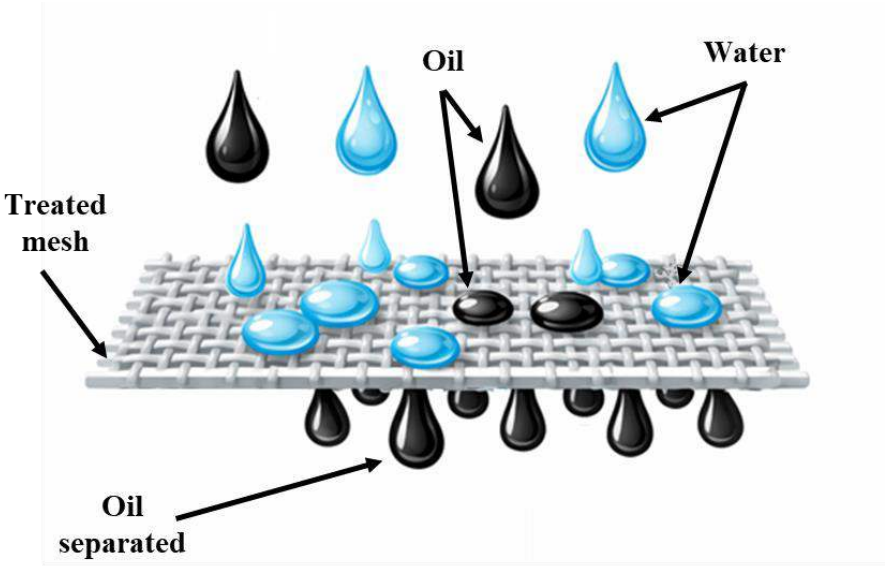


***Figure 8.*** *A stainless steel mesh traps water droplets while allowing oil to pass through.*

### 2.5.1. The mechanisms of oil-water separation by stainless steel mesh

Early research indicates that for an oil-water separation mesh to work efficiently, the surface must possess superhydrophobic-oleophilic properties [80, 88]. To effectively separate oil-water mixtures, the contact angle of water on the solid surface must be significantly greater than that of oil, thereby substantially impeding oil movement while permitting water to pass. The resistance can be quantified as the incursion pressure determined by equation (4) [32].

$$\rho = \frac{4\gamma \cos(180-\theta_A)}{\varphi} \tag{4}$$

where: $\rho$= the intrusion pressure, $\gamma$= the interfacial tension, $\theta_A$= the advancing contact angle of one phase submerged in the other, and $\varphi$= the size (length) of the square pore.

According to equation 1, the most significant resistance to water flowing through a mesh can be achieved with an oleophilic mesh having a high-water contact angle ($\theta_A$) and a small mesh size. These meshes are commonly known as oil-selective meshes [97]. Compared to other oil-water separation devices, meshes can separate a greater volume of oily water per unit time (flux) because meshes have submicron pore diameters [98].

Nevertheless, the main drawback of meshes is their larger pore width, which results in a lower inclusion pressure than that of membranes. Consequently, they are less effective at preventing the targeted phase from passing through the filtration process, unlike other devices. Additional benefits of utilising mesh include its straightforwardness and affordability, as well as the minimal pressure needed to propel liquid through it. Gravity can often serve as the driving force for flow.

Oil and water are two distinct materials with extraordinary physical properties that play an essential role in their behaviour and interactions, which in turn affect the separation mechanism, mesh properties, and environmental conditions. Here are the vital points influencing the separation efficiency with the aid of a metal mesh:

a. Differential density: Oil and water have different densities; water has a density of about 1 g/cm$^3$ at standard temperature and pressure, while oils generally have lower densities than water, ranging from approximately 0.8 to 0.95 g/cm$^3$. Depending on the type and composition of the oil, this difference causes it to float on the surface of the water. Steel mesh systems leverage this property by allowing oil to pass through while capturing and retaining the floating water droplets [99].

b. Surface tension: Water has an excessive surface tension due to the cohesive forces between its molecules. While oils have lower surface tension than water, which may affect the formation and balance of oil droplets in water, they are generally more likely to spread out, cling to the mesh surface, and skip through due to their lower surface tension. This asset can affect the performance of separation procedures by altering the behaviour of oil-water combos. This difference in conduct allows for more efficient separation of the two levels, with oil passing through the mesh while water is captured and retained [100].
c. Viscosity differences: Oil has a higher viscosity than water, making it far thicker and influencing its drift behaviour and interaction with the steel mesh. Water droplets, being less viscous, can also coalesce or merge whilst contacting the mesh, forming large droplets that might be easier to capture and become independent of oil [101]. The layout of the steel mesh takes advantage of this difference by allowing oil to move more freely through the pores and barriers, floating more easily through the mesh while trapping coalesced water droplets.

d. Pore size: The metallic mesh used in separation structures has a selected pore size engineered to be smaller than the dimensions of water droplets but larger than those of oil molecules [102]. This layout ensures that oil can pass through the mesh pores while water droplets are captured and retained on the mesh surface.
e. Boiling point and freezing point: The boiling point of water is 100 °C, and the freezing point is 0 °C at standard temperature and pressure (STP) at the same time as the boiling and freezing points of oils range relying on their composition, in well-known, oils have better boiling points and decrease freezing factors than water, and those temperature residences determine the segment of water (liquid, solid, or vapour) beneath one of a kind conditions from one side, and impact the phase conduct of oils and their interactions with water beneath exclusive conditions, affecting its conduct in oil-water separation strategies [103]. Where high temperature generally enhances oil–water separation by reducing oil viscosity and interfacial tension, allowing oil droplets to coalesce and separate more easily.
f. Coalescence: As oil droplets come into contact with the steel mesh, they coalesce into a collective, forming smaller droplets that are easier to separate from water. This coalescence system complements the performance of oil elimination by steel-mesh separators [104].
g. Polar and apolar nature: Water molecules are polar, which means they have a partial positive charge on one side and a negative charge on the opposite. This polarity allows water to engage with other polar substances and may affect the solubility and miscibility of oils in water. Unlike water, most oils are apolar materials, meaning they lack charged ends [105]. This non-polarity impacts the solubility and interplay of oils with water, often resulting in immiscibility and the formation of oil-water phases, and the separation could be simplified.

### 2.5.2. Effect of adhesion and surface free energy on the separation efficiency

By studying equilibrium conditions for binary systems with two-phase equilibrium with consideration of composition dependence of specific surface free energy, Hillert and Agren [106] start to evaluate common tangent construction for compressible liquids and solids, analysis of surface properties and their effects on phase equilibria, and examination of thermodynamic basis for phase equilibria diagrams. They found that the equilibrium condition is modified when surface properties vary with composition; the specific surface

free energy for an interstitial phase can be treated as that of any other phase, since partial volumes play a minor role in two-phase equilibrium in binary systems. The correlation between adhesion and surface energy is firmly established in systems where specific chemical interactions are improbable.

Giles Dillingham et al. [107] proposed that wetting measurements could be valuable for identifying specific chemical interactions crucial to adhesion in reactive systems, thereby establishing a more robust theoretical connection between wetting probe measurements and adhesive bond performance. Surface energy measurements indicated that treatments led to an increase in all facets of surface energy, including electron-donating, electron-accepting, and Lifshitz-van der Waals components. Consequently, this increases adhesion, with a strong correlation observed between the rise in the surface electron-donating character and enhanced adhesion. While surface energy can serve as a quantitative predictor of adhesive bond fracture toughness in systems where specific chemical interactions, such as covalent bonds, are highly unlikely [108, 109]. The relationship between surface energy and adhesive bond fracture toughness remains poorly understood in systems where specific chemical interactions play a significant role in the adhesive mechanism.

Wennerstrom [110] studied the interplay between the work of adhesion for similar surfaces and the forces acting between them within a given medium and showed that introducing the concept of contact adhesion energy, even in non-equilibrium states, establishes a mechanistic link between forces and adhesion in specific models. This perspective holds conceptual value, providing a criterion for mechanistic models of surface forces. The analysis reveals that merely understanding the distance dependence is inadequate for repulsive forces; one must also establish a connection to the adhesive energy at contact. It is beneficial for comprehending surface forces in systems involving adsorption from a solution. Adsorption from a bulk solution decreases the free energy of the surface. When two surfaces converge in equilibrium with the bulk, the integral of the force up to contact yields a higher, less negative, or more positive value than in the absence of adsorbed species.

Given that solid surfaces consistently aim to minimise surface energy and maintain stability, the surface energy of the solid plays a crucial role in determining whether droplets spread or contract upon contact. Wang and Zhang [111] analysed the relationship between surface energy and wettability (Fig. 9) to elucidate the mechanism by which roughness influences the wettability of mineral surfaces. The findings indicate that roughness significantly impacts the surface energy of both hydrophilic and hydrophobic calcite

surfaces. Furthermore, there is a noteworthy correlation between the wettability of calcite with varying degrees of roughness and its corresponding surface energy.

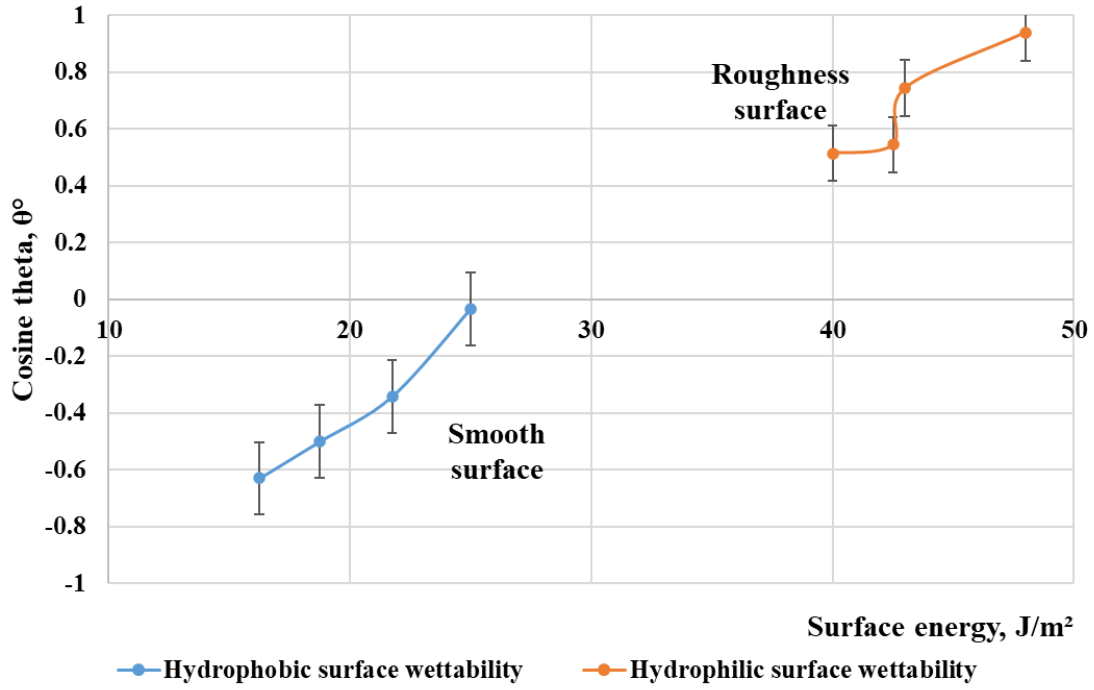


***Figure 9.*** *The effect of surface roughness on the surface energy and wettability for hydrophilic and hydrophobic surfaces [111].*

The surface free energy of a solid provides a direct measure of intermolecular interactions occurring at the surface, exerting a significant influence on wetting, adsorption, and adhesion behaviour. Several factors, including chemical composition, roughness, structure, and temperature, contribute to the modulation of surface free energy. The determination of a solid surface free energy through contact angle measurements relies on the principle that fluids possessing a liquid–air interfacial tension ($\gamma_L$) equal to or lower than the surface free energy of the solid ($\gamma_S$) will spread on the surface. In contrast, fluids with higher interfacial tension will form an angle with the solid, and this contact angle increases with the liquid–air interfacial tension ($\gamma_L$).

For highly energetic surfaces, Aspenes et al. [112] prove that there is a limited selection of liquids suitable for determining the solid surface free energy. This determination assumes no interaction between air and the solid surface, treating air as equivalent to a vacuum. Additionally, it assumes that there are no chemical reactions between the solid and the probe fluid. Measuring surface free energy is challenging for highly energetic surfaces, such as metals and glass, because most probe fluids exhibit specific spreading behaviour. To

overcome this, the Equation-of-State (EOS) for interfacial tension method could be employed to determine the free surface energy of various surfaces, including stainless steel, aluminium, and those coated with epoxy, fluoropolymers, polyethene, and polyurethane. Fig. 10 shows how the average surface free energies and their corresponding standard deviations differ depending on whether metallic substrates or coating materials are used [112].

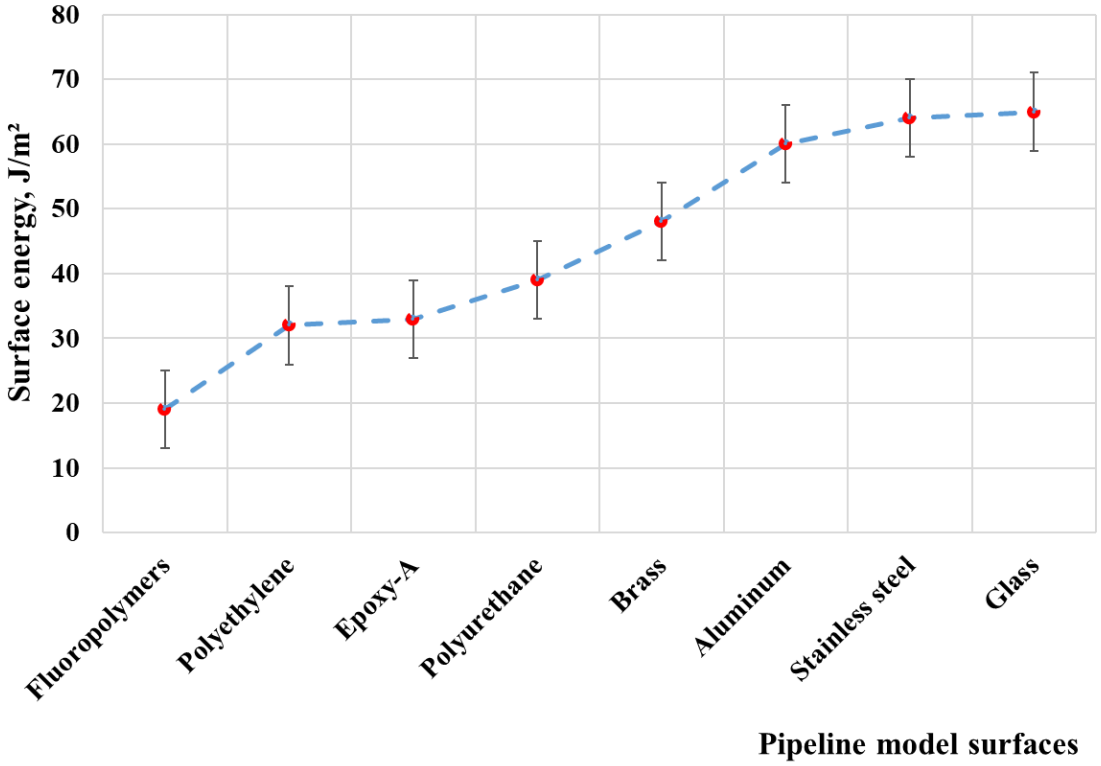


***Figure 10.*** *Surface free energies vary with the materials used for corrosion resistance [112].*

### 2.5.3. Enhancing stainless steel mesh surface with the coatings

Recent advancements in surface modification technologies have enabled these meshes to selectively separate oil from water, or vice versa, depending on the mechanisms, adhesion, and surface free energy, as required by specific applications. Such modifications ensure that water droplets are repelled, while oil readily permeates through the mesh. To achieve hydrophobic and oleophilic surfaces, many methods and techniques are used, including surface chemistry modification (chemical functionalization with low-energy molecules), surface topography engineering (hierarchical micro/nano structures, and re-entrant and special geometries), combined chemistry and texture (one-step nano structuring and coating, and two-step approaches), hydrothermal synthesis, self-assembly method, template-based

method, anodization, chemical etching, nanocomposite coating, coating and deposition techniques [113, 114].

Many researchers have successfully developed superhydrophobic coatings for corrosion protection on metal and alloy surfaces, including aluminium, copper, magnesium, and steel [115], by either roughening the surface of a low-surface-energy material or by depositing low-surface-energy materials to modify a rough surface. They demonstrate that chemical composition and surface roughness are essential factors in the formation of superhydrophobic surfaces [116]. Therefore, researchers [117-120] rushed to focus on enhancing the separation process and extending their life by adding coatings to the surface of the metal meshes, which improve the durability and hardness necessary to extend their life (such as immersion in a solution of fatty acids, electrodeposition, chemical modification with low surface energy materials, and electroless galvanic deposition, electrodeposition, electroplating, etching, sandblasting, solution-immersion, spray-and-dry method, dip coating, spray coating, electrospinning, plasma treatment, PVD, CVD and other methods).

Many researchers have started with stainless steel mesh coated with silica, including a one-layer silica-coated stainless steel mesh [121] and a double-layer modified silica-coated stainless steel mesh [122]. The results demonstrated effective separation of oil-water mixtures. However, a limitation was found in separating oil-water emulsions, attributed to the size of the prepared oil droplets in water, and a detailed benchmark against alternative materials and coatings for oil-water separation has not yet been fully developed, as there is limited discussion of the sustainability of the materials and economic feasibility for large-scale industrial deployment.

Other researchers focused on $TiO_2$ coating, depositing it via atomic layer deposition [123] and hydrothermal synthesis [83]. These articles [123, 83] present significant findings on the $TiO_2$-coated stainless steel mesh for oil-water separation, but do not address the environmental impact of $TiO_2$ coatings, particularly the potential leaching of materials or byproducts during operation or cleaning. The studies primarily focused on a few types of oils (e.g., n-hexane, soybean oil). Still, they did not explore performance across a broader range of oils with similar crude-oil properties or under varying environmental conditions, which could affect separation efficiency. Sustainability and eco-friendliness are critical considerations for widespread adoption, especially in environmental remediation applications.

Seongjae Myeong et al. [124] developed a hydrophobic mesh filter by coating with carbon and treating with fluorine plasma using Physical Vapour Deposition (PVD). PVD can uniformly coat materials at the nanoscale, and the carbon coating enhances hydrophobicity, with a water contact angle of 120.41 degrees. The study primarily focuses on the immediate separation efficiency and flux of the mesh filters. However, there is a lack of comprehensive data on the long-term performance and durability of the filters under various operational conditions, and it was focused on a specific type of oily wastewater (soybean oil), leaving a gap in understanding how the mesh filter performs with different types of oils.

One promising approach involves coating stainless steel meshes with nickel to impart superhydrophobic (water-repelling) and oleophilic (oil-attracting) properties. The nickel coating not only enhances the physical properties of the meshes but also enables the formation of micro- and nanoscale surface structures that optimise wettability. Qian Gao et al. [125] used electrodeposition techniques to coat stainless steel meshes with a nickel layer. This process involved depositing Ni onto the mesh surface, creating a hierarchical micro-nanostructure. Subsequent modification with low-surface-energy materials rendered the mesh superhydrophobic (extremely water-repellent) and superoleophilic (highly oil-attractive).

Other researchers have enhanced Ni coatings on stainless steel mesh using various methods, such as electrochemically depositing a layered double hydroxide (LDH) by Liu et al. [126]. The preparation took a few minutes and significantly improved production efficiency. The positive charge of LDH promotes the rupture of emulsion droplets and improves emulsion separation efficiency. While Hou et al. [127] prepared nickel-coated meshes via electrodeposition in a deep eutectic solvent (DES) composed of choline chloride (ChCl) and ethylene glycol (EG), the resulting materials exhibit superior chemical stability in acidic, alkaline, and salt solutions.

Much research [128-130] has demonstrated the efficacy of Ni-coated meshes for separating oil-water mixtures, owing to their enhanced chemical stability and mechanical strength. It was reported that nickel-coated meshes achieved high separation efficiencies, with oil flux rates exceeding 98%, even under challenging conditions involving high oil viscosity and dynamic flow environments and highlighted that the hierarchical structure formed by nickel coatings significantly improves the long-term durability and reusability of the meshes, making them suitable for continuous industrial applications. In addition to chemical stability and mechanical strength, these studies have proven that Ni coatings allow

the creation of micro- and nanoscale surface structures that optimise their wettability and highlight that the hierarchical structure (multilevel structural arrangement) formed by nickel coatings significantly improves the long-term durability and reusability of the meshes, making them suitable for continuous industrial applications. Still, they did not determine the separation efficiency when using emulsion or study the effect of differences in hole mesh size on it.

### 2.6. Physical Vapour Deposition (PVD) coating technology

Although the current results are satisfactory, it is necessary to employ contemporary methods to ensure precision and consistent dimensions, as well as to enhance production speed. This will allow us to save time while adhering to a clean, eco-friendly, and low-cost procedure, for example, Physical Vapour Deposition coating. Physical vapour deposition (PVD) is a widely recognised technology for depositing thin films to meet various requirements, such as improving tribological behaviour, enhancing optical properties, improving visual aesthetics, and supporting applications across many fields. PVD has already been extensively applied in a wide range of established applications [131, 132]. Machining tools are a frequent application of this deposition technology, often used in conjunction with chemical vapour deposition (CVD) to enhance durability, reduce friction, and improve thermal characteristics. This method is most often used when the desired coating can only be achieved through this specific procedure. Numerous studies have been conducted to optimise the PVD method [132], focusing on increasing plasma ionisation, reducing dark areas (regions where deposition does not occur in the reactor), improving target utilisation, enhancing atomic bombardment efficiency, increasing the deposition rate, and optimising gas selection. These investigations demonstrate significant potential to enhance thin-film quality by adjusting parameters and to improve substrate adhesion.

PVD is a coating process that involves transferring material from a solid phase to a vapour phase, then back to a solid phase, to form a thin film on the surface of a substrate. This process applies coatings that enhance the performance, durability, and aesthetics of various components. Here are the detailed steps and techniques involved in the PVD coating process [133]:

a. Preparation of Substrate: The substrate (the object to be coated) must be thoroughly cleaned to remove any contaminants, such as oils, dirt, or oxides. This is typically done using ultrasonic, chemical, or plasma cleaning. And Parts of the substrate that should not be coated are masked using appropriate materials.

b. Loading the Substrate: Cleaned, masked substrates are placed in the coating chamber. The substrates are often mounted on fixtures or rotating holders to ensure even coating.
c. Evacuation of the Chamber: The coating chamber is evacuated to create a high vacuum environment. A high vacuum is essential for removing contaminants and ensuring a pure coating process.
d. Introduction of Process Gases: Process gases, such as argon, nitrogen, or oxygen, are introduced into the chamber, depending on the coating type. These gases facilitate plasma formation and the desired chemical reactions.
e. Generation of Vapour Phase: The coating material is heated in a crucible until it vapourises. The vapour then condenses on the substrate to form a thin film (Thermal Evaporation). An electron beam is directed at the coating material to heat it to its vapourisation point (Electron Beam Evaporation). The ions (typically argon ions) are accelerated towards the target material (the coating material), causing atoms to be ejected from the target and deposited on the substrate. Arc Vapourisation: An electric arc is used to vapourise the coating material (Sputtering).
f. Deposition: The vapourised atoms or molecules travel through the vacuum chamber and condense on the substrate to form a thin film. The thickness and uniformity of the coating are controlled by deposition time and substrate positioning.
g. Coating Techniques: Involves introducing reactive gases (e.g., nitrogen, oxygen) into the chamber, which react with the vapourised material to form a compound coating, such as nitrides or oxides (Reactive PVD). No reactive gases are used, and the coating material is deposited directly onto the substrate (Non-Reactive PVD).
h. Cooling and Unloading: After the deposition process is complete, the substrates are allowed to cool in the vacuum chamber. Once cooled, they are removed from the chamber.
i. Post-Processing: The coated substrates are inspected for coating thickness, uniformity, and adhesion (Inspection). Depending on the application, additional treatments such as heat treatment or annealing may be applied to enhance coating properties (Additional Treatments).

There are numerous advantages of PVD coatings. PVD offers distinct, exclusive benefits that enhance product durability and value. Deposition techniques play a crucial role in machining processes. Machining tools are highly demanding applications that require

specific qualities, including high-temperature hardness, exceptional abrasion resistance, chemical stability, toughness, and stiffness [134, 135]. Furthermore, PVD can generate coatings that exhibit excellent adhesion, uniform layers, predetermined structures, varying properties, controlled morphology, and a wide range of materials and properties [136, 137].

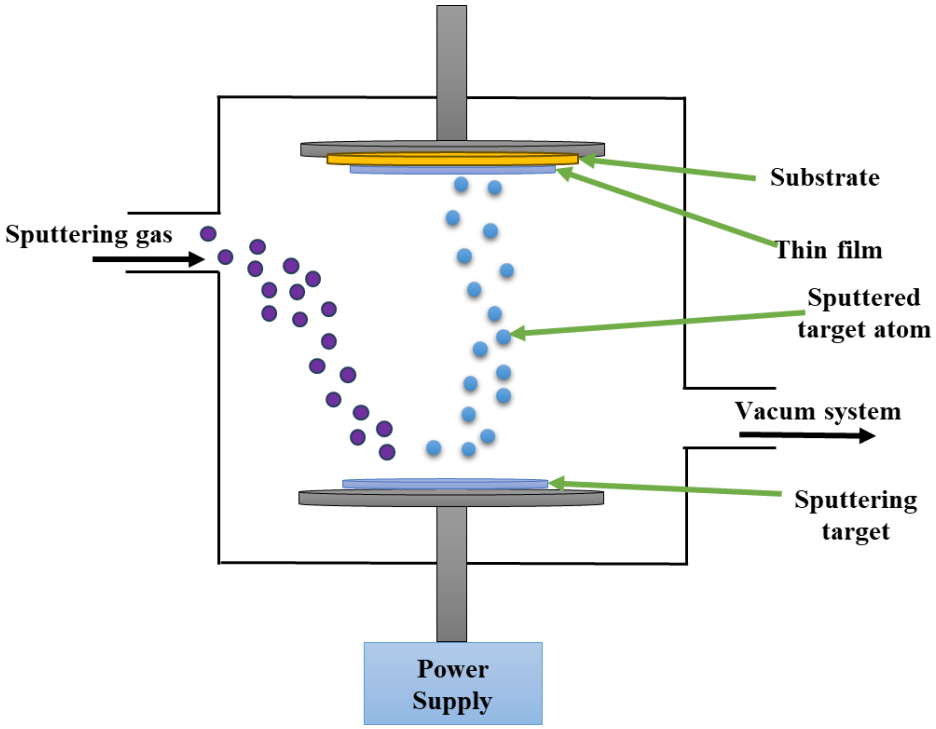


***Figure 11.*** *Schematic diagram representing the PVD coating technique.*

## 3. Knowledge gaps

The following points outline the knowledge gaps that could not be addressed previously, according to the reported literature:

1) Previous studies did not investigate the effect of differences in chromium content in stainless steel on the wettability behaviour of water and oil.
2) Previous studies did not establish a mathematical relationship between the atomic radius of pure metals and the wettability behaviour of oil and water.
3) Previous studies used only one or two types of stainless steel mesh, and they did not provide a practical comparison of the available types within the same mixture under the same conditions, nor did they explain the rationale for selecting a specific type.
4) Previous studies have reported coating stainless steel meshes with various metals, but these methods were often costly or environmentally damaging. Furthermore, they did not use pure nickel but mixed it with other compounds, which increased the cost of the process.
5) Previous studies did not utilise a two-layer separation method using nickel-coated stainless steel meshes to investigate its effect on the separation process and efficiency.
6) In all the stainless steel meshes used, the holes (opening areas) were square, and they did not explain the rationale for this shape, nor did they study the effect of changing the shape to on the oil-water separation efficiency.

# 4. Materials and Methods

The material and methods chapter is provided for the reproducibility of the results by the reader. The study focuses on wettability phenomena of oil and water on various metal surfaces and the benefits of these behaviours for oil-water separation potential, using stainless steel meshes before and after nickel coating.

## 4.1. Polar and apolar wetting behaviour investigation

### 4.1.1. Materials and liquids

In this subchapter, I used as substrates four types of steel samples include ($CrMo_4$, CK60, 1.4050 steel, and 1.4301 steel) size of (10mm×6mm×3mm) (Fig. 12), and two types of ceramics samples (TiC and WC) size of (10mm×6mm×3mm) (Fig. 12), both of the steel and ceramic samples chemical compositions listed in Table 2, additional to eight types of pure metals (Fig. 13) include (Ni, Cu, Ag, Al, W, Sn, Fe, and Cd) with 99.99% purity, and the size was around (10 mm×8 mm×5 mm) in all cases. The substrates were ground and polished mechanically immediately before the measurement. The average surface roughness of the pure metal substrates (Ra) was 0.02 µm using a surface roughness measurement device (MARSURF M 40). The preparation was performed at room temperature and under normal air, with a relative humidity of ~56%, under the same conditions as in [138].

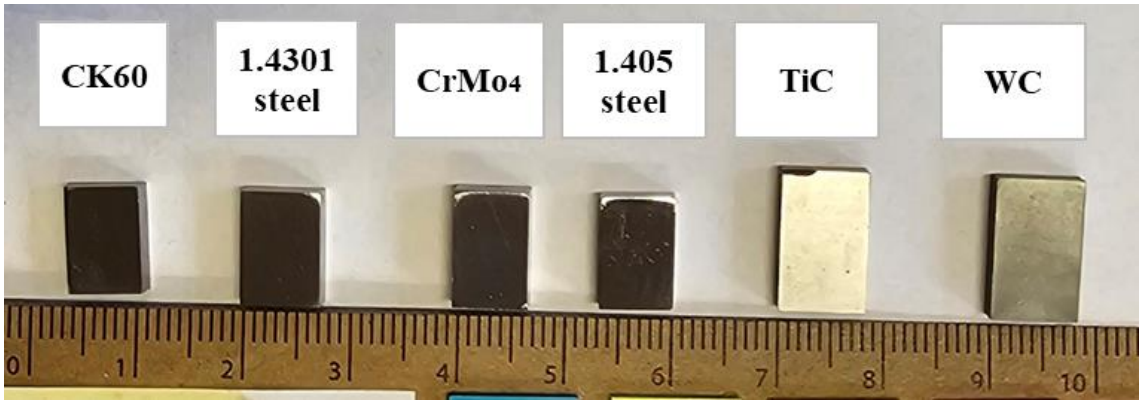


***Figure 12.*** *The dimensions of the steel and ceramic samples.*

***Table 2.*** *Chemical compositions of the steel and ceramics samples.*

| No. | Samples types | %C | %Si | %P | %S | %Mn | %Ni | %Cu | %Cr | %Mo | %Fe |
|---|---|---|---|---|---|---|---|---|---|---|---|
| **1** | Ck60 steel | 0.61 | 0.40 | 0.3 | 0.035 | 0. 75 | 0.4 | - | 0.4 | 0.1 | Balance |
| **2** | 1.4050 steel | 0.12 | 0.32 | 0.012 | 0.005 | 0.51 | 0.15 | 0.18 | 8.55 | 0.88 | Balance |
| **3** | $CrMo_4$ steel | 0.38-0.45 | 0.10-0.40 | 0.025 | 0.035 | 0.60-0.90 | - | 0.40 | 0.9-1.2 | 0.15-0.30 | Balance |
| **4** | 1.4301 steel | 0.07 | 1 | 0.045 | 0.015 | 2 | 8-10.5 | - | 17.5-19.5 | - | Balance |
| **5** | TiC | 14.49 | 7.19 W | | - | 0.45 | 60.26 Ti | | 5.25 | - | 12.38 |
| **6** | WC | 6.1 | > 93 W | | - | - | - | - | - | - | < 0.03 |

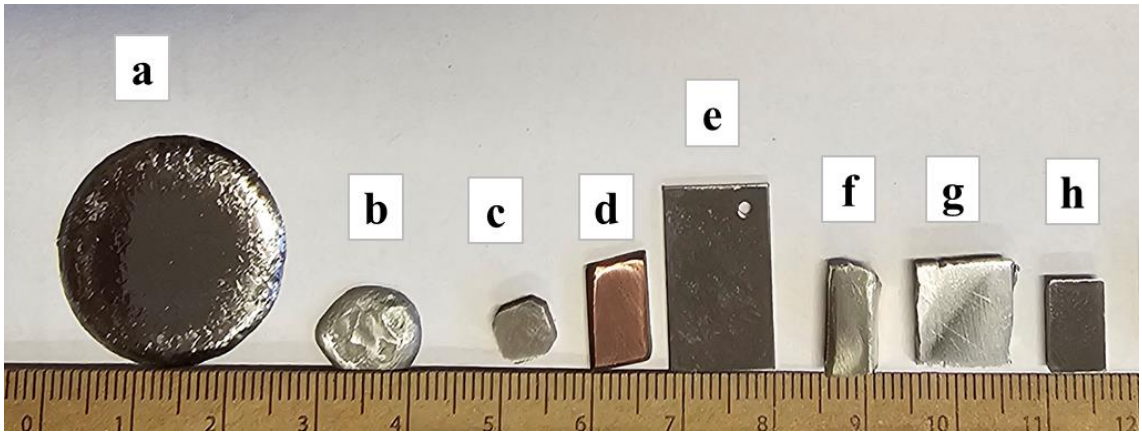


***Figure 13.*** *The pure metal samples (a: Iron-Fe, b: Cadmium-Cd, c: Silver-Ag, d: Copper-Cu, e: Nickel-Ni, f: Tin-Sn, g: Aluminium-Al, h: Tungsten-W).*

For the wettability behaviour test studying on these freshly polished surface, a eight types of liquids were used are distilled water, glycerin, hydraulic oil (HME10) (MOL Group), refined petroleum (MOL Group) (88–92 wt.% hydrocarbon, C10-C13, n-alkanes, iso-alkanes, cyclic compounds, <2% aromatics, 8–12 wt.% hydrocarbon, C15-C20, n-alkanes, iso-alkanes, cycloalkanes, <0.03% aromatics), and hydraulic oil/petroleum mixture (10 vol.% petroleum + 90 vol.% hydraulic oil, 30 vol.% petroleum + 70 vol.% hydraulic oil, 50 vol.% petroleum + 50 vol.% hydraulic oil, and 20 vol.% petroleum + 80 vol.% hydraulic oil), with its properties listed in Table 3.

***Table 3.*** *Liquids properties [139-142].*

| No. | Liquid | Density ($g/cm^3$) | Viscosity (Pa·s) |
|---|---|---|---|
| 1 | Distilled water | 0.9982 | 1.0034 |
| 2 | Glycerin | 1.261 | 1.412 |
| 3 | Hydraulic oil | 0.860 | 10.1 |
| 4 | Petroleum | 0.760 | 6.21 |
| 5 | (10 vol. % petroleum + 90 vol. % hydraulic oil) mixture | - | 9.43 |
| 6 | (30 vol. % petroleum + 70 vol. % hydraulic oil) mixture | - | 8.37 |
| 7 | (50 vol. % petroleum + 50 vol. % hydraulic oil) mixture | - | 7.83 |
| 8 | (80 vol. % petroleum + 20 vol. % hydraulic oil) mixture | - | 7.11 |

### 4.1.2. The measurement of the contact angle (CA)

Polishing, washing, and alcohol cleaning of all the samples were performed before the test began. To measure the contact angle, the sessile drop method was used for each liquid listed in Table 3. Using an automatic pipette, five μL of liquid was placed on the polished surface of each sample (steel types, ceramics, and pure metals) for 5 min. A CCD camera was used to record changes in the droplet silhouette as it formed (Fig. 14). The CCD camera was connected to a computer with KSV software (CAM2008, KSV Instruments Ltd., Helsinki, Finland) to determine the contact angle (Fig. 15). The experiments were performed at room temperature, and the liquid contact angles were measured at least 10 times for each sample.

The process of measuring and analysing the liquid contact angle on metal surfaces is depicted in Fig. 16. The experimental procedures were conducted using the sessile drop technique, utilising equipment developed by Sunplant Ltd. (Miskolc, Hungary).

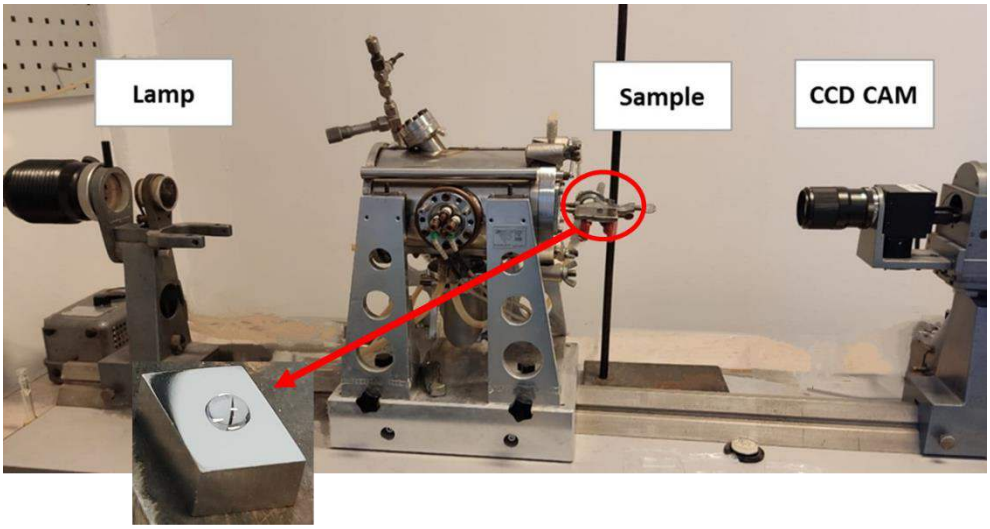


***Figure 14.*** *The wetting test equipment and the liquid droplet on the substrate surface.*

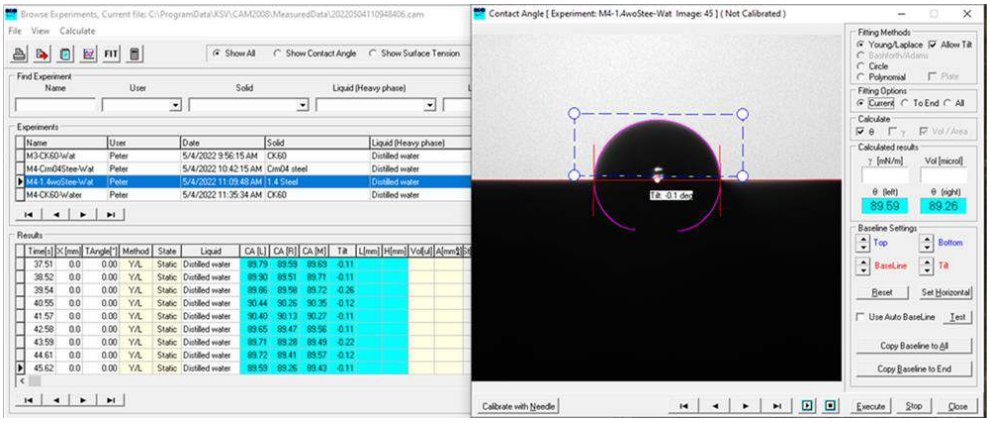

***Figure 15.*** *The KSV program interface and the contact angle measurement.*

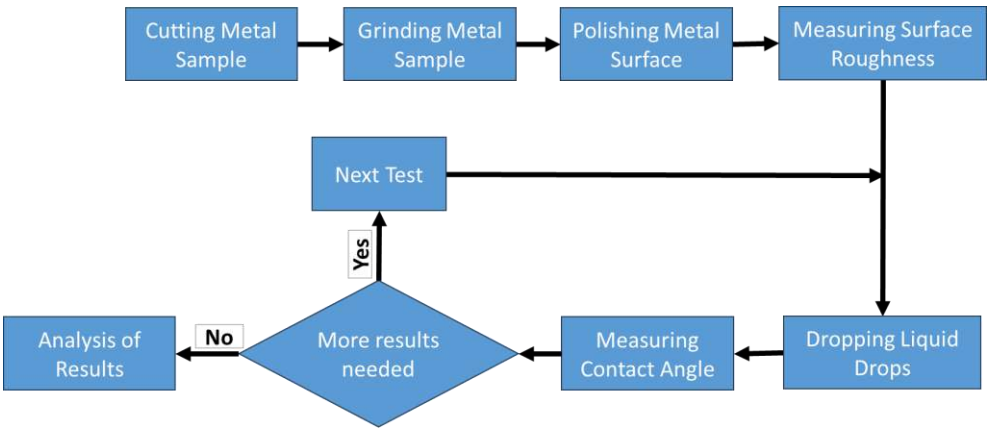


***Figure 16.*** *Sketch of the measurement process.*

## 4.2. Separation potential by stainless steel meshes

### 4.2.1. Materials

In this subchapter of the experiment, the samples were meshes (Fig. 17, Table 4 and Table 5) made of stainless steel with different sizes (500, 400, 300, 200, and 180 meshes), were purchased from (Putian Xinyu District Blue Sky Electronic Commerce Co. Ltd. - China), and from (Yiwu Huili Metal Product Firm Co. Ltd - China). The stainless steel surface was coated with Ni by physical vapour deposition (PVD) (see subchapter 4.2.2.2). In my experiment, I also investigated coated and uncoated meshes (see subchapter 4.2.4). Two types of liquids, refined petroleum and distilled water (Table 2, subchapter 4.1.1), were used to prepare emulsions with different compositions, and the emulsion preparation is detailed in subchapter 4.2.2.3.

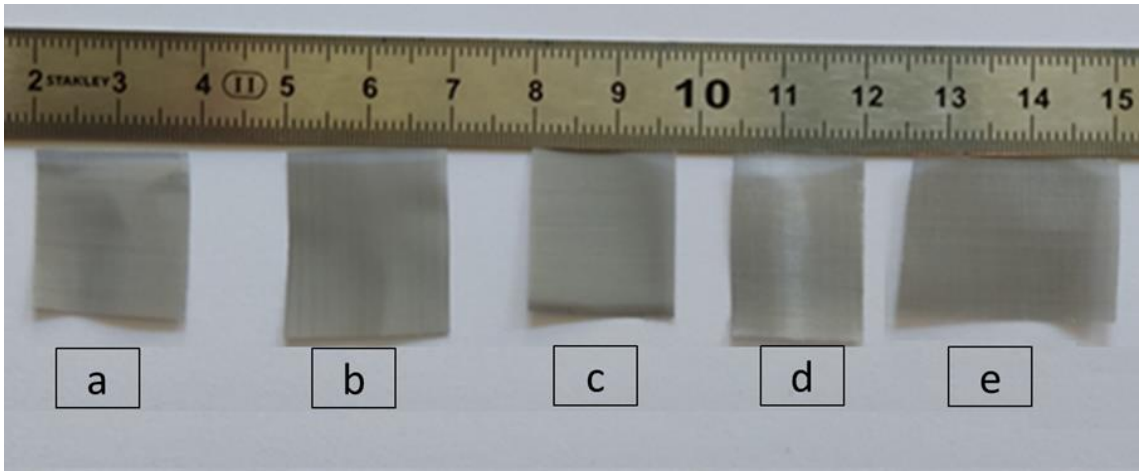


***Figure 17.*** *The stainless steel mesh samples (a: 500, b: 400, c:300, d:200, e:180 mesh sizes).*

***Table 4.*** *The stainless steel mesh properties.*

| No | Mesh size | Hole diameter mm | Wire diameter mm |
|---|---|---|---|
| a | 500 | 0.026 | 0.0254 |
| b | 400 | 0.033 | 0.0254 |
| c | 300 | 0.040 | 0.0381 |
| d | 200 | 0.080 | 0.0533 |
| e | 180 | 0.082 | 0.08 |

***Table 5.*** *The Chemical composition of the stainless steel mesh samples before coating.*

| No | Mesh size | %Fe | %Cr | %Ni | % Others |
|---|---|---|---|---|---|
| a | 500 | 68.31 | 18.33 | 11.54 | 1.82 |
| b | 400 | 68.63 | 18.40 | 11.12 | 1.85 |
| c | 300 | 68.89 | 18.45 | 11.16 | 1.50 |
| d | 200 | 73.33 | 19.41 | 7.26 | - |
| e | 180 | 73.88 | 18.62 | 7.50 | - |

### 4.2.2. Preparation of the samples

#### 4.2.2.1. Stainless steel mesh preparation

The meshes were cut into square shapes with a size (10 mm× 10 mm), they were fixed on the wood frame made by hand to keep plain level (Fig. 18), before each test they were ultrasonically treated in 0.1 M of $H_2SO_4$ solution, and ethanol, respectively, for 5 min to remove any organic impurities, and prevent unwanted side reactions, or any changes to surface chemistry during the experiment, to ensure the reproducibility and consistency in results; finaly under room temperature they were dried.

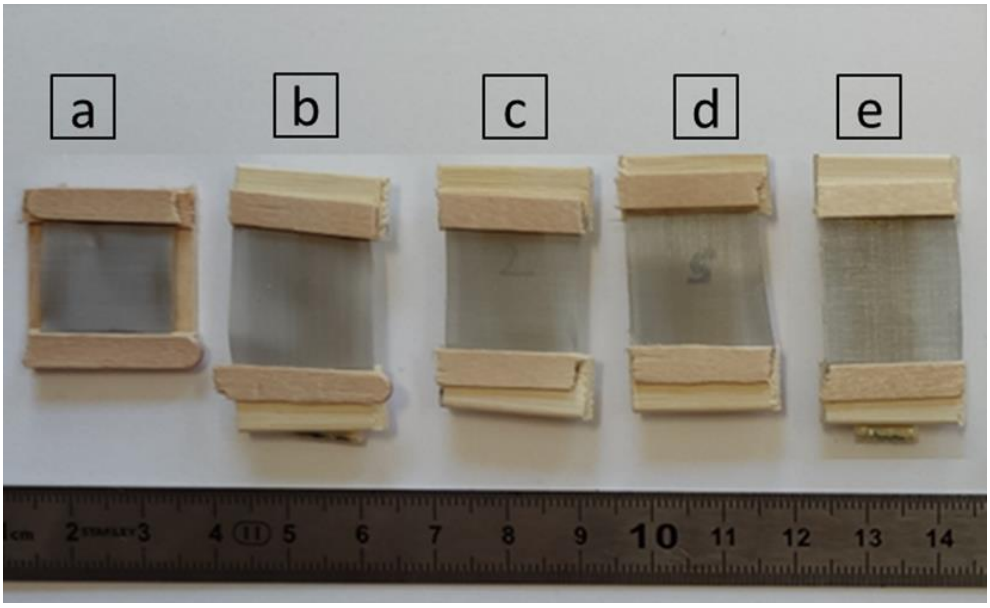


***Figure 18.*** *Fixation of stainless steel meshes (a: 500, b: 400, c: 300, d: 200, e: 180) before Ni coating.*

#### 4.2.2.2. The stainless steel mesh coating by physical vapour deposition (PVD)

As I mentioned in subchapter 4.2.1, the meshes were coated with Ni; in this subchapter, I show the details of the Ni coating process. The 0.10 μm of Ni coatings were deposited when the meshes were static in front of the target in an argon atmosphere by the PVD technique. The samples were placed on a plate and then inserted into the upper device chamber (Fig. 19), while the Ni plate was mounted in the shutter. The deposition parameters were (chamber pressure= 5.7 $*10^{-3}$ mbar, argonne= 90 sscm, voltage= 250 V, current = 250 mA, tooling factor = 100, and the temperature was 25 °C), the device that be used was from Korvus Technology company, and using the Niobium software interface to control the process and parameters.

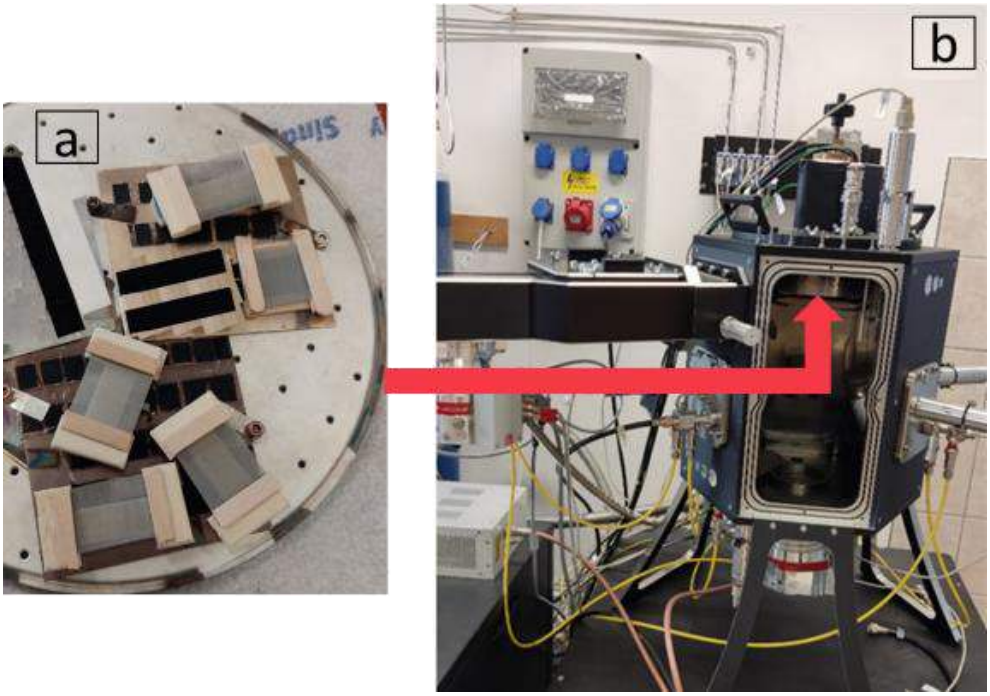


***Figure 19.*** *Setting up the samples for the PVD coating (a: samples placed on the PVD plate base; b: The plate base with samples fixed was inserted inside the upper device chamber).*

#### 4.2.2.3. Preparation of the petroleum-water emulsion

To mix petroleum with water, stabilising powders such as cetyltrimethylammonium bromide (CTAB) are often used in petroleum-water mixtures (emulsions) to maintain stability and prevent separation of the petroleum and water phases. Where stabilisers help keep the dispersed phase (petroleum or water) within the continuous phase by reducing interfacial tension and forming a protective barrier around droplets and prevent the merging of dispersed droplets into larger ones, which could lead to separation. It means stabilisers maintain homogeneity, preventing sedimentation or creaming, and ensuring the long-term

stability of the emulsion during the experiment. CTAB powder (0.1 gram) was added to 100 mL of water and shaken by hand to ensure mixing. This solution was used in the experiment and blended with petroleum as follows:

a. First, to establish a calibration standard for evaluating the separation results later, additional to petroleum and water, there are seven mixtures with known volume ratios that were prepared (20% petroleum + 80% water; 35% petroleum + 65% water; 50% petroleum + 50% water; 65% petroleum + 35% water; and 80% petroleum + 20% water;) of petroleum-water mixing. Then they were examined using an element analyser device (EA1108.) from Carlo Erba Instruments, and the hydrocarbon ratios in each sample were calculated using Clarity software version 8.8.1.1.6.
b. Equal proportions of (50% vol.) water and (50% vol.) petroleum were mixed for use in a primary phase separation experiment (see subchapter 4.2.4).

### 4.2.3. Petroleum and water contact angles measured on the surface of stainless steel meshes before and after Ni coating

To simulate the results proven by [77, 138] and provide insights into the wetting characteristics of liquids (petroleum and water) and the possibility to apply this behaviour on stainless steel mesh surfaces, the sessile drop and captive bubble techniques were employed to determine the contact angle, using an automatic pipette a drops of 5µl of distilled water and petroleum separately, were placed on the surface of cleaned meshes (before and after coating) for 5 minutes for each sample, then used same technique procedure mentioned in subchapter 4.1.2 to record and determine the value of the contact angle by using a CCD camera to record the changes in the silhouettes of the formed drop and controlled with KSV software. The experiments were performed at room temperature, and the liquid contact angle was measured about 10 times for each sample.

### 4.2.4. The separation process and investigation

To evaluate the emulsion (petroleum-water) separation ability with the prepared meshes (coated and uncoated by Ni), emulsion separation tools were collected, and an experiment was conducted to separate petroleum from water at room temperature. As shown in Fig. 20, the stainless steel meshes were held in place by the holder. An amount of 20 µL of the previously prepared emulsion (50% vol. water + 50% vol. petroleum) (as mentioned

in subchapter 4.2.2.3, point b) was placed on the stainless steel mesh surfaces by using a laboratory pipette. After one minute of the equilibrium state, the petroleum began to pass through the mesh and collect at the bottom of the container. The petroleum-water separation process was repeated 8 times for each stainless steel mesh, both before and after Ni coating.

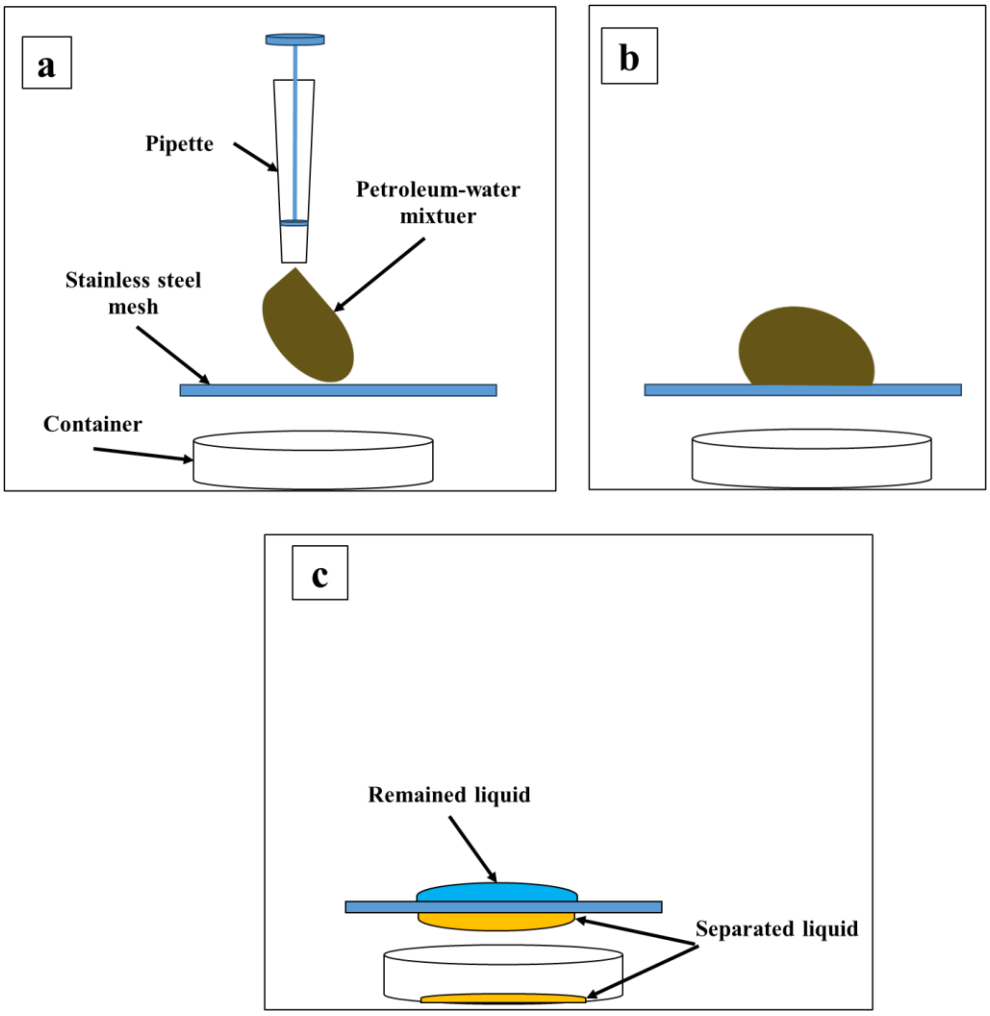


***Figure 20.*** *Schematic diagram of the emulsion (petroleum-water) separation process by stainless steel meshes coated and uncoated with Ni (a: Place of the emulsion droplet on the stainless steel mesh surface; b: Equilibrium phase; c: The separation).*

Only the liquid collected under the mesh is used for examination and calculation of the hydrocarbon content percentage. Small laboratory capsules are filled from the separated liquid, and the weight of each filled capsule is measured with an accurate electronic balance (Fig. 21). The weighed and numbered capsules are transferred and placed into the holes of a rotating disc, from which they will fall into the Element Analyzer device in sequence after each analysis of the previous capsule (Fig. 22). The Element Analyzer device is connected to the computer, through which, using the Clarity program, the results will be collected and detailed by sample numbers.

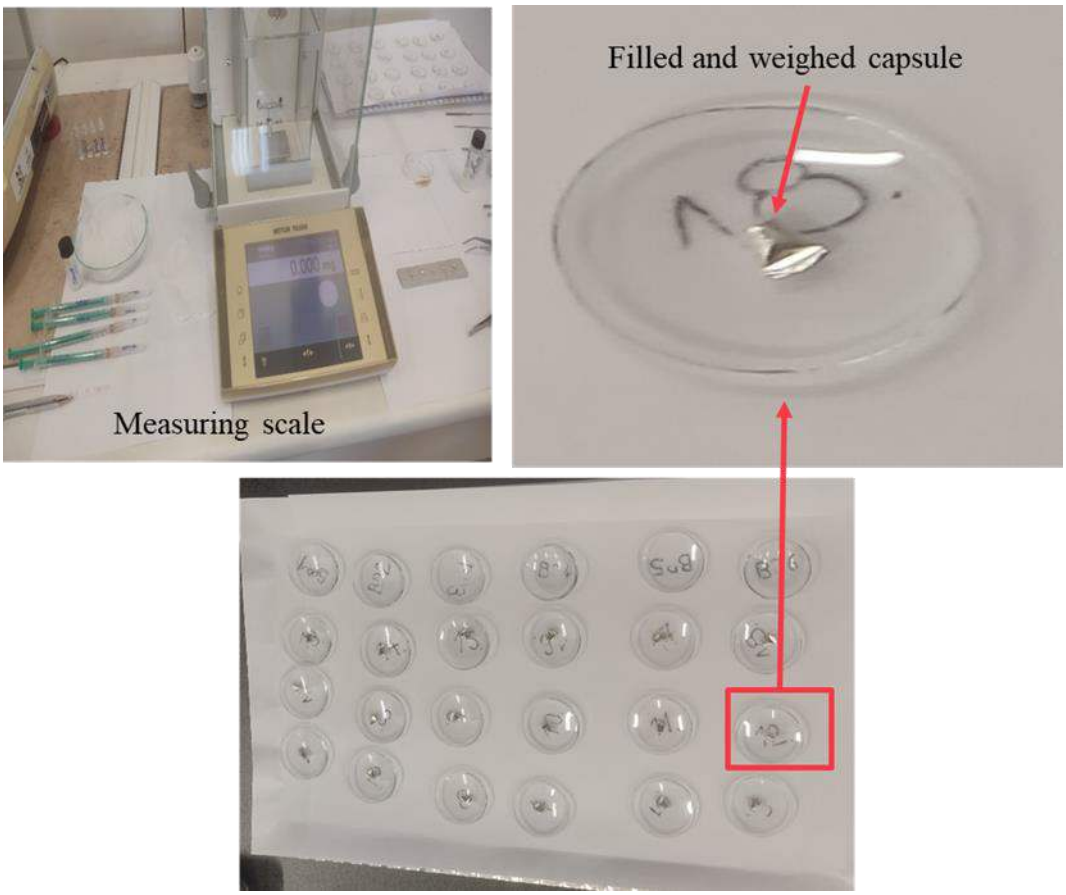


***Figure 21.*** *The filled capsules with the resulting solution, and precisely weighing them.*

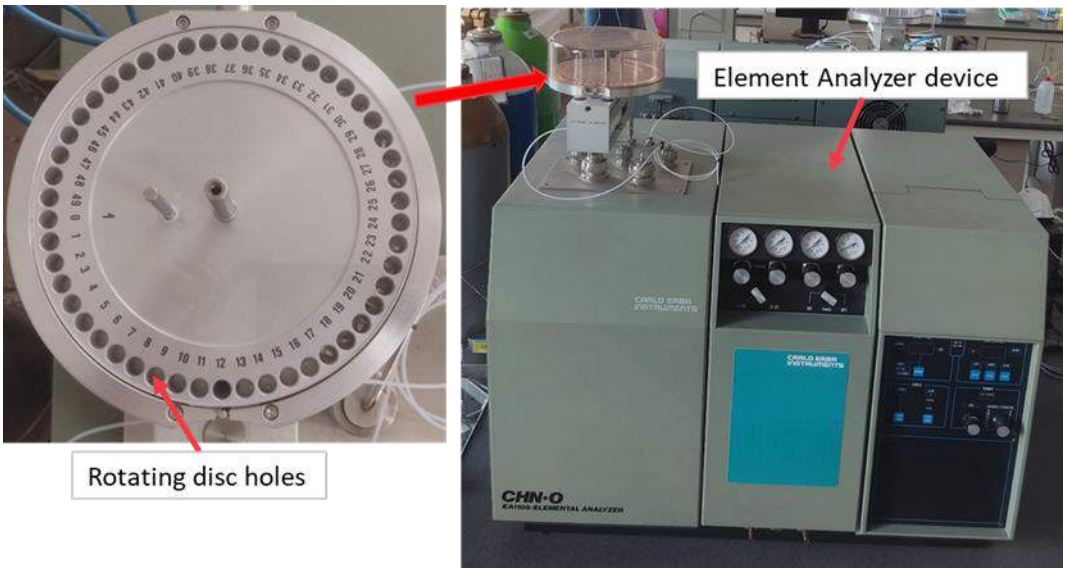


***Figure 22.*** *Placed capsules in the rotating disc holes of the Element Analyzer device.*

## 4.3. Effect of employing a double-layer configuration of Ni-coated stainless steel mesh on the petroleum-water separation efficiency.

### 4.3.1. Designing and producing the separation system

A plastic test tube with an outer diameter of 12 mm and two layers of nickel-coated stainless steel mesh (400 mesh), each 12 mm in diameter, matching the horizontal cross-section of the tube, was used to set up the separation system. The tube is cut into three sections, and a layer of mesh is added between each pair of sections. These sections are then resealed and secured with adhesive to prevent liquid leakage and to create a new separation tube system with three chambers (upper, middle, and lower) and two separation stages, each consisting of one layer of nickel-coated stainless steel mesh between the two chambers (Fig. 23).

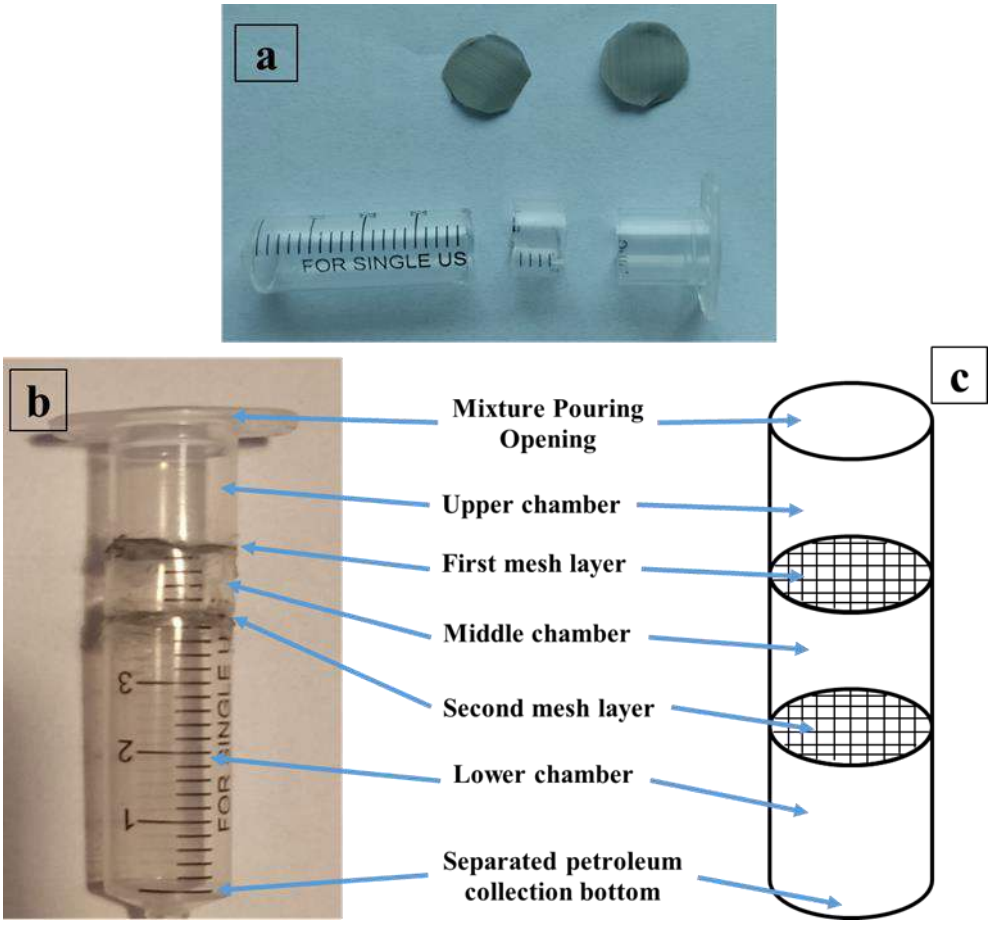


***Figure 23.*** *A new separation system preparation (a: System parts before assembly, b: System parts after assembly, c: Schematic diagram of the system after parts assembly).*

### 4.3.2. The separation process and results calculation

A red-colored food powder is mixed with water before being combined with the petroleum, allowing it to be differentiated after separation. The petroleum-water mixture was poured into the filtration system through the top opening of the new tube system using a 1-mL pipette. Separation begins in the first chamber, and the petroleum mixed with a small amount of water flows into the second chamber. The second layer performs the final separation, and the separated petroleum then flows into the third chamber, where it settles to the bottom (Fig. 24).

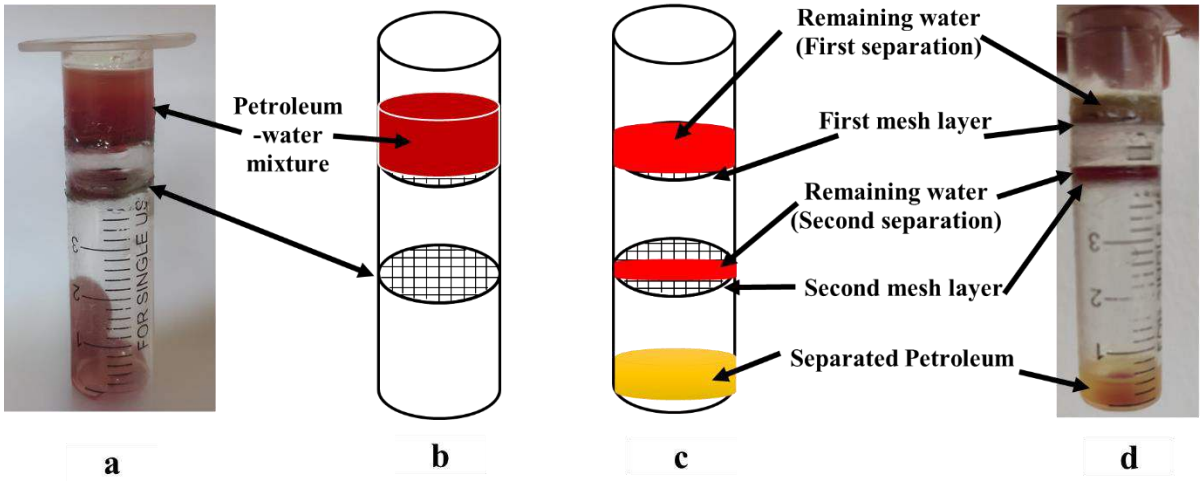


***Figure 24.*** *Schematic diagram of the separation process with a new tube system (a, b: Before the separation, c, d: After the separation).*

The volume percentage for the separated petroleum can be calculated based on the gradient of the tube, and the separation efficiency can be determined using the following equation [143]:

$$E\% = \left(\frac{M_1}{M_0}\right) * 100\% \quad (5)$$

where $M_0$= is the oil concentration of the original oil–water mixture, and $M_1$ = is the oil concentration of the collected oil after one separation cycle.

For the durability test, the same separation process was repeated 20 times for the same system containing Ni-coated meshes (400 mesh).

# 5. Results and discussion

## 5.1. The effect of Cr-containing steels on the wettability behaviour of polar and apolar liquids

### 5.1.1. The effect of Cr-containing steels on the wettability behaviour of polar liquids (water and glycerin)

Contact angle measurements with distilled water showed a similar wettability profile across all stainless steel type surfaces. Wettability behaviour decreased with increasing chromium content, and the contact angle exceeded 72° (Fig. 25), suggesting that chromium is hydrophobic. The spreading behaviour of the water droplet is happen when the height decreases and the diameter increases at the same time, but after 3 minutes of placement on the substrate surface, I noticed that the volume decreasing with the height decreases, but the diameter remains fixed, this behaviour refers to the water start evaporation and not spreading, then the contact angle measurement after 3 minutes is not real (Figs. 26 and 27).

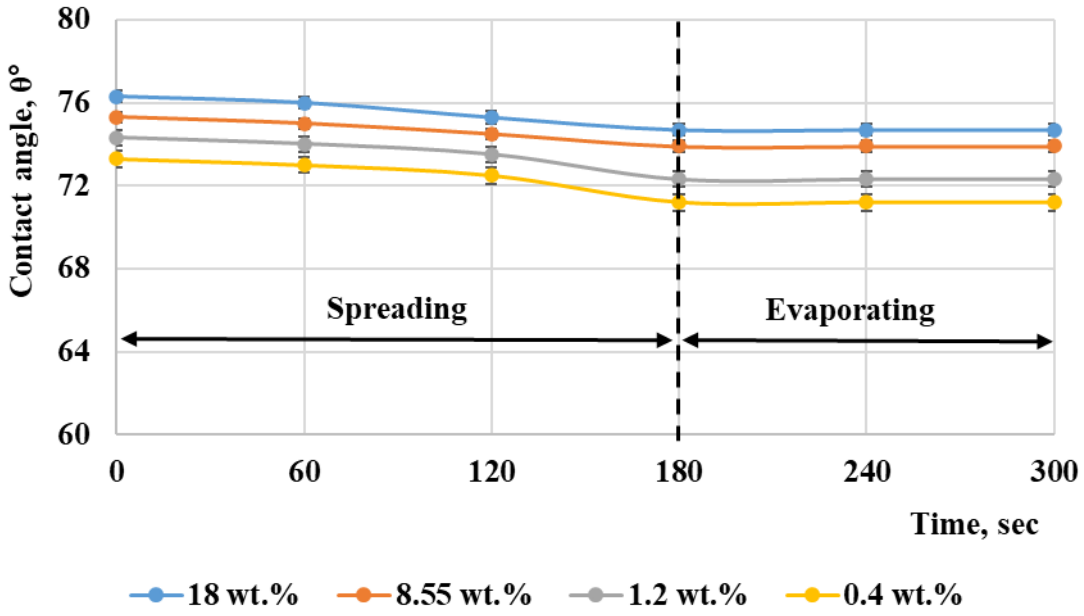


***Figure 25.*** *The wettability behaviour of distilled water by different Cr-containing steels as a function of holding time.*

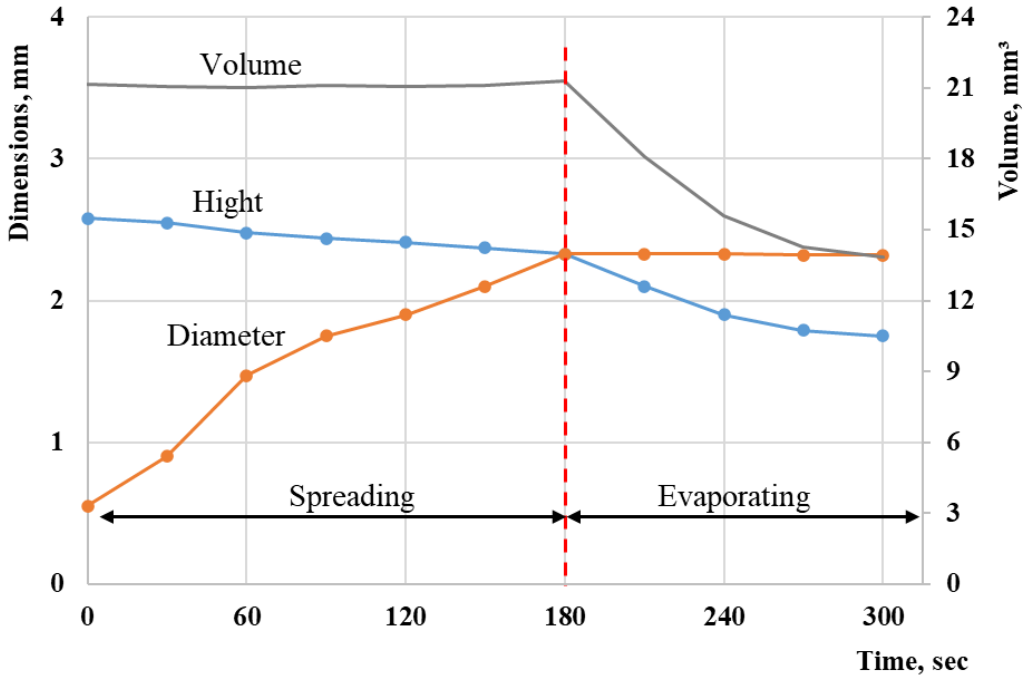


***Figure 26.*** *Water droplet dimensions behaviour as a function of holding time.*

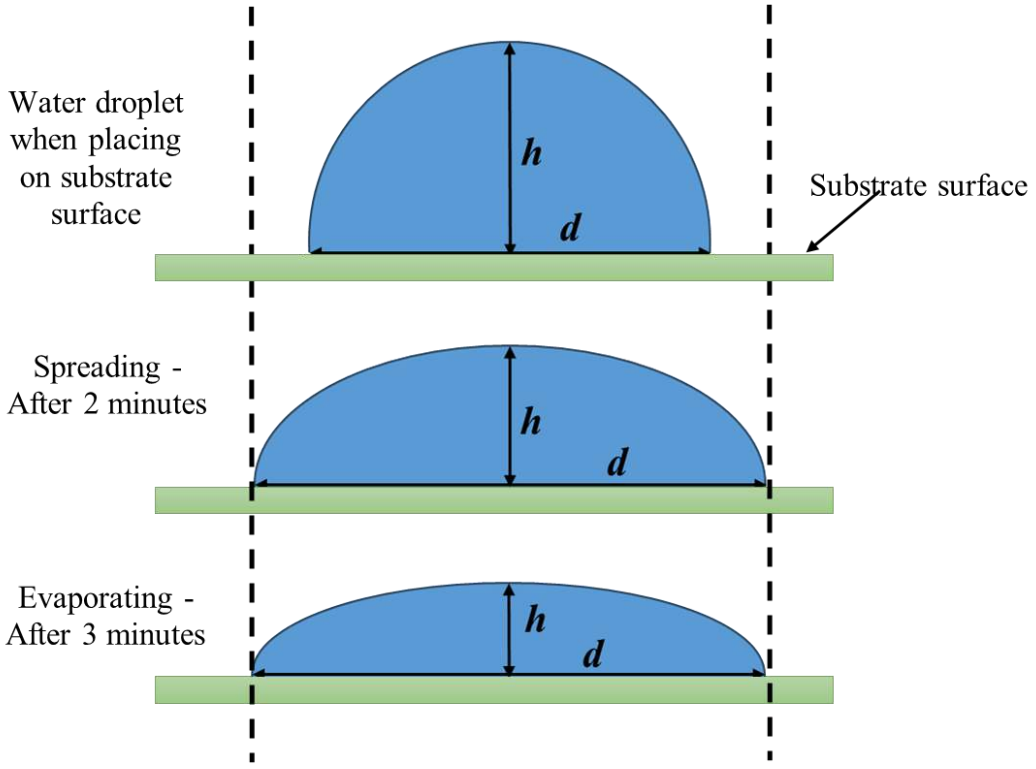


***Figure 27.*** *The expansion and contraction behaviour of water on the CK60 steel substrate surface.*

On the other hand, the results showed that the wettability function of glycerin on the same stainless steel surfaces was similar. It is not significantly different, and wettability decreases with increasing chromium content. The contact angle was greater than 78°, indicating that chromium dislikes glycerin, as shown in Fig. 28. One can observe that both water and oil, which represent polar liquids, exhibit significant similarities in their wettability functions on the surfaces of different steel types. Therefore, it can be said that the wettability of polar liquids decreases on the surface of steel with increasing chromium content, due to the formation of Cr oxide. Cr-rich oxide surfaces often have fewer accessible polar bonding sites for water molecules, reducing the adhesive component of the solid–liquid interaction.

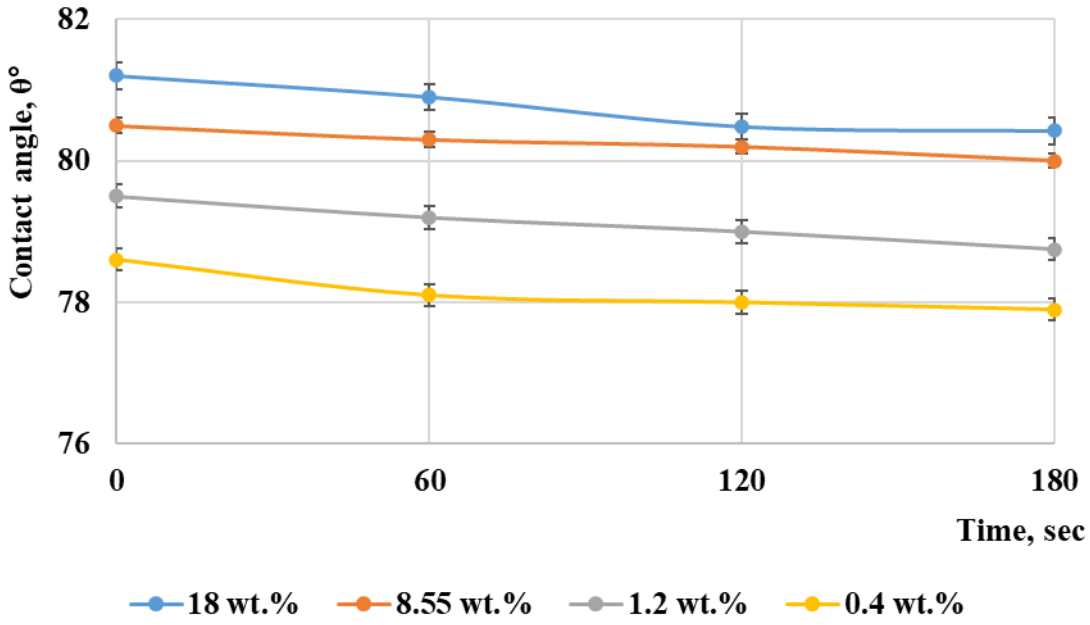


***Figure 28.*** *The wettability of different Cr-containing steels by glycerin as a function of holding time.*

### 5.1.2. The effect of Cr-containing steels on the wettability behaviour of apolar liquids (hydraulic oil, petroleum, and their mixtures)

The results for both hydraulic oil and petroleum wettability on stainless steel surfaces showed a similar behaviour. The contact angle is too slight, being less than 13° for hydraulic oil and less than 9° for petroleum (Figs. 29, 30, and 31), due to a very low viscosity, which led to the very high speed of their expansion and diffusion on the stainless steel surfaces, because of chromium oxide formation. It suggests that hydraulic oil and petroleum are attracted to chromium.

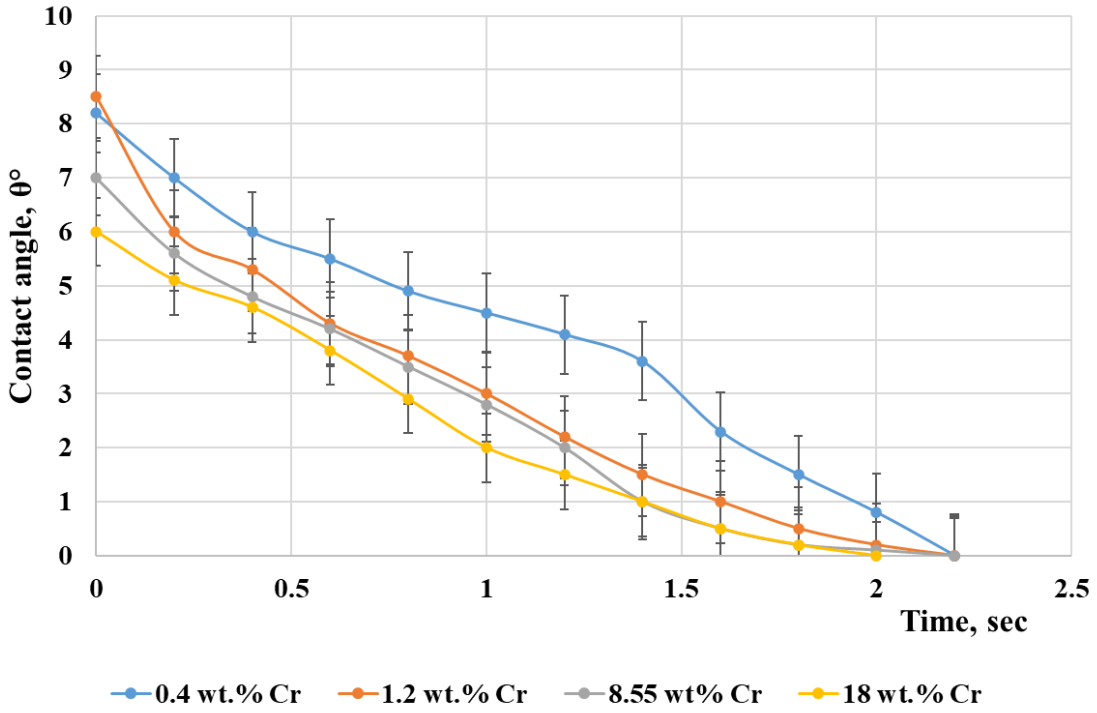


***Figure 29.*** *The wettability of different Cr-containing steels by petroleum as a function of holding time.*

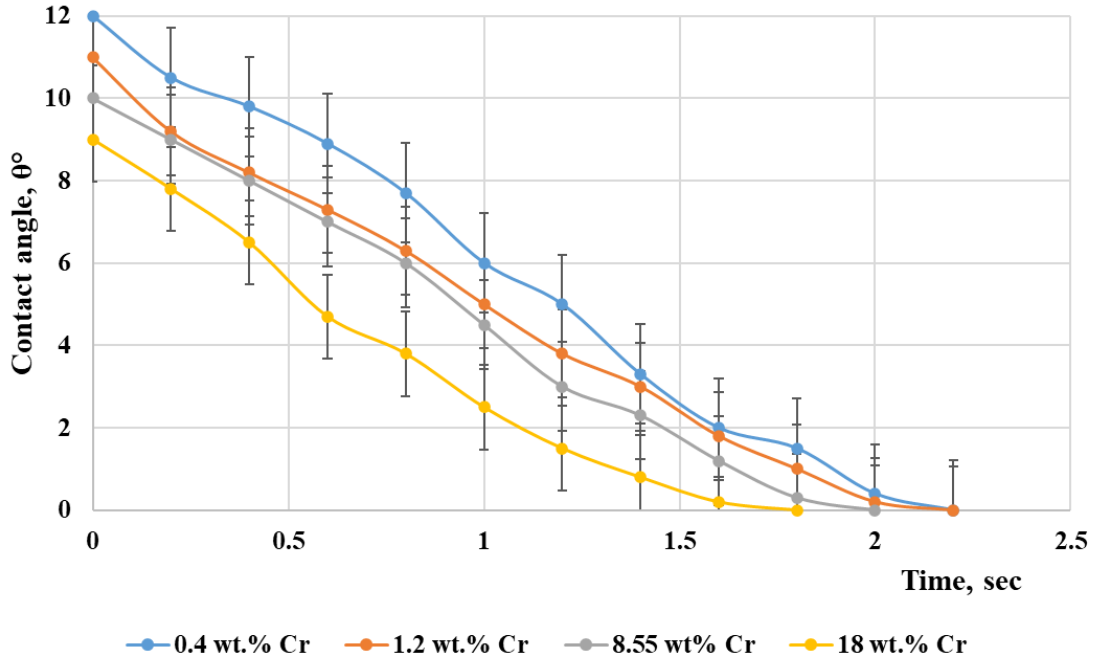


***Figure 30.*** *The wettability of different Cr-containing steels by hydraulic oil as a function of holding time.*

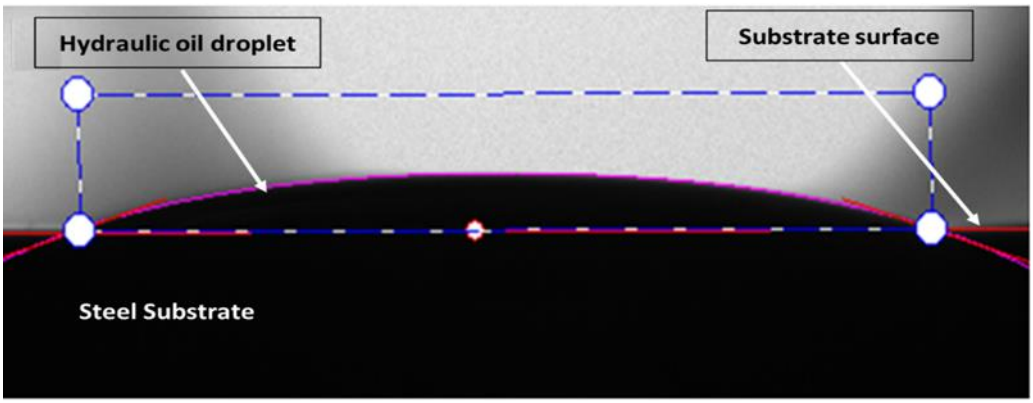


***Figure 31.*** *High hydraulic oil wetting behaviour on the CK60 steel surface.*

While all the petroleum and hydraulic mixtures (10 vol. % petroleum + 90 vol. % hydraulic oil, 20 vol. % petroleum + 80 vol. % hydraulic oil, 50 vol. % petroleum + 50 vol. % hydraulic oil, and 20 vol. % petroleum + 80 vol. % hydraulic oil) results that were prepared and investigated (in subchapter 4.1.1) have behaved similarly in the wettability function, they are similar relative to pure petroleum and hydraulic oil wettability behaviour. And the results range from 12 to 6 degrees due to the rapid expansion and diffusion of the mixture on the steel surface, driven by the formation of Cr oxide as the Cr content increases. Figs. 32 and 33 show that, regardless of composition, oils generally exhibit high wetting, and increasing the petroleum content enhances the wettability of the mixture. This behaviour applies to both steel types and ceramic surfaces.

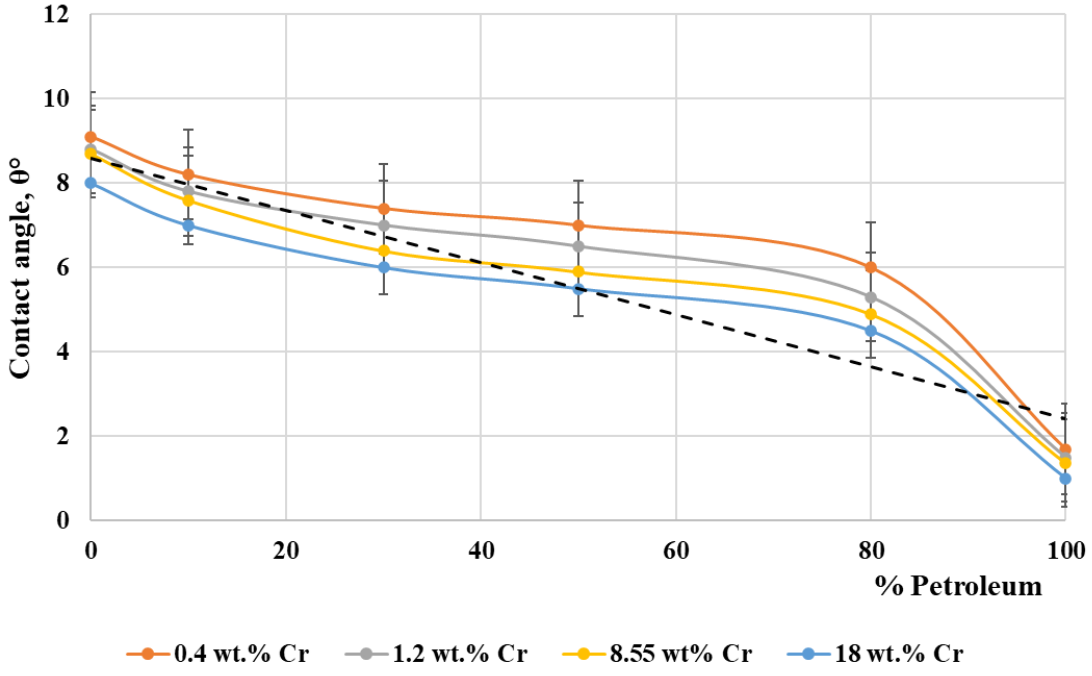


***Figure 32.*** *The wettability behaviour of a petroleum-hydraulic oil mixture on steel surfaces after two seconds.*

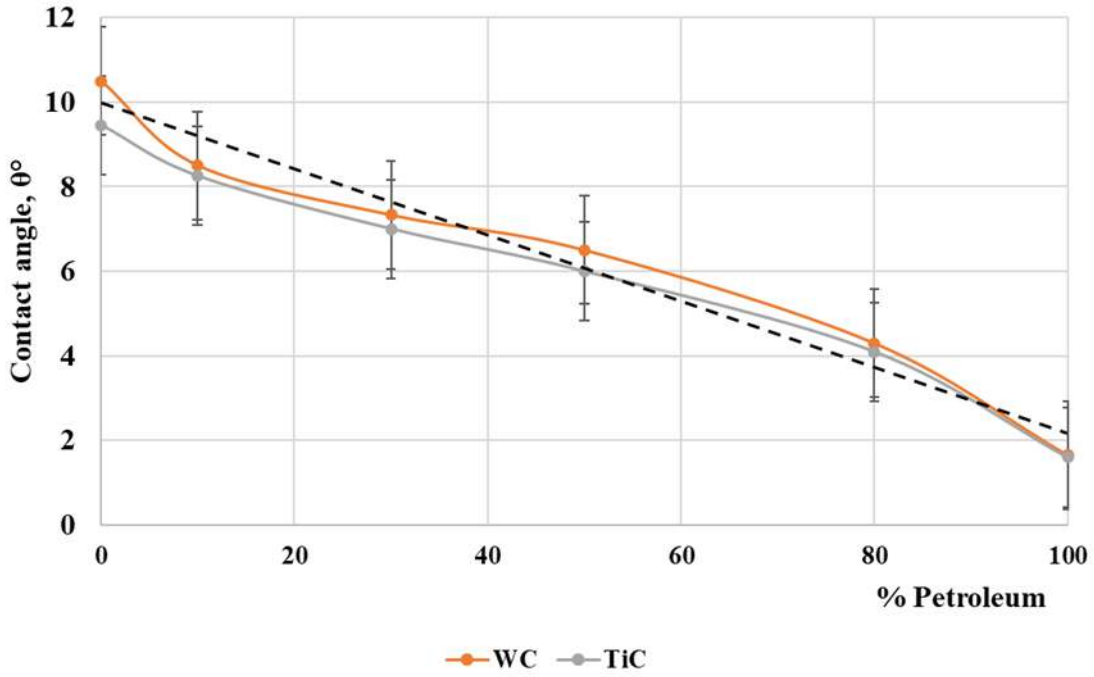


***Figure 33.*** *The wettability behaviour of a petroleum-hydraulic oil mixture on ceramic surfaces after two seconds.*

Therefore, we can note that all of petroleum, hydraulic oil, and all mixtures between petroleum and hydraulic oil have a remarkable similarity in the wettability function on the surfaces of different steel types, and they represent apolar liquids. The intermolecular interactions between the petroleum molecules and the surfaces primarily influence the wetting of petroleum on steel surfaces, where the degree of wetting, or how well the petroleum spreads over the surface, depends on the balance between adhesive forces (found between the petroleum and the metal) and cohesive forces (found within the petroleum). Different types of oils have varying chemical compositions, which influence their intermolecular forces and surface tension. Some oils have low surface tension and strong adhesive forces, enabling them to spread easily on steel surfaces and exhibit good wetting properties. When Cr content increased, a more stable Cr-oxide surface film forms. That film often has reduced polarity (less hydroxylation). It supports dispersive forces, since the surface tension of the oil types is relatively low; a suitably prepared high-energy/dispersive surface promotes wetting, allowing the oil to spread more readily. Therefore, the wettability of apolar liquids exhibits a very high rate of expansion and diffusion as the chromium content increases, due to the formation of chromium oxide on the steel surface.

## 5.2. Polar and apolar wetting behaviour on pure metal surfaces

### 5.2.1. Experimental results

This subchapter focused on the wettability behaviour of polar and apolar liquids on pure metals; the wettability test results are summarised in Table 6. Firstly, I remeasured the contact angle of distilled water, which ranged from 63° to 77°; the results show that water does not readily spread on metal surfaces free of oxide layers, confirming the findings in [138]. Averaged values are shown here; deviation is ±3°.

***Table 6.*** *The measured contact angle θ (in degrees) of the liquids on the surface of pure metals.*

| **Liquid** | **Al** | **Fe** | **Ni** | **Cu** | **Sn** | **Ag** | **W** | **Cd** |
|---|---|---|---|---|---|---|---|---|
| Hydraulic oil | 20 | 12 | 8 | 15 | 19 | 20 | 18 | 22 |
| Petroleum | 9 | 3 | 2 | 5 | 9 | 11 | 8 | 11 |
| Distilled water | 69 | 77 | 80 | 78 | 70 | 67 | 71 | 63 |
| Glycerin | 73 | 80 | 84 | 82 | 75 | 72 | 76 | 69 |

Glycerin, which differs in viscosity and density from water, has a contact angle of about (69–84°). Fig. 34 shows the silhouettes of the contact angle and its measurement on Ag surface, it has a similarity in the wettability function of the water on the same metal surfaces; the reason is that both water (72 mN/m) and glycerin (64.7 mN/m) have relatively high surface tensions, and liquids with higher surface tension tend to form rounded droplets on surfaces to minimize their surface area. Water is inherently a highly polar molecule, resulting in partial positive charges on its hydrogen atoms and a partial negative charge on its oxygen atom. This polar nature enables water molecules to form hydrogen bonds not only with one another but also with other polar molecules, such as those on various solid surfaces. Glycerin also has polar hydroxyl (-OH) groups, which can form hydrogen bonds with water molecules and with solid surfaces; these hydrogen bonding interactions contribute to the wetting behaviour of both substances.

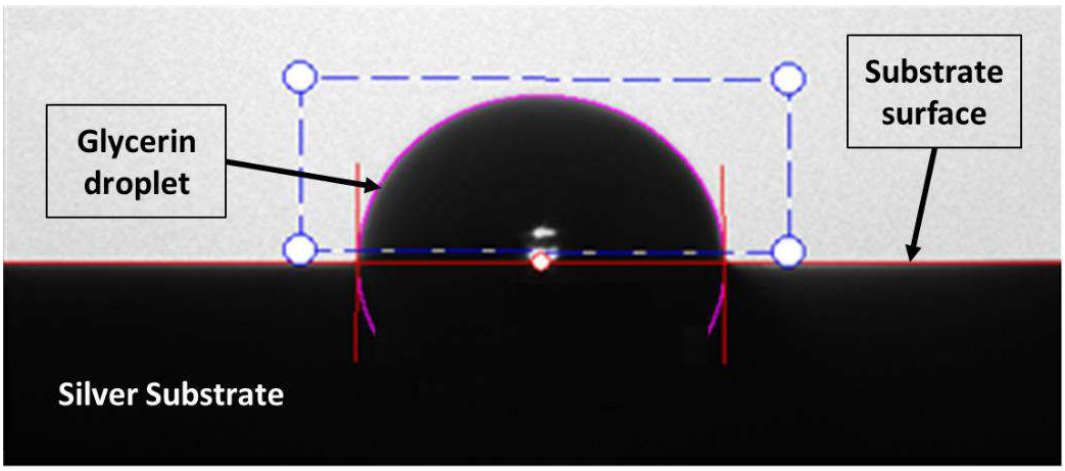


***Figure 34.*** *The silhouette of the glycerin droplets on the silver substrate surface.*

In contrast to water and glycerin wetting behaviour, in experiments with the different types of apolar liquids, the contact angle on metal surfaces (see Table 6) approached a lower value after only 3–4 seconds, demonstrating that apolar liquids has a very high speed of liquid spreading on all types of metal surfaces (Fig. 35) because of its low surface tension. The wettability of petroleum was better than that of hydraulic oil on all kinds of substrates (for example, on Sn surface, $\Theta_{petroleum}$= 9°, but $\Theta_{hydraulic}$ = 19°). These differences depend on the balance between adhesive forces (between the apolar liquid and the metal) and cohesive forces (within the apolar liquids).

On the other hand, the high carbon content of an apolar liquid primarily influences its wettability behaviour through the nature of the carbon compounds present. Apolar liquids with a higher concentration of light hydrocarbons (such as petroleum, 92 wt.%) tend to maintain wet conditions on surfaces, thanks to their lower surface tension and apolar nature. Moreover, I observed that apolar liquids behave more similarly, whereas polar liquids exhibit other behaviours. Oil properties under wetting conditions affect the ability to improve and control oil–water wetting; Buckley et al. [144] found that different crude oil species determine the wetting behaviour of the oil.

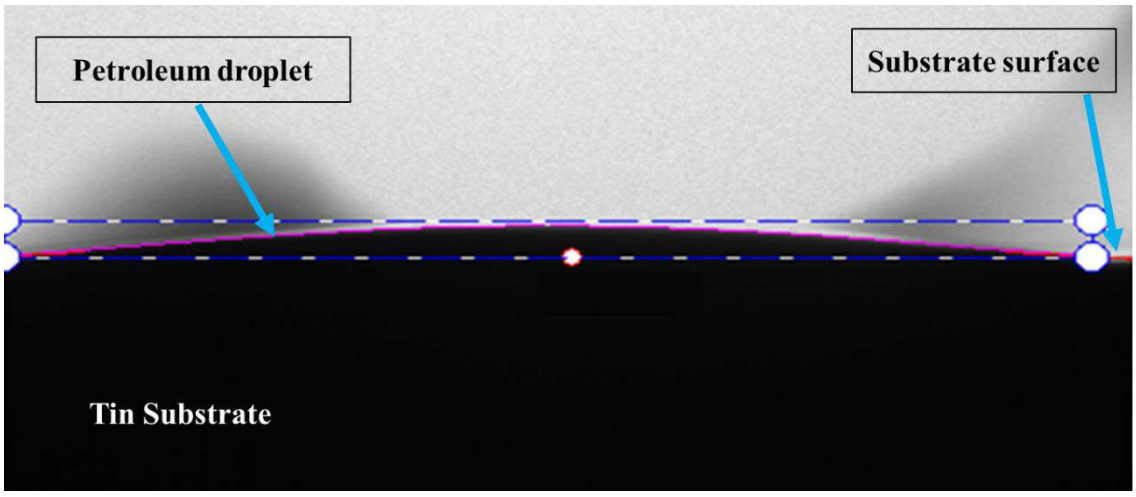


***Figure 35.*** *The silhouette of the hydraulic oil droplets on the silver substrate.*

The different types of oils have varying chemical compositions, which influence their intermolecular forces and surface tension, and, in turn, their wettability behaviour, as indicated by the test results in Fig. 36, which show that increasing petroleum content in the mixture can affect its wettability behaviour on metal surfaces. In addition to the chemical structure and surface tension of the oil, many factors, such as the presence of additives, the surface roughness and surface energy of the metals, temperature, and pressure, play a role in determining the wetting behaviour and influencing its properties.

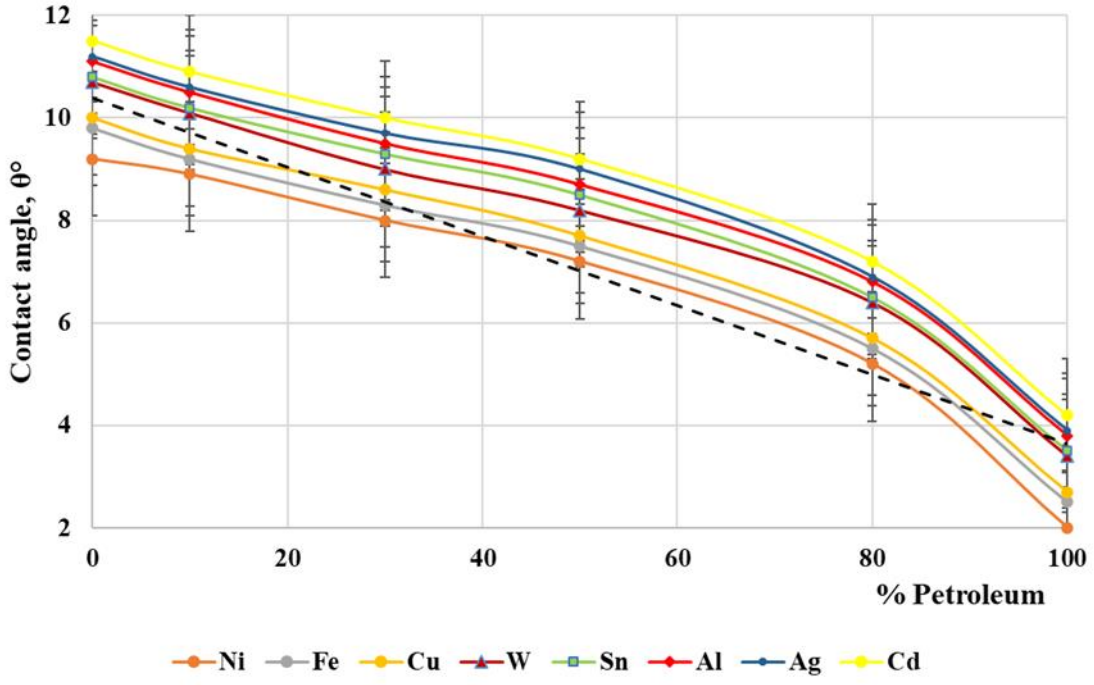


***Figure 36.*** *The wettability behaviour of a petroleum-hydraulic oil mixtures on the metal surfaces over two seconds.*

By examining the contact angles of different oil types on metal surfaces in relation to their atomic numbers, and comparing them with those of distilled water and glycerin, it becomes evident that the contact angles align with the periodicity of the atomic number of the substrates. As illustrated in Fig. 37, the atomic radius of the substrate can affect the contact angle value measured on its surface due to the interactions between the substrate, the liquid, and the surrounding environment, proving the difference in behaviour between the polar liquids (distilled water and glycerin) and apolar liquids (hydraulic oil and petroleum). While the variations observed in the results for the relationship between oil and water contact angles and the atomic number occur because the atomic number can correlate with electronic properties (e.g., electron density), which influence surface energy, this relationship may not be linear or consistent across all metals due to differences in their crystal structure and surface chemistry, this may explain the variations in results for different metals.

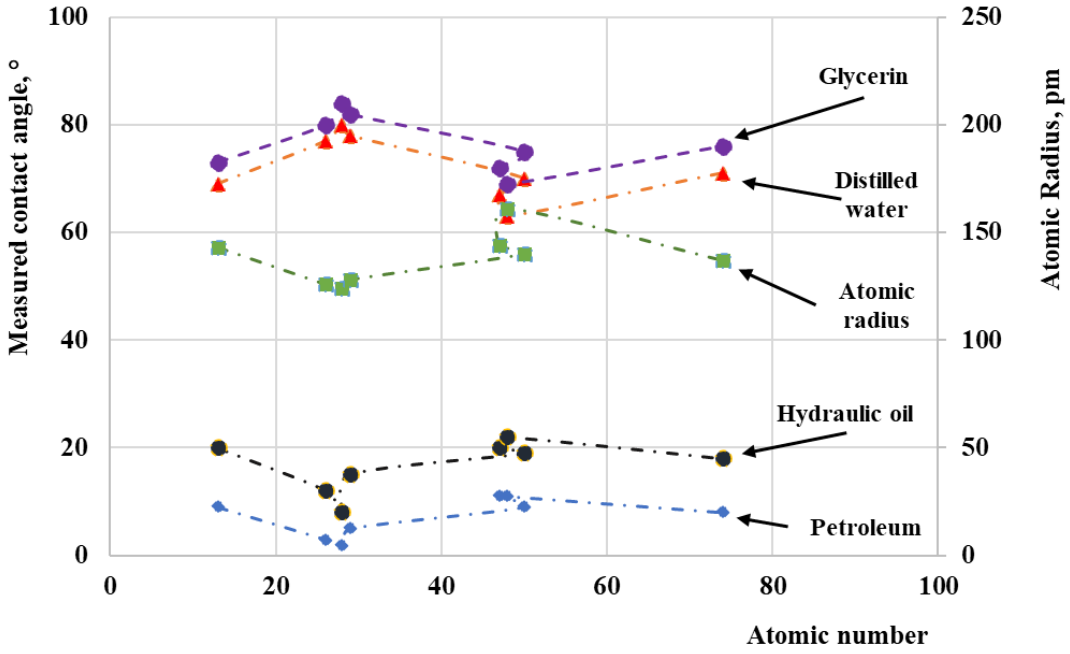


***Figure 37.*** *Measured contact angles of the liquids (polar and apolar) and atomic radius of the substrates as a function of the substrate atomic number.*

The atomic radius is a crucial parameter for understanding wetting behaviour and surface interaction influences on contact angle for the following points:

a. Atomic Interactions: The strength and type of interactions between liquid molecules and the solid surface can affect the atomic radius of the substrates. A larger atomic radius often corresponds to a larger surface area and more available

interaction sites. The concept is based on the idea that as atomic radius increases, the overall size of atoms or molecules increases, potentially providing more surface area for interactions, especially in chemical reactions, adsorption processes, or catalytic activity [145, 146]. Substrates with larger atomic radii might have more surface sites capable of forming hydrogen bonds, dipole-dipole interactions, or van der Waals forces with liquid molecules.

b. Pore size and Roughness: In porous substrates or surfaces with nanoscale roughness, the atomic radii of the atoms that make up a porous material can influence the overall pore structure; larger atomic radii may lead to a more open structure that allows easier infiltration of the liquid, resulting in a lower contact angle. However, pore size is more directly related to the material structure (like the crystal lattice, the arrangement of the atoms, or even the way the particles are packed) rather than only atomic radius. Pore size and surface roughness directly affect liquid infiltration and contact angle, while a larger atomic radius can indirectly contribute to a more open structure [147, 148].
c. Surface Energy and Wetting: The surface energy of a solid substrate plays a significant role in wetting behaviour. If the cohesive forces of the liquids are stronger than their adhesive forces to the solid, the liquid tends to bead up and form a higher contact angle. On the other hand, if the adhesive forces are stronger, the liquid spreads out, forming a lower contact angle [149].
d. Capillary Action: The ability of a liquid to flow in a narrow area against the force of gravity is called capillary action, which can also be affected by the atomic radius, this is usually a structural effect of the material rather than a direct result of atomic size, where capillary action is influenced by the dimensions of the capillaries, which in turn can be affected by the atomic structure of the materials. It is determined by how atoms or molecules are arranged within the material, rather than just by their atomic radii, which can lead to capillaries with different dimensions. A material composed of atoms with a larger atomic radius might exhibit different pore or capillary sizes, indirectly influence capillary action, and potentially alter the contact angle [149-151].
e. Chemical Interactions: The atomic radius is often linked to the chemical properties of the substrates. Substrates with larger atomic radii might have more polarizable electrons, affecting the strength of van der Waals forces or inducing stronger dipole interactions with the liquid [152].

### 5.2.2. Atomic radius effect and broken bond model

When figuring out the results of the liquids, the contact angle relation to the atomic radius (Fig. 38) shows the best correlation between the cosine of the contact angles of the liquid-metal system and the atomic radius of the metals. A robust correlation exists, as indicated by the high correlation coefficients, between the atomic radius parameter and the cosine of the calculated contact angles (petroleum=0.91, hydraulic=0.88, distilled water=0.95, and glycerin=0.91). This underscores a strong association within the data.

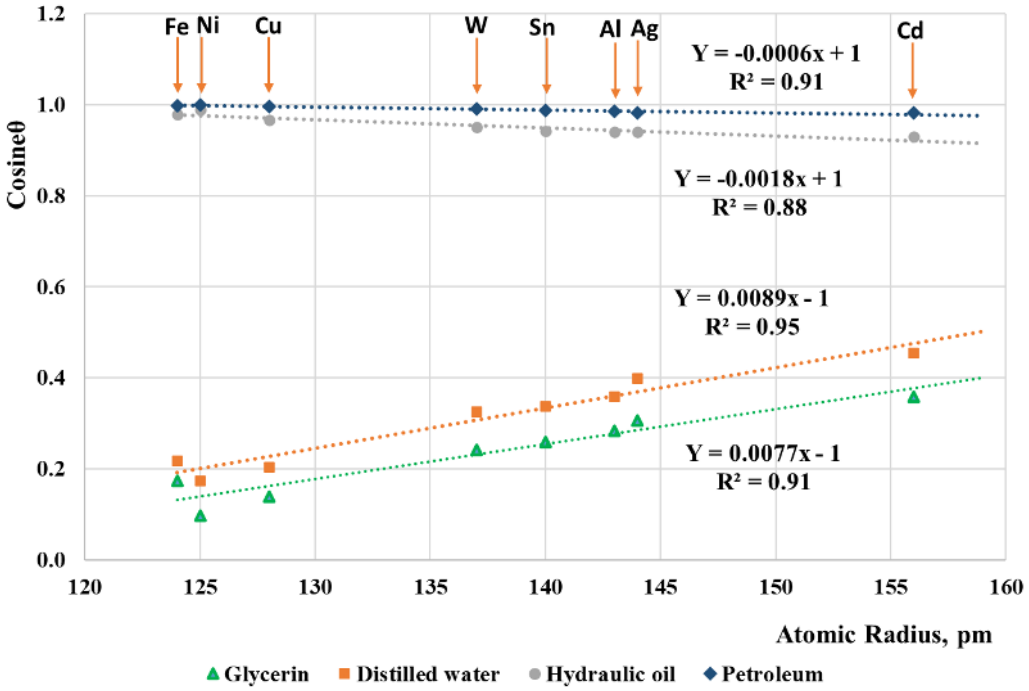


***Figure 38.*** *Cosine of the contact angle of liquids as a function of the atomic radius parameter of the substrate.*

For more accurate predictions in a specific liquid/metal system, I will turn to Becker's broken-bond model [153, 154] and establish the relationship between the contact angle and the atomic radius (half the bond length). In this model, the interfacial energy between two phases (*A* and *B*) can be calculated as follows:

$$\sigma_{AB} = n_{AB}\left(V_{AB} - \frac{V_{AA}+V_{BB}}{2}\right) \tag{7}$$

where $n_{AB}$ is the number of cross bonds per unit area, and $V_{ij}$ are the bond energies of interatomic pairs in phases *A* and *B*. Thus, for the solid–gas (*SG*), solid–liquid (*SL*), and liquid–gas (*LG*) interfaces, the interfacial energies are:

$$\sigma_{SG} = n_{SG}\left(V_{SG} - \frac{V_{SS}+V_{GG}}{2}\right) \quad (8)$$

$$\sigma_{SL} = n_{SL}\left(V_{SL} - \frac{V_{SS}+V_{LL}}{2}\right) \quad (9)$$

$$\sigma_{LG} = n_{LG}\left(V_{LG} - \frac{V_{LL}+V_{GG}}{2}\right) \quad (10)$$

If we assume that the solid–gas ($V_{SG}$), liquid–gas ($V_{LG}$) and gas–gas ($V_{GG}$) pair interaction energies are negligible compared to the others, then Equations (8) and (10) are simplified as follows:

$$\sigma_{SG} = -\frac{1}{2}n_{SG}V_{SS} \quad (11)$$

$$\sigma_{LG} = -\frac{1}{2}n_{LG}V_{LL} \quad (12)$$

These are formulas often used for surface energies in the literature [154]. Substituting Equations (9), (11), and (12) into Young's equation, we obtain:

$$cos(\Theta) = \frac{\sigma_{SG}-\sigma_{SL}}{\sigma_{LG}} = \frac{-\frac{1}{2}n_{SG}V_{SS}-n_{SL}V_{SL}+\frac{1}{2}n_{SL}V_{SS}+\frac{1}{2}n_{SL}V_{LL}}{-\frac{1}{2}n_{LL}V_{LG}} \quad (13)$$

If we use the approximation that $n_{SL} \approx n_{LG} \approx n_{SG}$, Equation (13) takes the following form:

$$cos(\Theta) = 2(\frac{V_{SL}}{V_{LL}}) - 1 \quad (14)$$

Note that this equation returns the expected limiting cases, namely, if the solid–liquid interaction is strong ($V_{SL} \approx V_{LL}$), then $\cos(\Theta) \approx 1$, making $\Theta \approx 0°$, i.e., the liquid perfectly wets the surface, but if the solid–liquid interaction is negligible compared to the liquid–liquid interaction ($V_{SL} \ll V_{LL}$), then $\cos(\Theta) \approx -1$, i.e., $\Theta \approx 180°$, i.e., the liquid does not wet the surface.

It is clear from equation (14) that the dependence of $\cos(\Theta)$ on the atomic radius ($r_a$) is determined by the dependence of $V_{SL}$ on $r_a$, since this varies as the substrate changes. The simplest approximation is to assume a linear dependence.

$$V_{SL} = \alpha r_a + \beta \quad (15)$$

where $\alpha$ and $\beta$ are semi-empirical parameters (which are placeholders for values adjusted to match real measurements, not derived solely from theory). In this case, $\cos(\Theta) \propto r_a$. Fig. 38 shows that the experimental data fits very well with a linear function on the $\cos(\Theta) - r_a$ diagram.

Note that for water and glycerin $\alpha < 0$, while for petroleum and hydraulic oil $\alpha > 0$. This is probably due to the difference in the metal–liquid bond, as distilled water and glycerin are composed of polar molecules, whereas hydraulic oil and petroleum are composed of apolar molecules. It is obvious that, for example, for covalent bonds, increasing the atomic radius would result in a larger distance and a weaker bond, while for ion–dipole or dipole–dipole interactions, increasing the atomic radii would cause higher polarizability, and thus greater intermolecular attraction. Substrates with larger atomic radii may have more polarizable electrons, thereby affecting the strength of interactions with the liquid. Since ion–dipole and dipole–dipole interactions are weak bonds, this may explain why the dependence on the radius of the substrate atoms (see Fig. 38) two orders of magnitude is weaker for distilled water and glycerin than for petroleum and hydraulic oil (see the slopes of the fitted lines in Fig. 38).

To verify the prediction of the result of the equation that I obtained, I used Bismuth metal as an example, wetted by the polar and apolar liquids, where the experimentally identified contact angles are $\Theta_W = 79° \pm 3°$, $\Theta_G = 83° \pm 3°$, $\Theta_H = 14° \pm 3°$, and $\Theta_P = 9° \pm 3°$ for water, glycerin, hydraulic oil, and petroleum, respectively. Using the equations from Fig. 38, the calculated contact angles are $\Theta_W = 73° \pm 3°$, $\Theta_G = 82° \pm 3°$, $\Theta_H = 17° \pm 3°$, and $\Theta_P = 10° \pm 3°$.

### 5.2.3. Free electron density effect

A Free electron density is the number of conduction (delocalized) electrons per unit volume in a metal. These electrons originate primarily from the outer (valence) electrons of metal atoms that are not tightly bound to any single nucleus; for that reason, they are called “free” because they are not bound to individual atoms but instead move throughout the crystal lattice, forming what is often called an electron gas or electron sea. At a metal surface, the electron gas does not abruptly stop at the last atomic plane. Instead, electron density spills out slightly into the vacuum or into the adjacent phase, creating a surface dipole layer [155].

Free-electron density influences wettability through electronic screening and polarisation mechanisms, allowing strong image charge formation as the liquid approaches, thereby affecting the solid–liquid interfacial energy ($\gamma_{sl}$) [150, 155]. This metallic surface energy ($\gamma_s$) arises from broken metallic bonds at the surface, the redistribution of free electrons near the surface, and electrostatic and quantum-mechanical effects. This concept arises from the Drude–Sommerfeld model of metals [156, 157], which successfully explains electrical and thermal conductivity by treating electrons as delocalized charge carriers [158]. The surface electron density is therefore a critical parameter in determining how a metal interacts with its environment, which can influence its surface properties, including interactions with liquids that affect wetting behaviour, as well as differences among metals [159].

The relationship between adhesion energy and free electron density in the context of liquid wettability is often discussed within the framework of the Young-Dupré equation and the concept of interfacial tension. The Young-Dupré equation is crucial in interfacial science for more accurate predictions in a specific liquid/metal system. It is related to the contact angle and the thermodynamics of wetting, and it describes the equilibrium contact angle (θ) of a liquid droplet on a solid surface in terms of the interfacial tensions involved. The Young-Dupré equation is given by equation (3):

$$W_a = \sigma_{lg}(1 + \cos\theta) \tag{3}$$

where: $W_a$: is the adhesion energy (J/m$^2$), $\sigma_{lg}$: is the surface tension of the liquid/air phase (J/m$^2$), and θ is the contact angle (°) between the liquid and solid surface.

The adhesion energy was calculated using the Young-Dupré equation (equation 3), according to the wetting results (subchapter 5.2.1 - Table 6) and illustrated as a function of the free electron density parameter ($r_S^{-4}$) based on the $W \sim f(r_S^{-4})$, where ($r_s$) is the free-electron density for metals, the values are sourced from Perrot and Rasolt [159]. The results show that an increase in free-electron density increases adhesion energy and enhances wettability for apolar liquids, as indicated by the correlations (y = 10.228x + 49.429 and y = 36.544x + 57.369) for petroleum and hydraulic oil, respectively (Figs. 39 and 40). While the increase in free-electron density will decrease adhesion energy, then wettability for polar liquids will be decreased according to the correlation (y = 281.58x + 88.259, and y = 384.97x + 109.21) for glycerin and water, respectively (Figs. 41 and 42).

A strong correlation exists between the free-electron density parameter ($r_S^{-4}$) and the calculated adhesion energy ($W_a$), as indicated by the high correlation coefficient $R^2$ (0.88, 0.92, 0.91, and 0.91) for (water, glycerin, hydraulic oil, and petroleum ), respectively, as shown in Figs. 39, 40, 41, and 42. This underscores a strong association within the data.

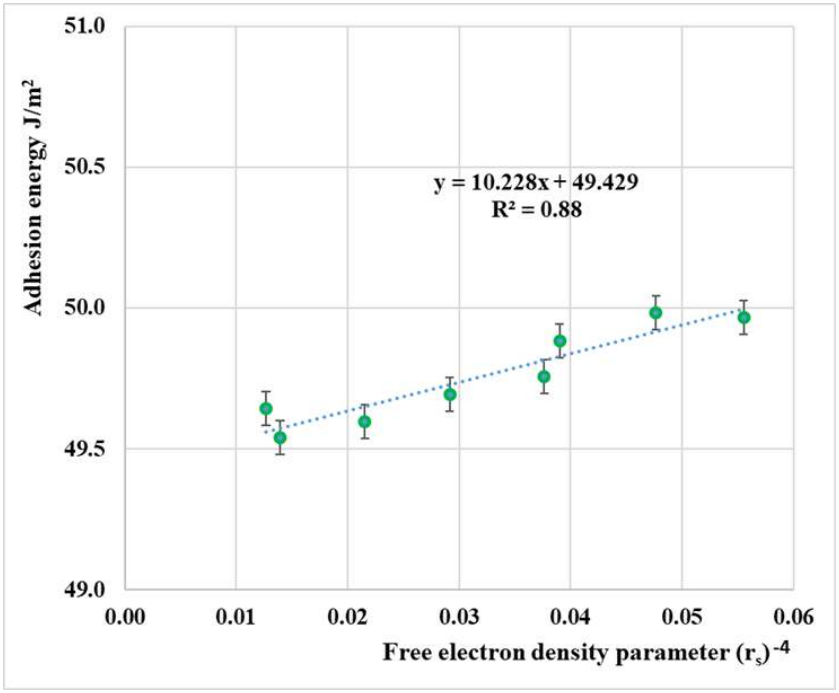


***Figure 39.*** *Adhesion energy (W) for petroleum as a function of the free electron density parameter following the $W \sim f(r_S^{-4})$ correlation.*

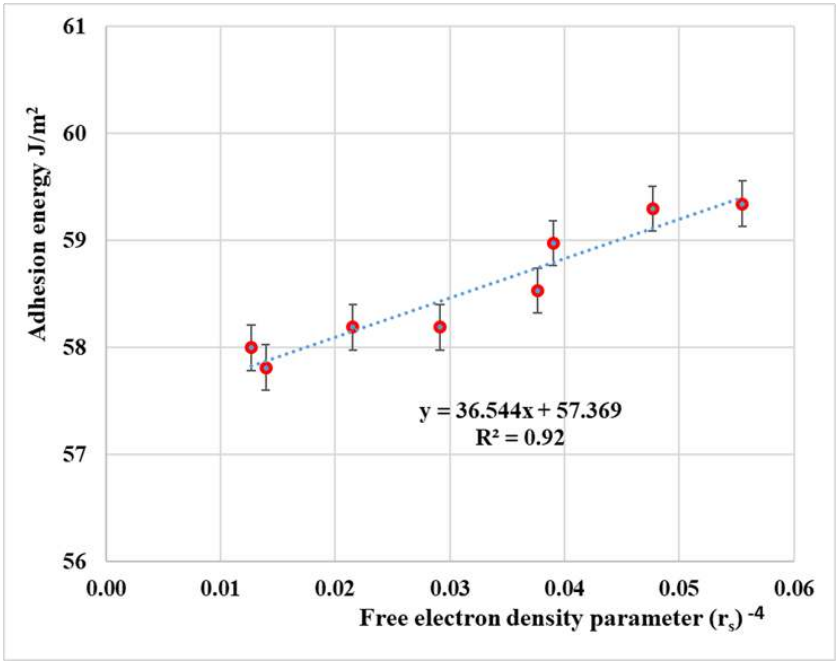


***Figure 40.*** *Adhesion energy (W) for hydraulic oil as a function of the free electron density parameter following the $W \sim f(r_S^{-4})$ correlation.*

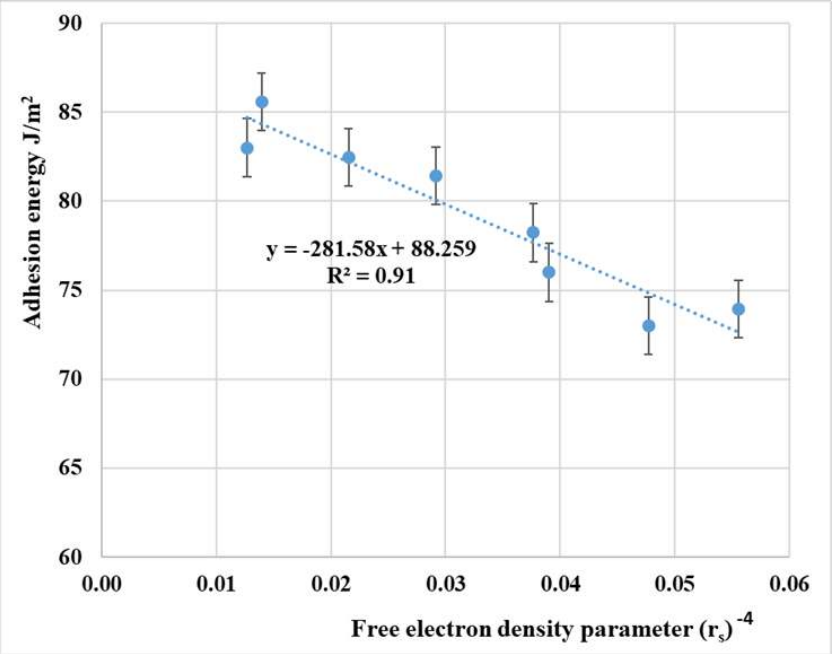


***Figure 41.*** *Adhesion energy (W) for glycerin as a function of the free electron density parameter following the W~f($r_S^{-4}$) correlation.*

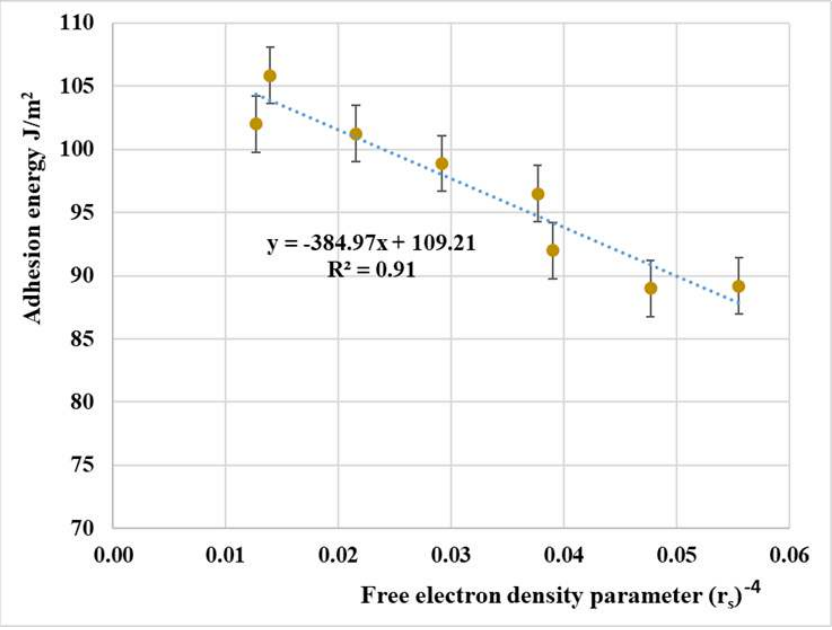


***Figure 42.*** *Adhesion energy (W) for distilled water as a function of the free electron density parameter following the W~f($r_S^{-4}$) correlation.*

## 5.3. Separation potential by stainless steel meshes

### 5.3.1. The Ni coating investigation

The results of the Ni coating investigation show uniform coatings (Fig. 43 and Table 7) with an average thickness of 90 ± 10 nm. A uniform Ni coating ensures that the entire surface of the stainless steel mesh exhibits uniform hydrophobic and oleophilic properties. This consistency is critical because any uncoated or unevenly coated areas could allow water to penetrate through the mesh, thereby reducing the overall separation efficiency. The uniform coating ensures that the entire mesh surface actively contributes to the separation process, optimising performance and ensuring that the mesh holes are evenly modified, thereby maintaining uniform hole size and shape, enabling better control over the passage of petroleum while blocking water. So, the nickel layer protects the underlying stainless steel from humidity and corrosive agents present in the petroleum-water emulsion, maintaining the performance of the meshes over time and preventing degradation under mechanical stress or during repeated separation cycles.

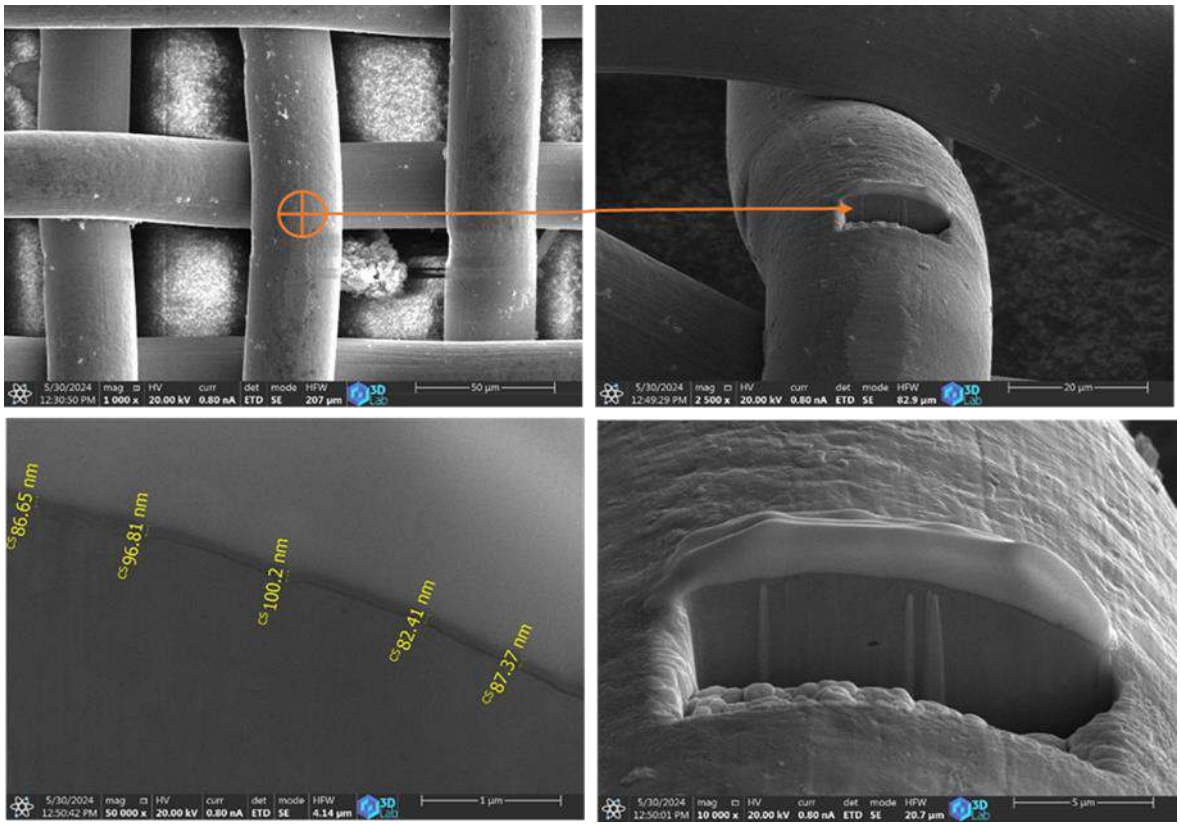


***Figure 43.*** *SEM image of the Nickel coating on stainless steel mesh wire (400 mesh size) using PFIB-SEM.*

***Table 7.*** *The Chemical composition of the stainless steel mesh samples after Ni coating.*

| No | Mesh size | %Fe | %Cr | %Ni | % Others |
|---|---|---|---|---|---|
| a | 500 | 63.39 | 17.33 | 17.58 | 1.70 |
| b | 400 | 62.79 | 16.81 | 18.92 | 1.48 |
| c | 300 | 62.92 | 17.12 | 18.33 | 1.62 |
| d | 200 | 69.13 | 17.35 | 13.52 | - |
| e | 180 | 67.98 | 17.02 | 15.00 | - |

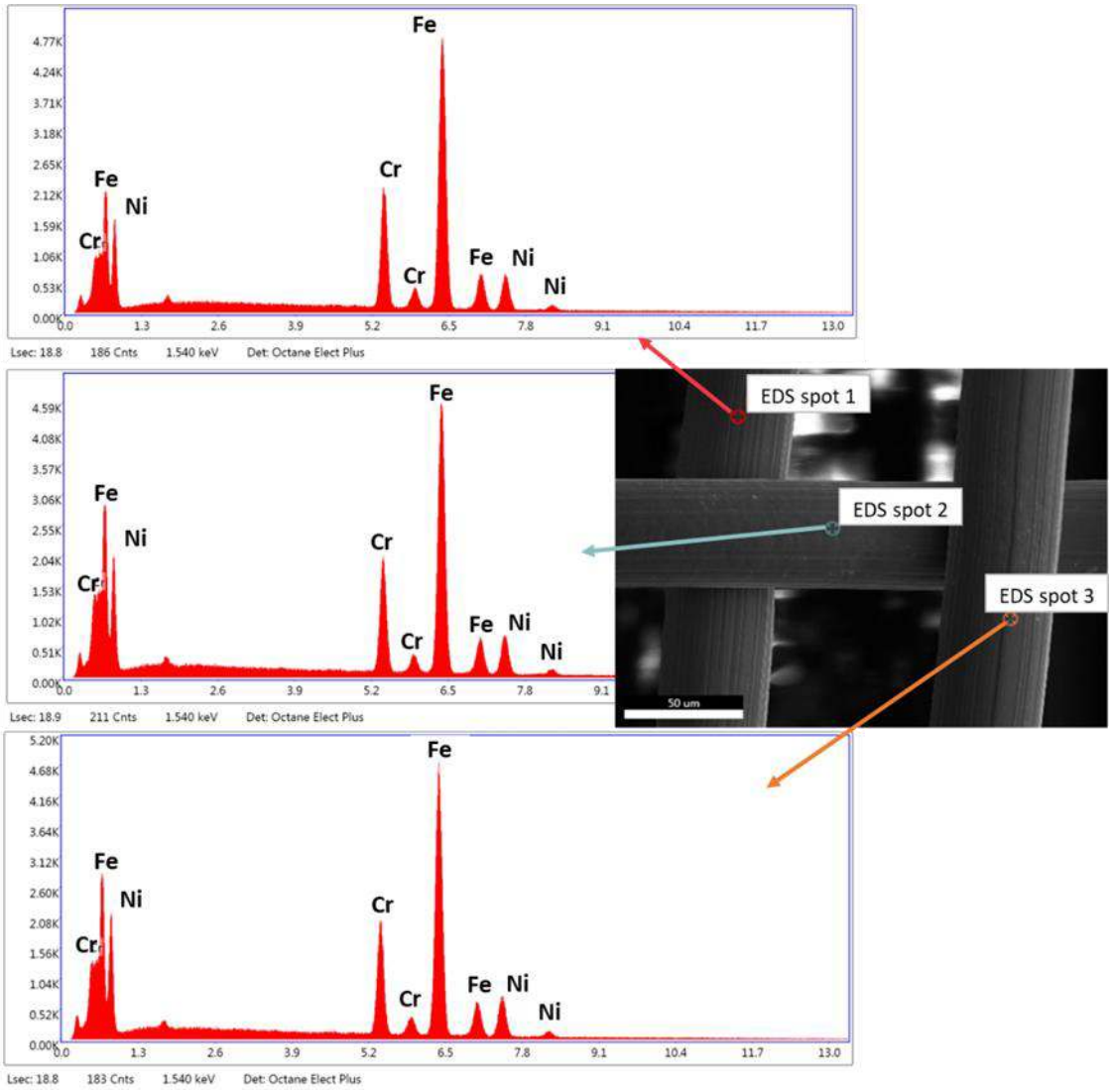


***Figure 44.*** *SEM image of the stainless steel mesh (400 mesh size) after Ni coating using an EDS specter from different places.*

### 5.3.2. The measurement of the contact angle (CA) before and after Ni coating

#### 5.3.2.1. The measurement of the contact angle (CA) before Ni coating

Based on the results in Table 8, obtained from the experiments, the differences in wettability behaviour across all stainless steel mesh types are insignificant. Still, the effect of varying mesh size on liquid wettability is evident. In some cases, the meshes were quickly wetted by petroleum, within a second. At the same time, a distilled water droplet remained on the surface for a longer time without spreading or passing through the mesh, with a contact angle greater than 106 degrees. Water droplets, being less viscous, can also coalesce or stick together when they come into contact with the mesh, forming larger droplets that experience higher surface tension due to stronger cohesive forces between their molecules. At the same time, petroleum tends to spread out, cling to the mesh surface, and skip through it due to its reduced surface tension [40], influencing its drift behaviour and its interplay with the steel mesh. In addition, the metallic meshes used have a different hole size, engineered to be smaller than the dimensions of water droplets but larger than those of petroleum molecules.

***Table 8.*** *The measured contact angle of the liquids on the stainless steel mesh surface before Ni coating.*

| | **liquid** | **Stainless steel mesh size** | | | | |
|---|---|---|---|---|---|---|
| | | **500** | **400** | **300** | **200** | **180** |
| Contact Angle θ° | Petroleum | 8 | 8 | 9 | 9 | 10 |
| | Distilled water | 129 | 121 | 115 | 110 | 106 |

When the petroleum droplet comes into contact with the Stainless steel mesh, it spreads directly on the surface and passes through the mesh at about 80% vol. in just seconds, while water droplets are captured and retained on the mesh surface, as seen in Fig. 45. Smaller hole sizes make surfaces smoother and less rough, which could decrease the contact angle of petroleum. However, when they are too large, they can cause water droplets to collapse, and the air in the large holes may no longer be confined. This layout provides a good opportunity to separate petroleum from water when the emulsion is placed on the mesh surface.

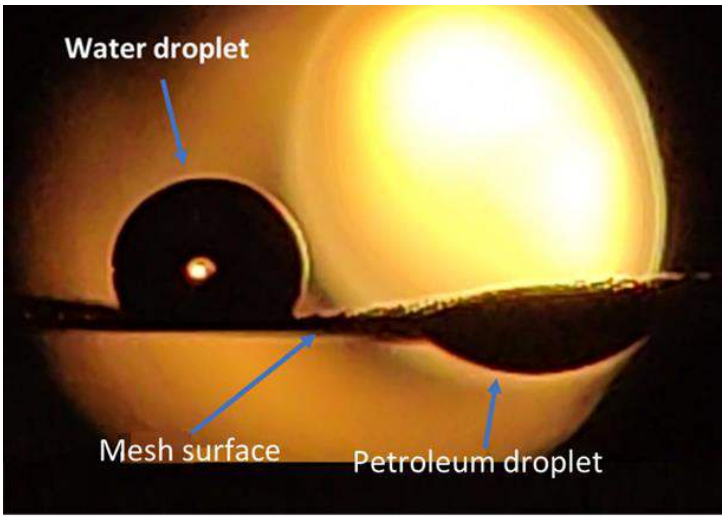


***Figure 45.*** *The silhouettes (after 1 minute) of water and petroleum droplet wetting behaviour on the stainless steel mesh (400-mesh) surface after Ni coating.*

#### 5.3.2.2. The measurement of the contact angle (CA) after Ni coating

Based on the results in Table 9, obtained from experiments, the surface wetting by distilled water decreases slightly as the Ni amount increases to twice the original amount after coating. In contrast, the petroleum continues to wet the surface with high-speed spreading. The change was not significant, but it could enhance petroleum-water separation. A decrease in petroleum flow was also observed as the stainless steel mesh count increased to 500, which will be another challenge for the separation process efficiency.

***Table 9.*** *The measured contact angle of the liquids on the stainless steel mesh surface after Ni coating.*

| | **liquid** | **Stainless steel mesh size** | | | | |
|---|---|---|---|---|---|---|
| | | **500** | **400** | **300** | **200** | **180** |
| Contact Angle θ° | Petroleum | 6 | 6 | 7 | 7 | 8 |
| | Distilled water | 131 | 123 | 118 | 112 | 110 |

### 5.3.3. Description of calibration measurements

To assess the separation efficiency, a calibration line was prepared using the known mixtures prepared in (subchapter 4.2.2.3, point a) and the investigation process in subchapter 4.2.4. The results show a linear relationship (Fig. 46) between the carbon content of the petroleum and its percentage in the mixture. The highest petroleum purity can be achieved when the carbon content is 81% wt.

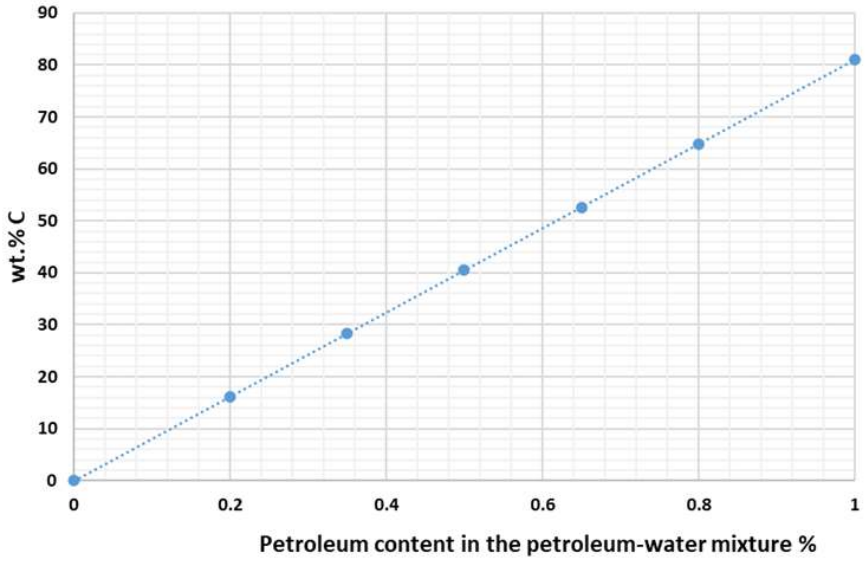


***Figure 46.*** *Calibration curve of the carbon content in the petroleum-water mixture.*

### 5.3.4. The petroleum-water separation efficiency

Based on the carbon content results (Table 10) obtained from experiments after emulsion separation using Ni-coated and uncoated stainless steel meshes, and according to the calibration line in Fig. 46, the separation ratio values for carbon content before and after Ni coating are shown in Figs. 47 and 48.

***Table 10.*** *The carbon content of the petroleum is measured after separation.*

| Stainless steel mesh size | wt.% C m/m | |
|---|---|---|
| | Before Ni-coating | After Ni-coating |
| 180 | 45 | 47 |
| 200 | 58 | 64 |
| 300 | 68 | 74 |
| 400 | 70 | 79 |
| 500 | 50 | 53 |

Separation results show the superiority of mesh size (400 meshes), which demonstrated the highest hydrophobicity and oleophilicity; the finer hole size and uniform Ni coating contributed to the superior separation of petroleum from water, achieving 97% separation, effectively blocking water while allowing petroleum to pass. The water droplets, being less viscous, can also coalesce or merge when they come into contact with the mesh

surface, forming larger droplets that experience higher surface tension due to stronger cohesive forces between their molecules. At the same time, petroleum tends to spread out, cling to the mesh surface, and skip across it due to its reduced surface tension, which influences its drift behaviour and interaction with the steel mesh. While the separation ratio for the stainless steel mesh (300 mesh) improved to 92%, it is a good ratio compared to the stainless steel mesh (200 mesh), which showed a slight increase in separation from 72% before coating to 80% after coating.

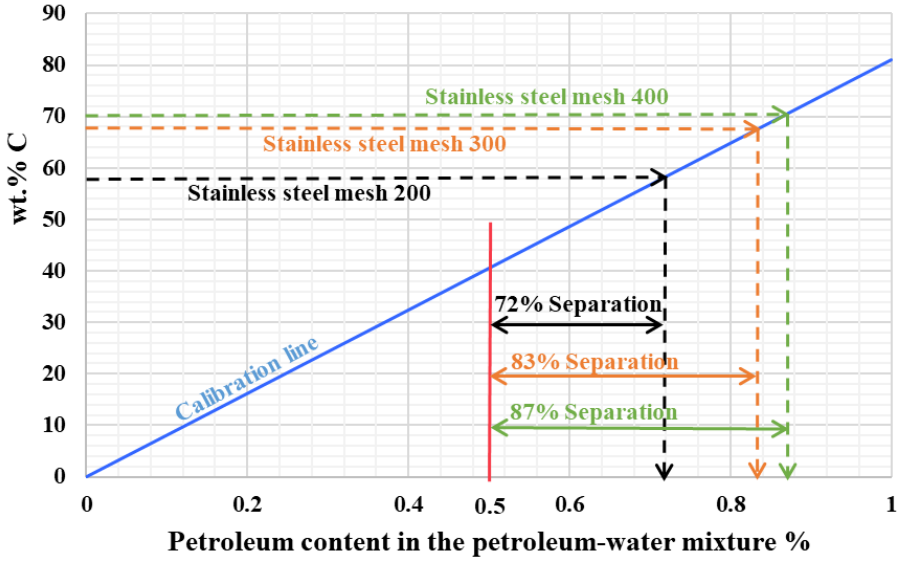


***Figure 47.*** *Identification of the C content for the separated liquid by the stainless steel meshes before coating with Ni, where the C content for the initial emulsion (50% vol. petroleum + 50% vol. water), see vertical red line in the figure.*

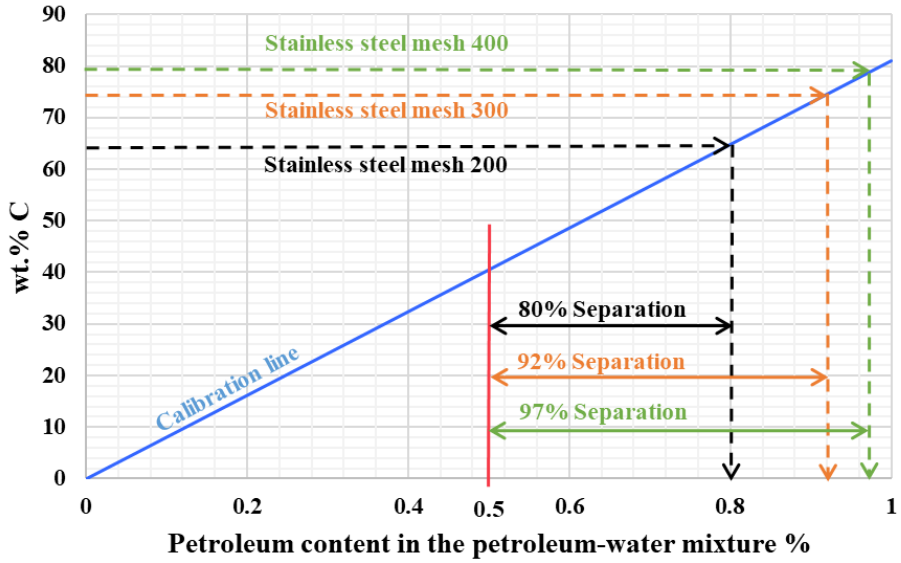


***Figure 48.*** *Identification of the C content for the separated liquid by the stainless steel meshes after coating with Ni, where the C content for the initial emulsion (50% vol. petroleum + 50% vol. water), see vertical red line in the figure.*

On the other hand, when comparing the efficiency of the separation for all the coated and uncoated stainless steel mesh samples Fig. 49 will find the samples with sizes (180 and 500 meshes) were bad in the separation process, because the size (180 meshes) allowed the emulsion to pass through the mesh holes with bad separation less than 58%, and the size (500 mesh) needed a long time to start the separation process and separation less than 66%.

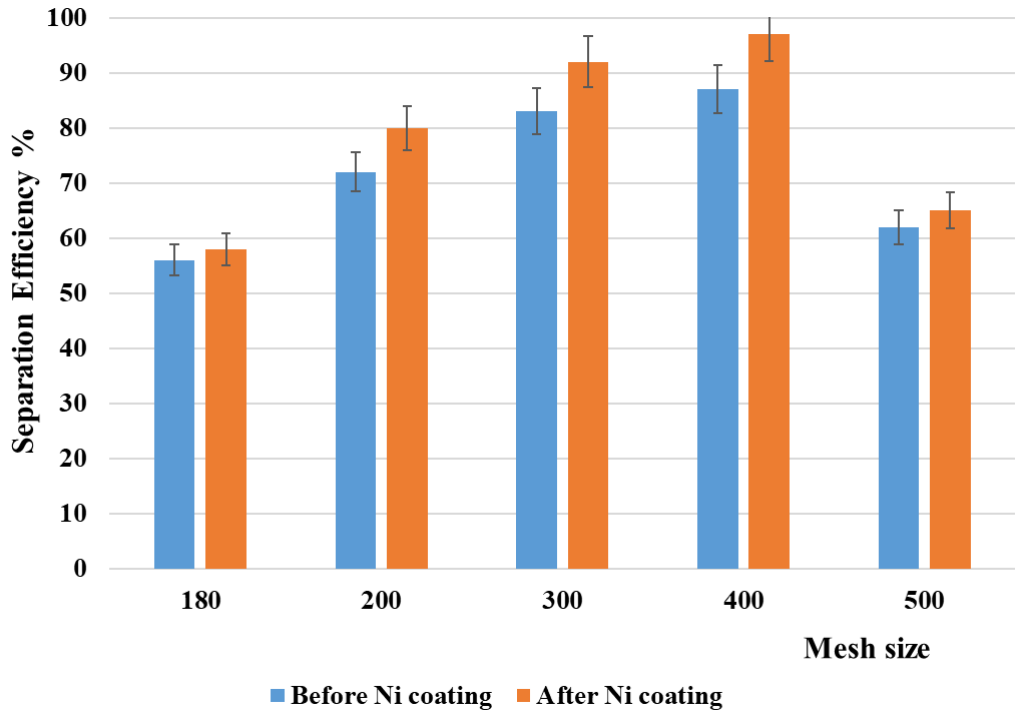


***Figure 49.*** *Influence of stainless steel mesh size on the efficiency of emulsion separation before and after coating with Ni.*

## 5.4. Effect of employing a double-layer configuration of Ni-coated stainless steel mesh on the petroleum-water separation

After collecting the remaining separated petroleum in the lower chamber of the new separation system and using equation 5 mentioned in subchapter 4.3.2 for efficiency paration calculation, the results that are obtained, Fig. 50 shows high separation efficiency for this system after 20 uses, reaching about 99.4±0.4%, where the first layer starts to separate 95±2% of water which is the same result that mentioned in subchapter 5.3.4. While water remaining after passing through the first layer as droplets will start to approach (collide with or touch the grid surface or each other) and coalesce to form larger droplets, the resulting larger droplets are heavier and therefore have a lower surface velocity, making them more susceptible to gravity or sedimentation. Since the percentage of droplets reaching the second

mesh is very small, this reduces noise and load on it, making selective separation easier. This separation system works in two stages together as a prefilter (coalescer) and an exclusion filter (separator). It offers greater flexibility and efficiency, especially when dealing with complex mixtures (e.g., micro-emulsions).

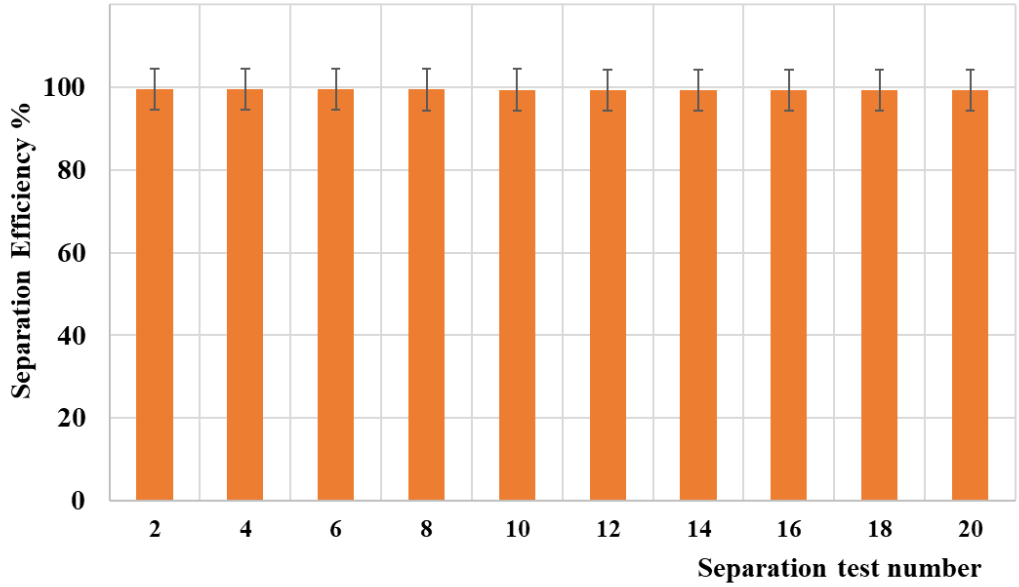


***Figure 50.*** *The separation efficiency of the new separation system after 20 uses.*

### 5.5. The Effect of changing the hole geometry of stainless steel mesh on the liquid wettability mathematically

In previous studies, the primary rationale for selecting stainless steel with a square-hole geometry for the separation process was not discussed. Here, I will mathematically show the difference in the wettability of the liquid as the hole geometry changes from square to triangular. According to Young–Laplace (capillary) relation for a meniscus, it gives the capillary pressure in terms of curvature [149]:

$$\Delta p = \gamma \left(\frac{1}{R_1} + \frac{1}{R_2}\right) \tag{16}$$

where $\Delta p$ is capillary pressure = $P_{\text{inside}}$- $P_{\text{outside}}$ in (P), $\gamma$ = surface/interfacial tension (N/m), and $R_1, R_2$ are the principal radii of curvature of the interface (m).

For a spherical meniscus: $R_1 = R_2 = R$, substitute into the equation (16), giving:

$$\Delta p = \frac{2\gamma}{R} \tag{17}$$

In a sufficiently narrow hole of circular cross-section (radius *r*), the interface with liquid forms a meniscus that is a portion of the surface of a sphere (liquid droplet) with radius *R* (Fig. 51). The radius of the sphere will be a function only of the contact angle, θ, which in turn depends on the exact properties of the fluids and the mesh material with which the fluids in question are contacting/interfacing. In capillary contexts, *R* is related to pore geometry and contact angle (θ) of the wetting phase on the surface of the porous medium via the following equation derived from Fig. 51 [160]:

$$R = \frac{r}{\cos\theta}, \tag{18}$$

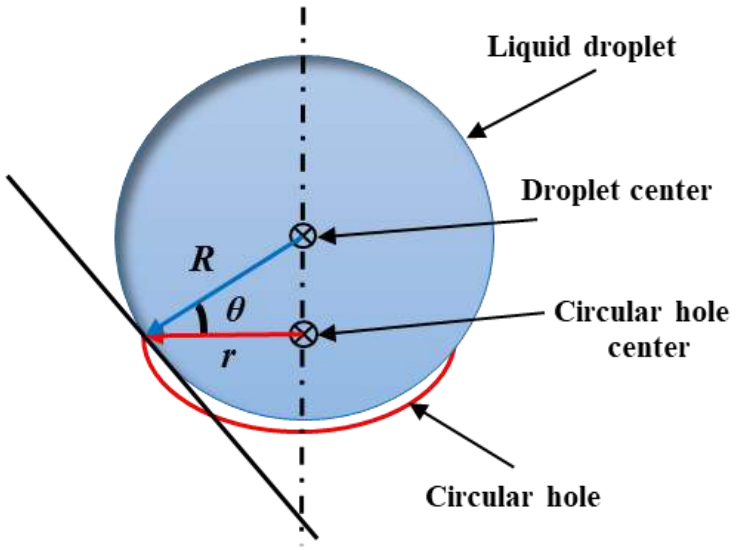


***Figure 51.*** *Schematic of the relationship between the radius of the droplet (spherical) and the radius of the hole (circular) at the point of contact.*

The pressure jump across this surface is related to the radius and the surface tension γ, so that the pressure difference may be written by substituting equation (18) into equation (17), leading to the practical form:

$$\Delta p = \frac{2\gamma\cos\theta}{r}$$

$$\Rightarrow \quad \cos\theta = r\,\frac{\Delta p}{2\gamma} \tag{19}$$

For noncircular pores, an accepted approximation is to replace the circular radius by an equivalent radius that reproduces the same area (A) to perimeter (P) relation as a circle, which reduces to the proper radius for a circular cross-section. This is widely used in porometry/pore-scale models (sometimes expressed as a "shape factor" correction for noncircular pores). One convenient form is [161], [162]:

$$r = \frac{2A}{P} \tag{20}$$

When a noncircular pore is square with side $a$: area ($A$)=$a^2$, perimeter ($P$)= $4a$, then the equivalent radius in equation 20 is:

$$r = \frac{2A}{P} = \frac{2\,a^2}{4a} = \frac{a}{2} \tag{21}$$

Substitute the equivalent radius in equation (21) into the capillary formula equation (19) to get:

$$\cos\theta = r\frac{\Delta p}{2\gamma} = \frac{a}{2} * \frac{\Delta p}{2\gamma} = \frac{a\,\Delta p}{4\gamma} \tag{22}$$

This is the same algebraic form used in capillary flow porometry, where the square opening is treated as having an equivalent circular diameter. Then, for a square hole, the liquid wettability can be found from equation (22):

$$\cos\theta_{Square} = \frac{\Delta p\, a}{4\gamma} \tag{22}$$

If I suppose a square pore is two isosceles triangles with length ($a$) of the triangle is the same as the side length of the square, and the diameter of the square represents the base ($b$) of the triangle and height is ($h$) (Fig. 52), then for isosceles triangle area ($A$)=$bh$/2, and perimeter ($P$)=2$a$+$b$, under geometrical facts the base ($b$)= $a\sqrt{2}$ , and the height ($h$) is half the diameter of the square, which represents the half base ($h = \frac{a}{2}\sqrt{2}$ ), then for an isosceles triangle, the equivalent radius in equation 20 is:

$$r = \frac{2A}{P} = \frac{2\frac{bh}{2}}{2a+b} = \frac{2\frac{a\sqrt{2}\frac{a}{2}\sqrt{2}}{2}}{2a+a\sqrt{2}} = \frac{a}{2+\sqrt{2}} \tag{23}$$

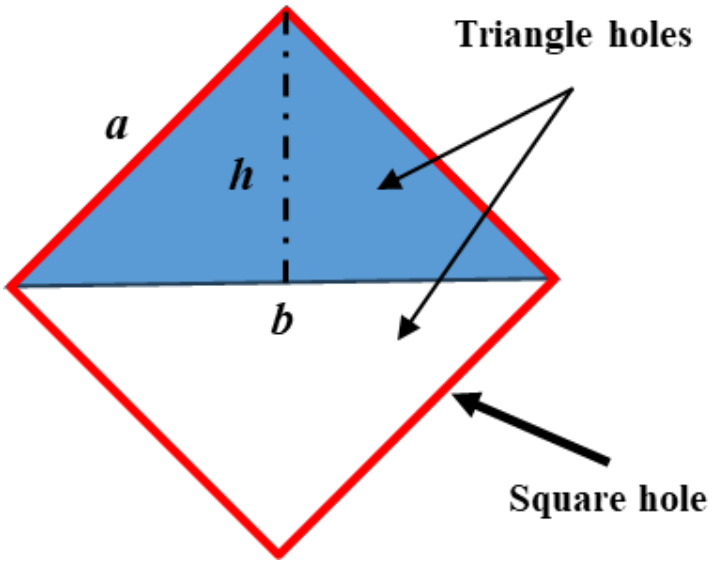


***Figure 52.*** *Schematic diagram to represent the triangle mesh hole shape dimensions relative to a square.*

Substitute equation 23 in equation 19, and the square equals two triangles, then the new liquid wettability equation by an isosceles triangle hole is:

$$\cos\theta = 2 * r \frac{\Delta p}{2\gamma} = \frac{2\,a}{2+\sqrt{2}} \frac{\Delta p}{2\gamma} = \frac{4}{2+\sqrt{2}} \frac{\Delta p\, a}{4\gamma}$$

$$\Rightarrow \quad \cos\theta_{Triangle} = 1.172 \frac{\Delta p\, a}{4\gamma} \tag{24}$$

If I suppose that both the triangle and the square mesh hole work under the exact conditions of liquid capillary pressure and surface/interfacial tension, then I can substitute the value $(\frac{a\Delta p}{4\gamma})$ in equation (24) with the corresponding value in equation (22), to get the liquid wettability relationship between the triangular and square holes:

$$\cos\theta_{Triangle} = 1.172\ \cos\theta_{Square}$$

So, the liquid wetting on the mesh surface with a triangular hole is 1.172 times that on the mesh surface with a square hole. Hereby, improving the separation efficiency could be achieved by changing the hole geometry.

## 6. New scientific results

All claim stages are based on a series of sequential, consistent, and complementary experiments, from selecting the most suitable stainless steel for the best oil-wetting behaviour relative to water, to identifying the best correlation between atomic number and wetting, studying the effect of free-electron density on adhesion energy and wettability. Then identify the optimal pore size for the separation and coat it with Ni to enhance it. Additionally, the separation efficiency with a double-layer mesh coated with Ni was increased. Finally, mathematically, I described the Effect of changing the hole geometry of stainless steel mesh on the liquid wettability. All preparations and experiments were performed under room conditions, at room temperature and normal air, with a relative humidity of ~56%. The purpose of the separation is to reduce corrosion on the inner surface of the oil pipeline by minimising the amount of water carried with oil after extraction.

**Claim 1: I identified the effect of chromium content in stainless steel on the wettability behaviour of polar and apolar liquids.**

Four types of steel samples were used as substrates, with a size of (10mm×6mm×3mm), including (CrMo4, CK60, 1.4050 steel, and 1.4301 steel) with Cr-content percentage (0.9-1.2, 0.4, 8.55, 17.5-19.5 %Cr) respectively. The following findings:

**1a.** I established that the polar liquid (water and glycerin) decreased in wettability with the increase of the chromium percentage, and the contact angle was greater than (Θ=75 ± 5°) on all steel type surfaces (Figs. A1 and A2).

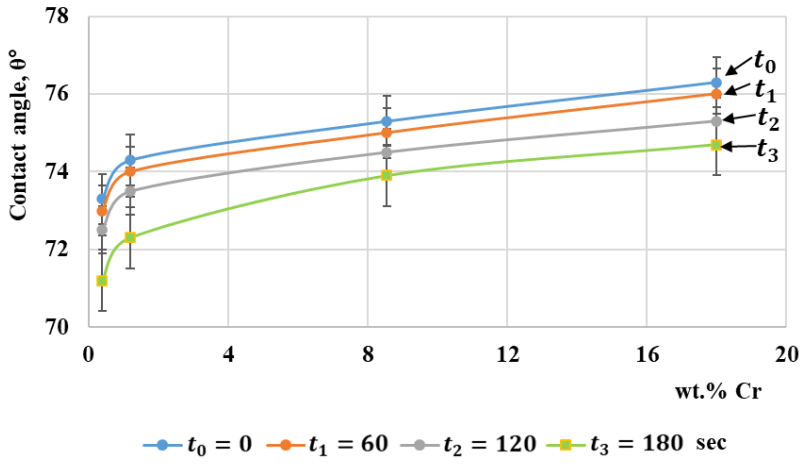


**Figure A1.** *The wettability behaviour of distilled water by different times (in seconds) as a function of Cr-containing steels.*

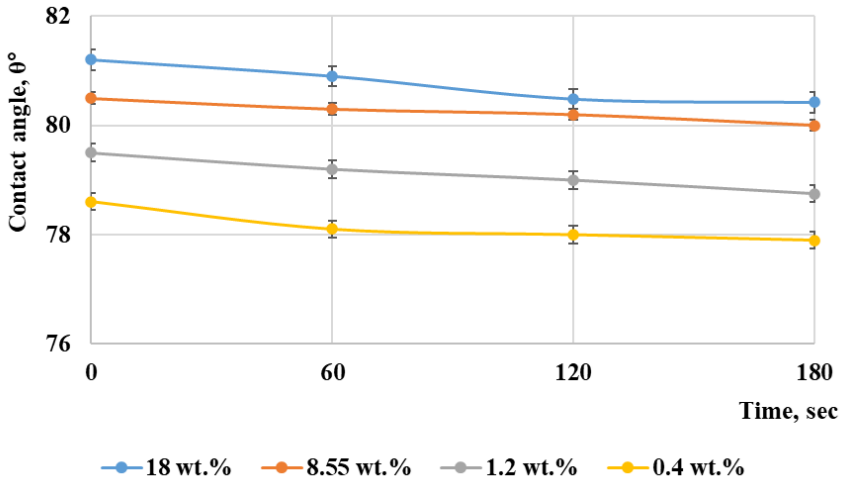


**Figure A2.** *The wettability of different Cr-containing steels by glycerin as a function of holding time.*

**1b.** I established that the apolar liquid (petroleum and hydraulic oil) increases in wetting behaviour with the increase of the chromium percentage on all steel surfaces, where the contact angle is too slight, less than (Θ= 9 ± 3°), it approached its lowest value only in the case of 1.4301 steel (Figs. B1, B2 and B3).

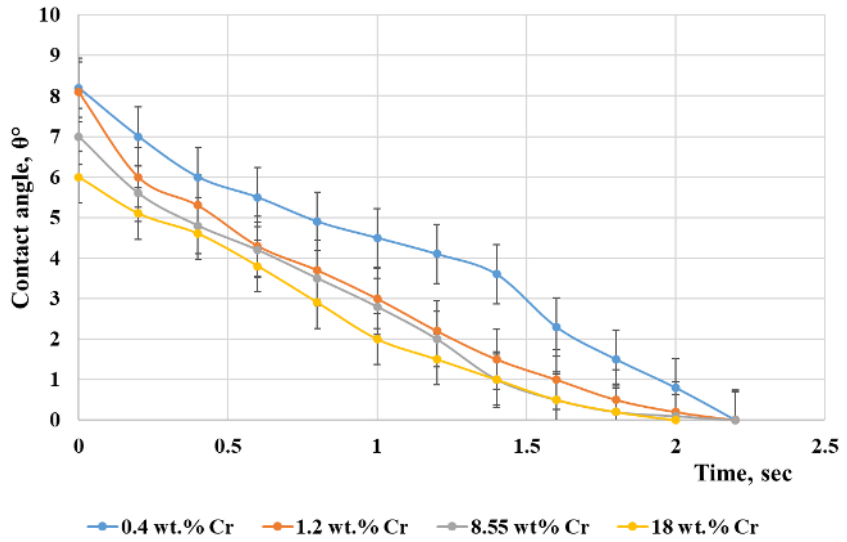


**Figure B1.** The wettability of different Cr-containing steels by petroleum as a function of holding time.

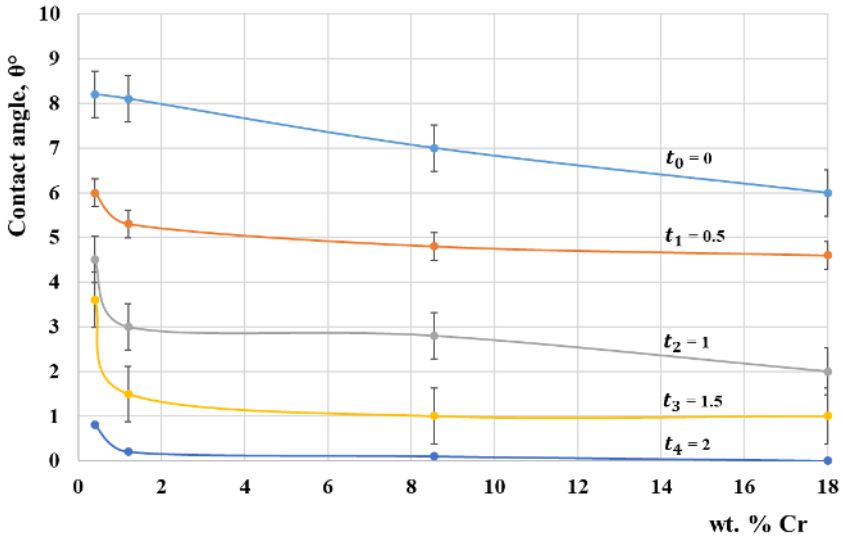


**Figure B2.** *The wettability behaviour of petroleum by different times (in seconds) as a function of Cr-containing steels.*

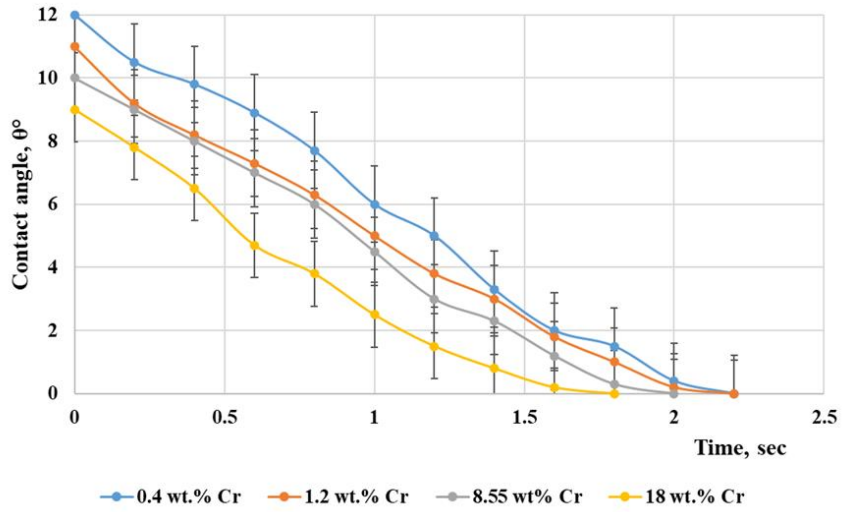


**Figure B3.** The wettability of different Cr-containing steels by hydraulic oil as a function of holding time.

**Claim 2: A new correlation between the wetting properties and the atomic radius of the pure metal substrate was identified and mathematically described.**

According to my results in (Fig. C) and described mathematically by Becker's broken bond model [153, 154] which describes the interfacial energy between two phases (A and B). I proven that the relationship between the contact angle and the atomic radius (half the bond length) is linear for pure metals (Ni, Cu, Ag, Al, W, Sn, Fe, and Cd) used as substrates. I make the following new correlation findings:

**2a.** For polar liquids

From the experimental results, new equations are (y = 0.0089x - 1) and (y= 0.0077x - 1) for water and glycerin, respectively. And mathematically proven with Eq. (15) $V_{SL} = \alpha r_a + \beta$ when α < 0.

**2b.** For apolar liquids

From the experimental results, new equations are (y= -0.0006x +1) and (y= -0.0018x +1) for petroleum and hydraulic oil, respectively. And mathematically proven with Eq. (15) $V_{SL} = \alpha r_a + \beta$ when α > 0.

where: $V_{SL}$ is the bond energies of interatomic pairs in the phases solid-liquid, $r_a$ is the atomic radius, $\alpha$ and $\beta$ are semi-empirical parameters. In this case, $\cos(\Theta) \propto r_a$.

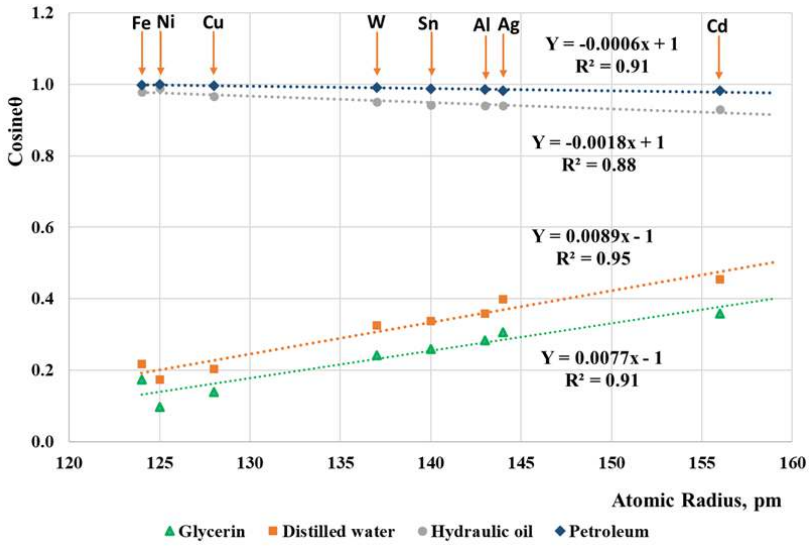


**Figure C.** Cosine of the contact angle of liquids as a function of the atomic radius parameter of the substrate.

**Claim 3: I have proven the effect of free-electron density on adhesion energy and wettability of liquids (polar and apolar) on a metal surface.**

Using the Young-Dupré equation, I established that the adhesion energy and wettability of liquids (polar and apolar) on metal substrates are strongly governed by the free-electron density of the substrate. I identified a strong correlation between the calculated adhesion energy and the free-electron density parameter ($r_s$), with the best fit described by the empirical relationship: $W \sim f(r_s^{-4})$.

I make the following findings:

**3a.** When the free-electron density increased, adhesion energy increased, and wettability for apolar liquids was enhanced, according to the correlations (y=10.228x+49.429, y=36.544x+57.369) for petroleum and hydraulic oil, respectively (Figs. D1 and D2).

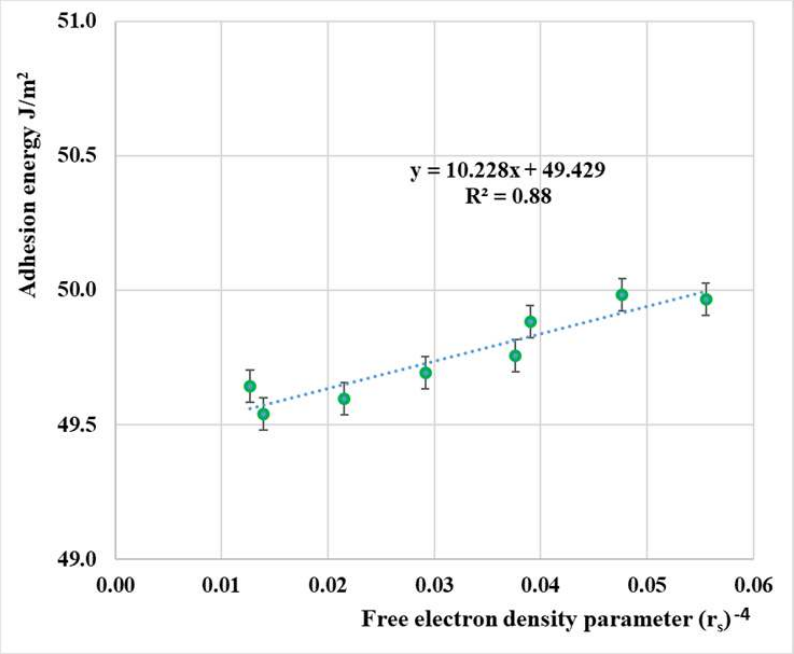


**Figure D1.** Adhesion energy (W) for petroleum as a function of the free electron density parameter following the $W \sim f(r_S^{-4})$ correlation.

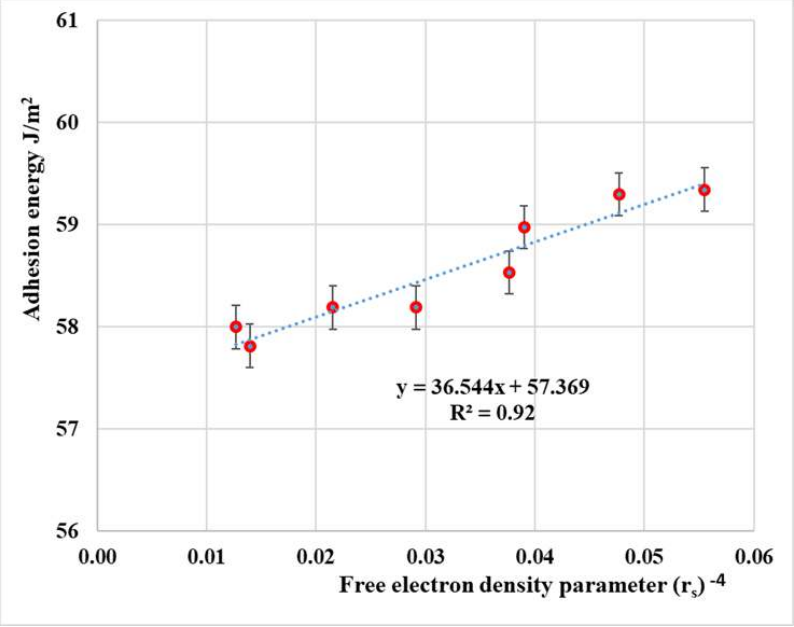


**Figure D2.** Adhesion energy (W) for hydraulic oil as a function of the free electron density parameter following the $W \sim f(r_S^{-4})$ correlation.

**3b.** The increase in free-electron density will decrease adhesion energy, then wettability for polar liquids will be decreased according to the correlation (y=281.58x+88.259, y=384.97x+109.21) for glycerin and water, respectively (Figs. D3 and D4).

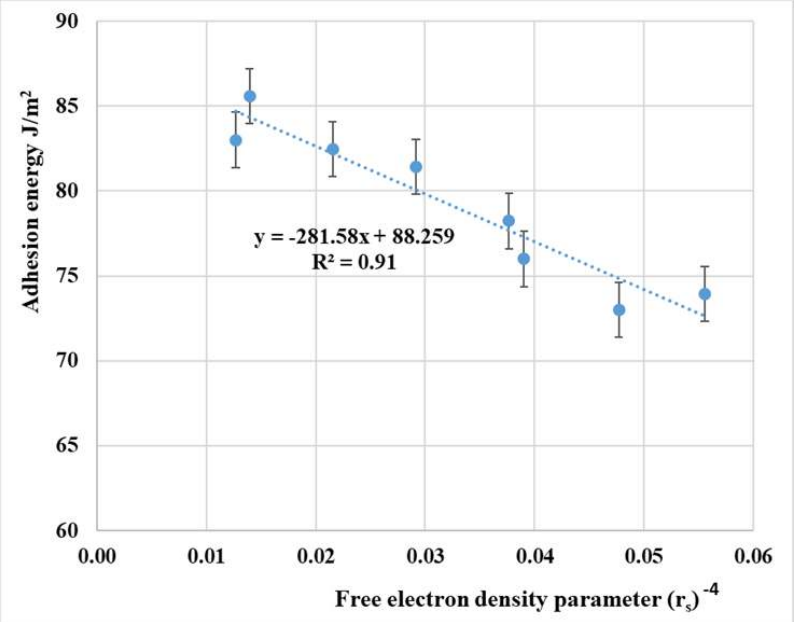


**Figure D3.** Adhesion energy (W) for glycerin as a function of the free electron density parameter following the $W \sim f(r_S^{-4})$ correlation.

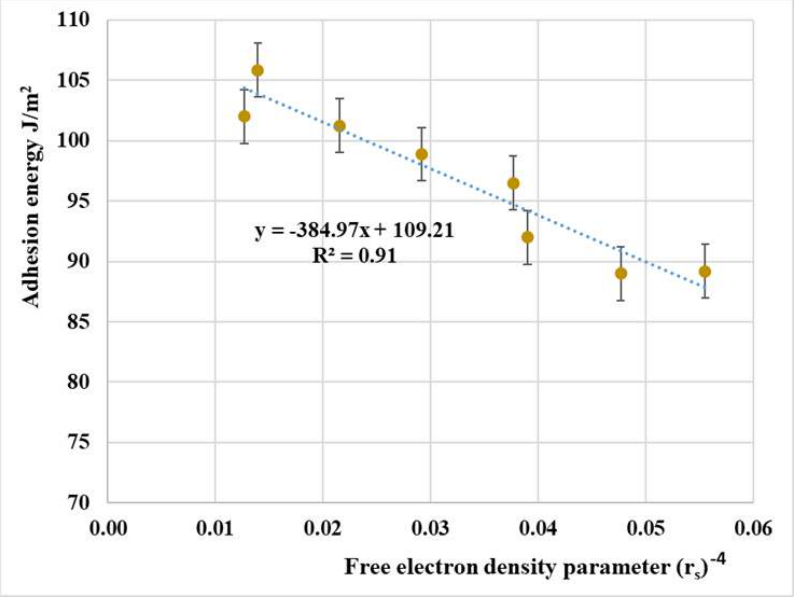


**Figure D4.** Adhesion energy (W) for distilled water as a function of the free electron density parameter following the $W \sim f(r_S^{-4})$ correlation.

**Claim 4: I established a comparative framework for evaluating the separation efficiency of stainless steel mesh with five different hole sizes (150, 200, 300, 400, 500 meshes) in a single emulsion system (petroleum-water).**

I used a single emulsion system (wt. 50% petroleum + wt. 50% water) on all types of mesh surfaces (500, 400, 300, 200, and 180 mesh) before and after Ni coating. I make the following findings:

**4a.** Determine the best hole size of the stainless steel mesh for separating petroleum from water before Ni coating. I have proved that the meshes with sizes of 300 and 400 mesh were the best in the separation, and reached up to 83% and 87% of the separation efficiency (Fig. E1), and other separation efficiencies are (56%, 72%, and 62%) for sizes (180, 200, and 500 mesh), respectively.

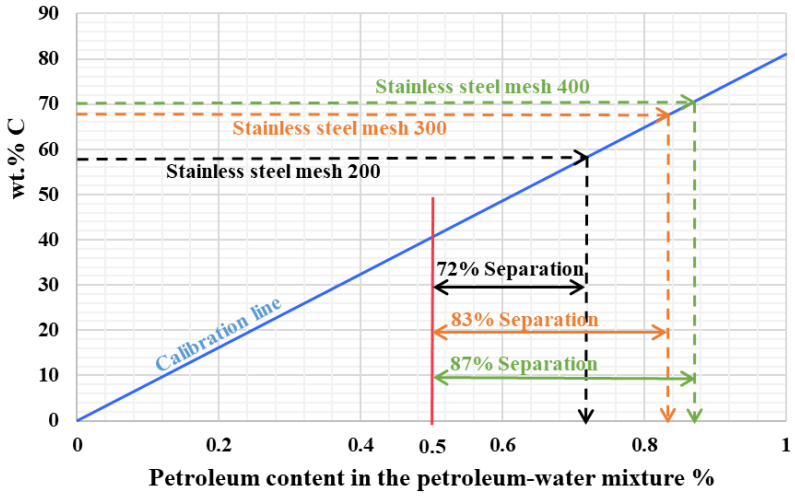


**Figure E1.** Identification of the C content for the separated liquid by the stainless steel meshes before coating with Ni, where the C content for the initial emulsion (50% vol. petroleum + 50% vol. water), see vertical red line in the figure.

**4b.** An increase of 9±1% in the separation efficiency with Ni-coating. I have proved that the 0.1 μm Ni coating on the stainless steel mesh surface could improve the separation efficiency up to (80%, 92%, and 97%) for sizes (200, 300, and 400 mesh), respectively (Fig. E2). On the other hand, the samples with sizes (180 and 500 meshes) were bad in the separation process, and the efficiency was about 58% and 65%. Fig. E3 shows the differences in the separation efficiency of meshes before and after Ni coating.

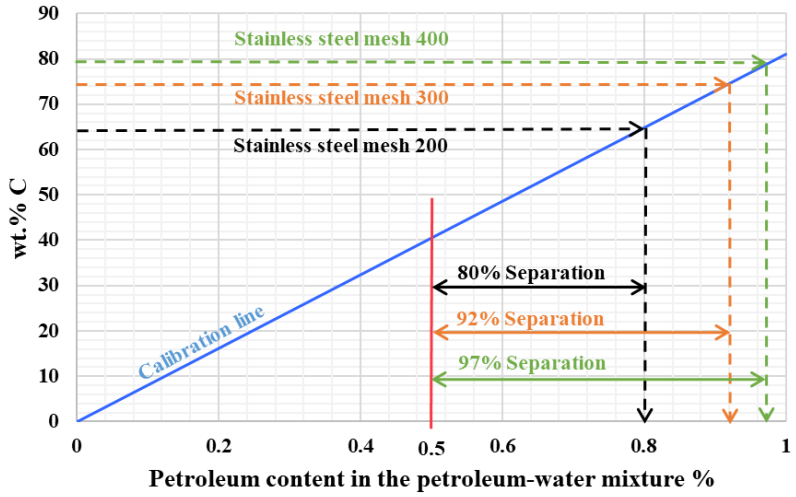


**Figure E2.** Identification of the C content for the separated liquid by the stainless steel meshes after coating with Ni, where the C content for the initial emulsion (50% vol. petroleum + 50% vol. water), see vertical red line in the figure.

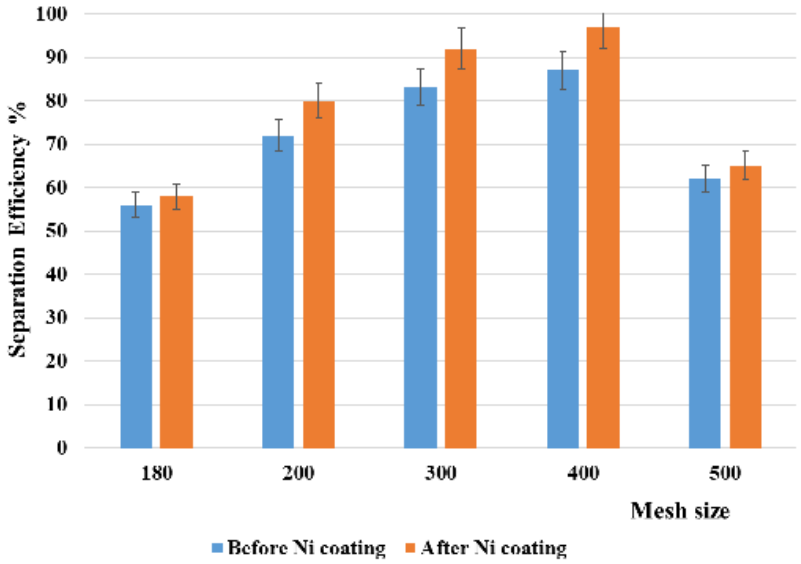


**Figure E3.** Influence of stainless steel mesh size on the efficiency of emulsion separation before and after coating with Ni.

**Claim 5: Enhanced the petroleum-water separation by employing a dual-layer configuration of stainless steel mesh with Ni-coated.**

I improved the separation efficiency by using a new separation system consisting of a dual-layer of nickel-coated stainless steel mesh with a 400-mesh size (Fig. F1), relative to the single-layer process. The efficiency of the separation reached about 99.4±0.4%, and it remained stable even after 20 uses (Fig. F2).

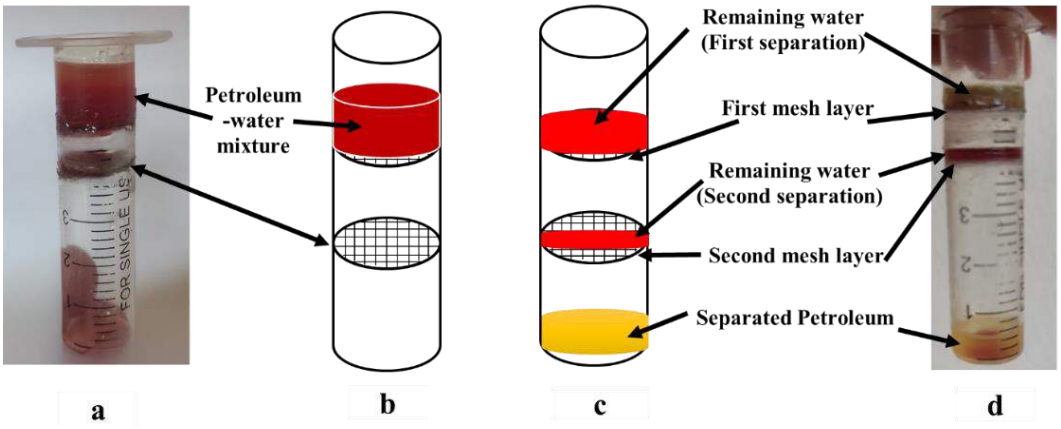


**Figure F1.** Schematic diagram of the separation process with a new tube system (a, b: Before the separation, c, d: After the separation).

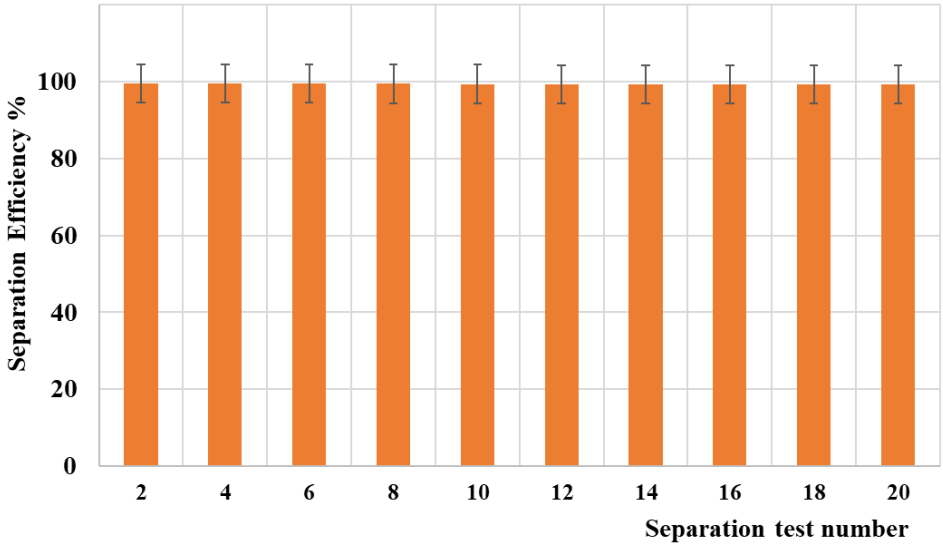


**Figure F2.** The separation efficiency of the new separation system after 20 uses.

**Claim 6: I identified the importance of changing the mesh hole geometry from square to triangular and proved that it could improveseparation mathematically.**

Mathematically, according to Young–Laplace (capillary) relation for a meniscus, after derivation relative to liquid droplet on circular hole (Fig. G1) I had Equations 22 and 24 that proved that using a mesh with a triangular hole shape will increase the liquid wetting by up to 1.172 times higher than the liquid wetting value on the mesh surface with a square hole shape (Fig. G2), under the same hole area value and work under the exact conditions of liquid capillary pressure and surface/interfacial tension, thus providing a clear physical and mathematical justification for improved oil-water separation performance when triangular meshes are employed instead of square ones.

$$\cos\theta_{Square} = \frac{\Delta p_c\, a}{4\gamma} \tag{22}$$

$$\cos\theta_{Triangle} = 1.172\ \frac{a\Delta p_c}{4\gamma} \tag{24}$$

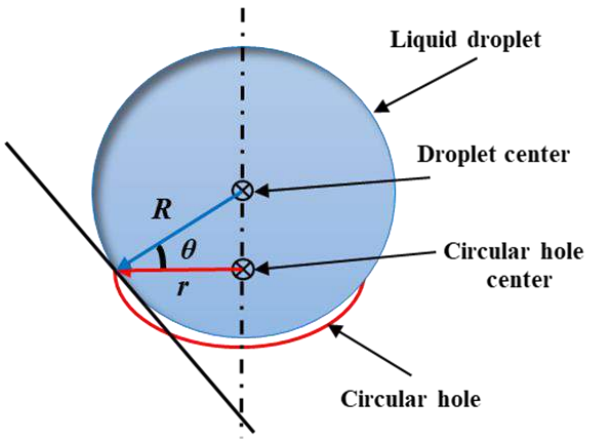


**Figure G1.** Schematic of the relationship between the radius of the droplet (spherical) and the radius of the hole (circular) at the point of contact.

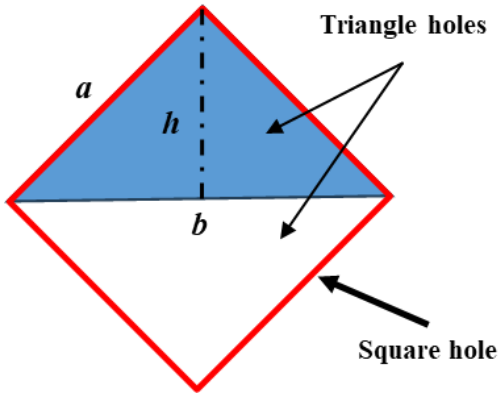


**Figure G2.** Schematic diagram to represent the triangle mesh hole shape dimensions relative to a square.

# 7. Author publications

## 7.1. Journal papers

- **J1: Mohanad Khairi**, Zoltán Erdélyi and Peter Baumli: Wettability of Polar and Apolar Liquids on Metal Surfaces, Metals Journal **2025. Q1**
- **J2: Mohanad Khairi**, and Peter Baumli: Nickel-Coated Stainless Steel Mesh Surfaces: A Corrosion Resistance Improvement Strategy via Oil-Water Separation, (*Under process*)
- **J3: Mohanad Khairi**, and Peter Baumli: An Empirical Investigation into the Chromium-Containing Percentage of Carbon Steel on Oil and Water Wettability Behavior, *(Under process*)
- **J4: Mohanad Khairi**, and Peter Baumli: A Study of Surface Hardening with Ni-Composites Coatings- A review, Doktorandusz Almanach/PhD Students Almanach **2022**, Page 254.

## 7.2. Proceeding paper

1- **Mohanad Khairi**, Peter Baumli: Oil–Water Separation and Corrosion Resistance Enhancement by Mesh Surfaces Nanocoated, ISCAME - 11th International Scientific Conference on Advances in Mechanical Engineering, Debrecen, Hungary **2025**, p.76.

2- **Mohanad Khairi**, Peter Baumli: Variations in the wettability behaviour of material surfaces caused by petroleum and hydraulic oil, ISDM Conference Proceedings, **2024**, p.55.

3- **Mohanad Khairi**, Peter Baumli: Comparative Analysis of Wettability of Metals and Ceramics by Oil, ISCAME - 9th International Scientific Conference on Advances in Mechanical Engineering, Debrecen, Hungary **2023**, p.73.

4- **Mohanad Khairi**, Peter Baumli: Study Influence of the Chromium on the Oil's Wettability, Adana-Turkey **2022**, p.348.

5- **Mohanad Khairi**, Peter Baumli: An Experimental Analysis of Mixture Oil Wettability on Three Types of Steel Surfaces, Adana-Turkey **2022**, p.405.

## 7.3. Conference presentations:

- **Con1: Mohanad Khairi**: Oil–Water Separation and Corrosion Resistance Enhancement by Mesh Surfaces Nanocoated, ISCAME - 11th International Scientific Conference on Advances in Mechanical Engineering, Debrecen, Hungary **2025**.

- **Con2: Mohanad Khairi**: Investigating the Influence of Nickel Physicochemical Properties on the Wetting Dynamics of Water and Hydrocarbon Liquids, 27th International Students' Day of Metallurgy, Freiberg, Germany **2024**.
- **Con3: Mohanad Khairi**: The Differences in Oil (Petroleum and Hydraulic) Wettability Behaivor on Materials Surfaces, Materials science day XXlll of PhD students, Veszprémben-Hungary **2023**.
- **Con4: Mohanad Khairi**: Comparative Analysis of Wettability of Metals and Ceramics by Oil, ISCAME - 9th International Scientific Conference on Advances in Mechanical Engineering, Debrecen, Hungary **2023**.
- **Con5: Mohanad Khairi**, Prof. Dr Peter Baumli: Study Influence of the Chromium on the Oil's Wettability, Adana-Turkey **2022**.
- **Con6: Mohanad Khairi**, Prof. Dr Peter Baumli: An Experimental Analysis of Mixture Oil Wettability on Three Types of Steel Surfaces, Adana-Turkey **2022**.

## 7.4. Publication out of the study

**a- Proceeding paper**

- Mohammed Qasim Kareem, Tamás Mikó, **Mohanad Khairi Fadhil**, Mahmood Alhafadhi: Manufacturing 3D SLMParts of 17-4PH Using Direct Scanning Strategy with 0 to 90° Rotation. ISCAME - 11th International Scientific Conference on Advances in Mechanical Engineering, vol.14 (**2025)**: pp 99-99, Debrecen, Hungary.

**b- Conference presentations**

- Mahmood ALHafadhi, Mundher Abdul-Zahra Dookhi, and **Mohanad Khairi**: Preparing Superconducting Compound (Pb (Bi) $Ba_2Ca_2Cu_{3-x}Zn_xO_{8+\delta}$) and Studying Its Electrical and Structural Properties. ISCAME - 11th International Scientific Conference on Advances in Mechanical Engineering, **2025**, Debrecen, Hungary.

**c- Poster**

- Mahmood Alhafadhi, Alsigar Masar Kadhim, Harinadh Vemanaboina, and **Mohanad Khairi**: Modeling and Measuring Residual Stresses in a Thick-Walled Pipe Structure Welded with a Buried-Arc Technique: A Comparative Study. ISCAME - 9th International Scientific Conference on Advances in Mechanical Engineering, Vol.2, (**2023):** pp 7-7, Debrecen, Hungary.

## 8. Reference


[1] V. Luzhetskyy: Peculiarities of Corrosion Degradation of Steel of Oil Pipelines, East European Journal of Advanced Technologies 4.5 (70) (2014).

[2] V. M. Pustovoi, and I. O. Reshchenko: Modeling of the In-service Degradation of Steels of Cargo Seaport Structures Under the Laboratory Conditions, Materials Science 48.5 (2013): 561-568.

[3] M. S. Khoma: Application of Electrochemical Methods to the Investigation of Corrosion Fatigue of Metals, Materials Science 36.1 (2000): 80-86.

[4] I. M. Dmytrakh: On Corrosion Fatigue Initiation From Notches and the Local Corrosion Fracture Approaches, Notch Effects in Fatigue and Fracture: NATO Science Series 11 (2001): 331-346.

[5] H. M. Nykyforchyn, and O. T. Tsyrulnyk: Specific Features of the In-service Bulk Degradation of Structural Steels Under the Action of Corrosive Media, Strength of Materials, Vol. 41, No. 6 (2009): 651-663.

[6] V. V. Panasyuk: Fracture Mechanics and Strength of Materials: Advances and Prospects, Materials Science, Vol. 40, No. 3 (2004): 305-319.

[7] D. Dardor, M. Al-Maas, J. Minier-Matar, A. Janson, R. Sharma, M. K. Hassan, A. Mariam, and S. Adham: Protocol for Preparing Synthetic Solutions Mimicking Produced Water From Oil and Gas Operations, ACS omega, Vol. 6, No. 10 (2021): 6881–6892.

[8] M. M. S. Yazdan, M. T. Ahad, I. Jahan, and M. Mazumder: Review on the Evaluation of the Impacts of Wastewater Disposal in Hydraulic Fracturing Industry in the United States, Technologies, Vol. 8, No. 4 (2020): 67.

[9] W. Zheng, J. Huang, S. Li, M. Ge, L. Teng, Z. Chen, and Y. Lai: Advanced Materials With Special Wettability Toward Intelligent Oily Wastewater Remediation, ACS App. Mater. Interfaces, Vol. 13, No. 1 (2020): 67-87.

[10] J. G. Speight: Chapter One - Gas and Oil in Tight Formations, Deep Shale Oil and Gas, Gulf Professional Publishing, (2017): 1-61.

[11] A. Marafi, H. Albazzaz, and M. S. Rana: Hydroprocessing of Heavy Residual Oil: Opportunities and Challenges, Catalysis Today, Vol. 329, (2019): 125–134.

[12] A. I.B. Ekejiuba: Natural Petroleum: Chemistry and Valuable Products Fractions, Inter World Journal of Science and Technology, Vol. 4, No. 2 (2011): 300-33.

[13] A. Al Madan, A. Hussein, and S. S. Akhtar: A Review on Internal Corrosion of Pipelines in the Oil and Gas Industry Due to Hydrogen Sulfide and the Role of Coatings as a Solution, Corrosion Reviews 43.2 (2025): 189-208.

[14] U. Dao, Z. Sajid, F. Khan, Y. Zhang, and T. Tran: Modeling and Analysis of Internal Corrosion Induced Failure of Oil and Gas Pipelines, Reliability Engineering & System Safety, Vol. 234 (2023): 109170.

[15] A. F. Al-Nouti and Z. M. Yaseen: Integration of Hybrid Machine Learning Model with Differential Evolution Algorithm for Underground Pipeline Corrosion Prediction, Engineering Applications of Artificial Intelligence, Vol. 158, part B (2025): 111511.

[16] S. Adumene, R. Islam, I. F. Dick, E. Zarei, M. Inegiyemiema, and M. Yang: Influence-Based Consequence Assessment of Subsea Pipeline Failure Under Stochastic Degradation, Energies, Vol. 15, No. 20 (2022).

[17] M. Askari, M. Aliofkhazraei, and S. Afroukhteh: A Comprehensive Review on Internal Corrosion and Cracking of Oil and Gas Pipelines, Journal of Natural Gas Science and Engineering, Vol. 71 (2019).

[18] M. S. Okyere: Assessment of Internal Corrosion Risk in Wet Sour Gas Pipeline Systems Utilizing Computational Fluid Dynamics: A Predictive Framework for Evaluating Pipeline and Structural Integrity, With a Case Study of the Kashagan 28-inch Offshore Pipeline, Okyere Journal of Engineering and Applied Science, Vol. 72, No.1 (2025).

[19] Z. Qiao, H. Yang, Y. Liu, X. Chen, X. Feng, X. Liu, B. Zhang, J. Huang, Y. Dan, AND N. Boshkov: A Comparative Study on Anti-corrosion and Antifouling Performance of Marine High Density Polyethylene-Capsaicin Composite Coatings with Different Biocide Content, Journal of Thermal Spray Technology, Vol. 33, No. 1 (2024): 88–100.

[20] H. M. H. Farh, M. E. A. B. Seghier, and T. Zayed: A Comprehensive Review of Corrosion Protection and Control Techniques for Metallic Pipelines, Engineering Failure Analysis, Vol. 143, Part A (2023): 106885.

[21] A. A. Tsynaeva: Cathode Protection Systems of Cross-country Pipelines, Procedia Engineering 111 (2015): 777-782.

[22] M. Kutz: Handbook of Environmental Degradation of Materials, William Andrew Publishing, (2005): 137.

[23] A. B. Khudhair and F. I. Hussein: Implementation of a Control and Monitoring System for a Cathodic Protection Cell to Mitigate Localized Corrosion in Fixed and Mobile Steel Structures, Results in Engineering, Vol. 23 (2024): 102553.

[24] S. Kokal, AND A. Al-Ghamdi: Performance Appraisals of Gas/Oil-Separation Plants, SPE Production and Operations 23.02 (2008): 287-296.

[25] L. M. Oshinowo and R. D. Vilagines: Modeling of Oil–Water Separation Efficiency in Three-phase Separators: Effect of Emulsion Rheology and Droplet Size Distribution, Chemical Engineering Research and Design, Vol. 159 (2020): 278–290.

[26] D. P. Subedi: Contact Angle Measurement for The Surface Characterization of Solids, The Himalayan Physics, Vol. 2 (2011).

[27] N. Sobczak, M. Singh, and R. Asthana: High-temperature Wettability Measurements in Metal/ceramic Systems - Some Methodological Issues, Curr Opin Solid State Mater Sci, Vol. 9, No. 4–5 (2005): 241–253.

[28] B. Doshi, M. Sillanpää, and S. Kalliola: A review of Bio-based Materials for Oil Spill Treatment, Water Research 135 (2018): 262-277.

[29] H. J. Butt, J. Liu, K. Koynov, B. Straub, C. Hinduja, I. Roismann, R. Berger, X. Li, D. Vollmer, W. Steffen, and M. Kappl: Contact Angle Hysteresis, Current Opinion in Colloid & Interface Science 59 (2022): 101574.

[30] T. Young. III: An Essay on the Cohesion of Fluids. Philosophical transactions of the royal society of London 95 (1805): 65-87.

[31] S. Ashokkumar, J. Adler-Nissen, and P. Moller: Factors Affecting the Wettability of Different Surface Materials with Vegetable Oil at High Temperatures and its Relation to Cleanability, Appl Surf Sci, Vol. 263 (2012): 86–94.

[32] R. K. Gupta, G. J. Dunderdale, M. W. England, and A. Hozumi: Oil/water Separation Techniques: A review of Recent Progresses and Future Directions, J. Mater. Chem. A, 5 (2017): 16025-16058.

[33] K. Liu and L. Jiang: Metallic Surfaces with Special Wettability, Nanoscale, Vol. 3, No. 3 (2011): 825–838.

[34] Y. C. Jung and B. Bhushan: Wetting Behavior of Water and Oil Droplets in Three-phase Interfaces for Hydrophobicity/philicity and Oleophobicity/philicity, Langmuir, Vol. 25, No. 24, (2009): 14165–14173.

[35] H. Wang, C. Wang, J. Fu, and G. Gu: Wetting Behavior and Mechanism of Wetting Agents on Low-energy Surface, Colloids Surf A Physicochem Eng Asp, Vol. 424 (2013): 10–17.

[36] M. S. Islam, L. Tong, and P. J. Falzon: Influence of Metal Surface Preparation on its Surface Profile, Contact Angle, Surface Energy and Adhesion with Glass Fibre Prepreg, Int J Adhes Adhes, Vol. 51 (2014): 32–41.

[37] M. Kalin and M. Polajnar: The Correlation Between the Surface Energy, the Contact Angle and the Spreading Parameter, and their Relevance for the Wetting Behaviour of DLC with Lubricating Oils, Tribol Int, Vol. 66 (2013): 225–233.

[38] D. Quéré. Wetting and Roughness: Annu Rev Mater Res, Vol. 38 (2008): 71–99.

[39] J. Wang, Y. Wu, Y. Cao, G. Li, and Y. Liao: Influence of Surface Roughness on Contact Angle Hysteresis and Spreading Work, Colloid Polym Sci, Vol. 298, No. 8 (2020): 1107–1112.

[40] H. Zhu, Z. Guo, and W. Liu: Adhesion Behaviors on Superhydrophobic Surfaces. Chem, Commun, Vol. 50, No. 30 (2014): 3900–3913.

[41] A. Samanta, W. Huang, H. Chaudhry, Q. Wang, S. K. Shaw, and H. Ding: Design of Chemical Surface Treatment for Laser-Textured Metal Alloys to Achieve Extreme Wetting Behavior, ACS Appl Mater Interfaces, Vol. 12, No. 15 (2020): 18032–18045.

[42] L. Guo, J. Liu, H. Xia, X. Li, X. Zhang, and H. Yang: Effects of Surface Treatment and Adhesive Thickness on the Shear Strength of Precision Bonded Joints, Polymer Testing, Vol. 94 (2021): 107063.

[43] T. Huhtamäki, X. Tian, J. T. Korhonen, and R. H. A. Ras: Surface-wetting Characterization Using Contact-angle Measurements, Nat Protoc, Vol. 13, No. 7, (2018): 1521–1538.

[44] J. W. Drelich, L. Boinovich, C. D. Volpe, L. Holysz, A. Marmur, S. Siboni: Contact Angles: History of Over 200 Years of Open Questions, Surface Innovations 8(1-2), (2020): 3-27.

[45] Q. Yin, C. Li, L. Dong, X. Bai, Y. Zhang, M. Yang, D. Jia, R. Li, and Z. Liu: Effects of Physicochemical Properties of Different Base Oils on Friction Coefficient and Surface Roughness in MQL Milling AISI 1045, Int. J. of Precis. Eng. and Manuf.-Green Tech., Vol. 8, No. 6 (2021): 1629–1647.

[46] Y. Chen, Q. Xie, A. Sari, P. V. Brady, and A. Saeedi: Oil/water/rock Wettability: Influencing Factors and Implications for Low Salinity Water Flooding in Carbonate Reservoirs, Fuel, Vol. 215 (2018): 171–177.

[47] F. Ding and M. Gao: Pore Wettability for Enhanced Oil Recovery, Contaminant Adsorption and Oil/water Separation: A review, Advances in Colloid and Interface Science, Vol. 289 (2021): 102377.

[48] Z. Pan, S. Cao, J. Li, Z. Du, and F. Cheng: Anti-fouling $TiO_2$ Nanowires Membrane for Oil/water Separation: Synergetic Effects of Wettability and Pore Size, Journal of Membrane Science, Vol. 572 (2019): 596–606.

[49] J. Xu, P. Che, H. Zhang, Y. Zhang, J. Wu, W. Li, J. He, Z. Ma, T. Li, Y. Dong, J. Yu, and R. Tong: Superhydrophobic Modification of Biomass Cuttlebone Applied to Oil Spill Remediation, Materials, Vol. 15, No. 13 (2022): 4401.

[50] Y. Sun, Z. Ke, C. Shen, Q. Wei, R. Sun, W. Yang, and Z. Yin: Facile Construction and Fabrication of a Superhydrophobic and Super Oleophilic Stainless Steel Mesh for Separation of Water and Oil, Nanomaterials, Vol. 12, No. 10 (2022): 1661.

[51] C. Li, B. Lee, C. Wang, A. Bajpayee, L. D. Douglas, B. K. Phillips, G. Yu, N. Rivera-Gonzalez, B. Peng, Z. Jiang, H. Sue, S. Banerjee, and L. Fang: Photopolymerized Superhydrophobic Hybrid Coating Enabled by Dual-purpose Tetrapodal ZnO for Liquid/liquid Separation, Mater. Horiz., Vol. 9, No. 1 (2022): 452–461.

[52] W. Ren, Z. Lian, J. Wang, J. Xu, and H. Yu: Fabrication of durable underoil superhydrophobic surfaces with self-cleaning and oil–water separation properties, RSC Adv., Vol. 12 (2022): 3838.

[53] B. Hou, R. Jia, M. Fu, Y. Wang, C. Jiang, B. Yang, and Y. Huang: Wettability Alteration of Oil-wet Carbonate Surface Induced by Self-dispersing Silica Nanoparticles: Mechanism and Monovalent Metal Ion's Effect, Journal of Molecular Liquids, Vol. 294 (2019): 111601.

[54] S. M. Gateman, O. Gharbi, M. Turmine, and V. Vivier: Measuring Changes in Wettability and Surface Area During Micro Droplet Corrosion Measurements, Electrochimica Acta, Vol. 399 (2021): 139402.

[55] W. Qu, S. Li, Z. Chen, C. Li, Y. Pei, and S. Gong: Hot Corrosion Behavior and Wettability of Calcium–magnesium–alumina–silicate (CMAS) on $LaTi_2Al_9O_{19}$ Ceramic, Corrosion Science, Vol. 162 (2020): 108199.

[56] M. Petkovšek, M. Hočevar, and P. Gregorčič: Surface Functionalization by Nanosecond-laser Texturing for Controlling Hydrodynamic Cavitation Dynamics, Ultrasonics Sonochemistry, Vol. 67 (2020): 105126.

[57] Y. Han, S. Wang, R. Zhou, L. He, and X. Luo: The Migration and Adherence of Oil Droplets on Surfaces with Different Wettability in a Laminar Flow Field, Langmuir, Vol. 36, No. 1 (2019): 109-118.

[58] B. Pan, X. Yin, and S. Iglauer: A Review on Clay Wettability: From Experimental Investigations to Molecular Dynamics Simulations, Vol. 285 (2020): 102266.

[59] S. Esmaeili, H. Sarma, T. Harding, and B. Maini: Review of the Effect of Temperature on Oil-water Relative Permeability in Porous Rocks of Oil Reservoirs, Fuel, Vol. 237 (2019): 91-116.

[60] M. Lokanathan, E. Wikramanayake, and V. Bahadur: Scalably Manufactured Textured Surfaces for Controlling Wettability in Oil-water Systems, Mater. Res. Express, Vol. 6, No. 4 (2019): 046507.

[61] L. Kang, B. Wang, J. Zeng, Z. Cheng, J. Li, J. Xu, W. Gao, and K. Chen: Degradable Dual Superlyophobic Lignocellulosic Fibers for High-efficiency Oil/water Separation, Green Chemistry, Vol. 22, No. 2, (2020): 504–512.

[62] F. Zaera: The Surface Chemistry of Atomic Layer Depositions of Solid Thin Films, J. Phys. Chem. Lett., Vol. 3 (2012): 1301−1309.

[63] Y. Jiang, Y. Sun, J. W. Drelich, and C. H. Choi: Spontaneous Spreading of a Droplet: The Role of Solid Continuity and Advancing Contact Angle, Langmuir, Vol. 34, No. 17 (2018): 4945–4951.

[64] J. W. Drelich: Contact Angles: From Past Mistakes to New Developments Through Liquid-solid Adhesion Measurements, Advances in Colloid and Interface Science, Vol. 267 (2019): 1-14.

[65] B. Li, Y. Ouyang, Z. Haider, Y. Zhu, R. Qiu, S. Hu, H. Niu, Y. Zhang, and M. Chen: One-step Electrochemical Deposition Leading to Superhydrophobic Matrix for Inhibiting Abiotic and Microbiologically Influenced Corrosion of Cu in Seawater, Colloids and Surfaces A: Physicochemical and Engineering Aspects, Vol. 616 (2021): 126337.

[66] L. Feng, H. Zhang, Z. Wang, and Y. Liu: Superhydrophobic Aluminum Alloy Surface: Fabrication, Structure, and Corrosion Resistance, Colloids and Surfaces A: Physicochemical and Engineering Aspects, Vol. 441 (2014): 319–325.

[67] K. Li, X. Zeng, H. Li, and X. Lai: Facile Fabrication of a Robust Superhydrophobic/superoleophilic Sponge for Selective Oil Absorption from Oily Water, RSC Adv., Vol. 4, No. 45 (2014): 23861–23868.

[68] C. Neinhuis and W. Barthlott: Characterization and Distribution of Water-repellent, Self-cleaning Plant Surfaces, Annals of Botany, Vol. 79 (1997): 667–677.

[69] R. Kumar, M. Rezapourian, R. Rahmani, H. S. Maurya, N. Kamboj, and I. Hussainova: Bioinspired and Multifunctional Tribological Materials for Sliding, Erosive, Machining, and Energy-Absorbing Conditions: A Review, Biomimetics, Vol. 9, No. 4 (2024): 209.

[70] B. N. Sahoo and B. Kandasubramanian: Recent Progress in Fabrication and Characterisation of Hierarchical Biomimetic Superhydrophobic Structures, RSC Adv., Vol. 4, No. 42 (2014): 22053–22093.

[71] P. Ragesh, V. A. Ganesh, S. V. Nair, and A. S. Nair: A Review on 'Self-cleaning and Multifunctional Materials', Journal of Materials chemistry A, Vol. 2, No. 36 (2014): 14773-14797.

[72] R. N. Wenzel: Resistance of Solid Surfaces to Wetting by Water, Industrial & Engineering Chemistry, Vol. 28, No. 8 (1936): 988-994.

[73] Y. Zhong, A. M. Jacobi, and J. G. Georgiadis: Effects of Surface Chemistry and Groove Geometry on Wetting Characteristics and Droplet Motion of Water Condensate on Surfaces with Rectangular Microgrooves, Int J Heat Mass Transf, Vol. 57, No. 2 (2013): 629–641.

[74] A. Shahraz, A. Borhan, and K. A. Fichthorn: A Theory for the Morphological Dependence of Wetting on a Physically Patterned Solid Surface, Langmuir, Vol. 28, No. 40, (2012): 14227–14237.

[75] Y. Lu, S. Sathasivam, J. Song, C. R. Crick, C. J. Carmalt, and I. P. Parkin: Robust Self-cleaning Surfaces that Function when Exposed to Either Air or Oil, Science, Vol. 347, No. 6226 (2015): 1132-1135.

[76] Y. Zhang, J. Zhang, and A. Wang: From Maya Blue to Biomimetic Pigments: Durable Biomimetic Pigments with Self-cleaning Property, J Mater. Chem. A, Vol. 4, No. 3 (2016): 901–907.

[77] M. Khairi, Z. Erdélyi, and P. Baumli: Wettability of Polar and Apolar Liquids on Metal Surfaces, Metals, Vol. 15, No. 1 (2024): 23.

[78] S. Pan, A. K. Kota, J. M. Mabry, and A. Tuteja: Superomniphobic Surfaces for Effective Chemical Shielding, J Am Chem Soc, Vol. 135, No. 2 (2013): 578–581.

[79] Y. Si, Z. Dong, and L. Jiang: Bioinspired Designs of Superhydrophobic and Superhydrophilic Materials, ACS Cent Sci, Vol. 4, No. 9 (2018): 1102–1112.

[80] H. Zhang and H. Q. Lan: A Review of Internal Corrosion Mechanism and Experimental Study for Pipelines Based on Multiphase Flow, Corros Rev., Vol. 35, No.6 (2017): 425–444.

[81] Z. Xue, Y. Cao, N. Liu, L. Feng, and L. Jiang: Special Wettable Materials for Oil/water Separation, J. Mater. Chem. A, Vol. 2 (2014): 2445.

[82] M. Nouri, M. T. Sadeghi, A. M. Rashidi, and R. Norouzbeigi: Hydrothermally Synthetized $WO_3$ Coated Stainless Steel Mesh for Oil–water Separation Purposes, J Pet. Explor. Prod. Technol., Vol. 14, No. 5 (2024): 1247–1258.

[83] Y. P. Zhang, Y. N. Wang, L. Wan, X. X. Chen, and C. H. Zhao: Superwetting Stainless Steel Mesh Used for Both Immiscible Oil/Water and Surfactant-Stabilized Emulsion Separation, Membranes, Vol. 13, No. 10 (2023): 808.

[84] D. D. Nguyen, N. H. Tai, S. B. Lee, and W. S. Kuo: Superhydrophobic and Superoleophilic Properties of Graphene-based Sponges Fabricated Using a Facile Dip Coating Method, Energy Environ. Sci., Vol. 5, No. 7 (2012): 7908–7912.

[85] X. Dong, J. Chen, Y. Ma, J. Wang, M. B. Chan-Park, X. Liu, L. Wang, W. Huang, and P. Chen: Superhydrophobic and Superoleophilic Hybrid Foam of Graphene and Carbon Nanotube for Selective Removal of Oils or Organic Solvents from the Surface of Water, Chem Commun., Vol. 48, No. 86 (2012): 10660–10662.

[86] L. Zhang, Z. Zhang, and P. Wang: Smart Surfaces with Switchable Superoleophilicity and Superoleophobicity in Aqueous Media: Toward Controllable Oil/water Separation, NPG Asia Mater., Vol. 4, No. 2 (2012): e8-e8.

[87] L. Feng, Z. Zhang, Z. Mai, Y. Ma, B. Liu, L. Jiang, and D. Zhu: A Super-Hydrophobic and Super-Oleophilic Coating Mesh Film for the Separation of Oil and Water, Angewandte Chemie International Edition, Vol. 43, No. 15 (2004): 2012–2014.

[88] M. Zhu, Y. Liu, M. Chen, Z. Xu, L. Li, and Y. Zhou: Metal Mesh-based Special Wettability Materials for Oil-water Separation: A Review of the Recent Development, Journal of Petroleum Science and Engineering, Vol. 205 (2021): 108889.

[89] P. Kumari, P. Chauhan, and A. Kumar: Superwetting Materials for Modification of Meshes for Oil/Water Separation, American Chemical Society, Vol. 2 (2022): 1–23.

[90] M. J. Kratochvil, U. Manna, and D. M. Lynn: Superhydrophobic Polymer Multilayers for the Filtration- and Absorption-based Separation of Oil/water Mixtures, J Polym Sci A Polym Chem, Vol. 55, No. 18 (2017): 3127–3136.

[91] X. Yang, D. Lang, Z. Wang, J. Cao, R. Wu, and W. Wang: Underwater Superoleophobic Polyurethane-coated Mesh with Excellent Stability for Oil/water Separation, RSC Adv., Vol. 8, No. 69 (2018): 39657.

[92] Z. Xue, S. Wang, L. Lin, L. Chen, M. Liu, L. Feng, and L. Jiang: A Novel Superhydrophilic and Underwater Superoleophobic Hydrogel-coated Mesh for Oil/water Separation, Advanced Materials, Vol. 23, No. 37 (2011): 4270–4273.

[93] Q. Wen, J. Di, L. Jiang, J. Yu, and R. Xu: Zeolite-coated Mesh Film for Efficient Oil-water Separation, Chem Sci., Vol. 4, No. 2 (2013): 591–595.

[94] J. Myeong, P. R. Deshmukh, and W. G. Shin: Facile Preparation of Superhydrophilic and Underwater Superoleophobic Stainless Steel Mesh for Oil–water Separation, Journal of Industrial and Engineering Chemistry, Vol. 120 (2023): 398–409.

[95] A. Melnik, A. Bogoslovtseva, A. Petrova, A. Safonov, and C. N. Markides: Oil–Water Separation on Hydrophobic and Superhydrophobic Membranes Made of Stainless Steel Meshes with Fluoropolymer Coatings, Water, Vol. 15, No. 7 (2023): 1346.

[96] H. Wang, X. Hu, Z. Ke, C. Z. Du, L. Zheng, C. Wang, and Z. Yua: Review: Porous Metal Filters and Membranes for Oil–Water Separation, Nanoscale Research Letters, Vol. 13 (2018): 284.

[97] G. J. Dunderdale, M. W. England, T. Sato, C. Urata, and A. Hozumi: Programmable Oil/Water Separation Meshes: Water or Oil Selectivity Using Contact Angle Hysteresis, Macromol Mater. Eng., Vol. 301, No. 9 (2016): 1032–1036.

[98] R. Ou, J. Wei, L. Jiang, G. P. Simon, and H. Wang: Robust Thermoresponsive Polymer Composite Membrane with Switchable Superhydrophilicity and Superhydrophobicity for Efficient Oil–water Separation, Environ. Sci. Technol., Vol. 50, No. 2 (2016): 906-914.

[99] I. K. Erabee, M. M. Mansour, and A. M. Lafta: Environmental Impact of Oil Spills on Water Resources Altering Physical Properties and Treatment Approaches, Applied Chemical Engineering, Vol. 8, No. 3 (2025).

[100] A. Ullah: The Influence of Interfacial Tension on Rejection and Permeation of the Oil Droplets Through a Slit Pore Membrane, Sep Purif Technol, Vol. 266 (2021): 118581.

[101] J. Yu, C. Cao, and Y. Pan: Advances of Adsorption and Filtration Techniques in Separating Highly Viscous Crude Oil/Water Mixtures, Advanced Materials Interfaces Vol. 8, No.16 (2021): 2100061.

[102] H. Ohya, J.J. Kim, A. Chinen, M. Aihara, S.I. Semenova, Y. Negishi, O. Mori, and M. Yasuda: Effects of Pore Size on Separation Mechanisms of Microfiltration of Oily Water, Using Porous Glass Tubular Membrane, Journal of Membrane Science, Vol. 145, No. 1 (1998): 1-14.

[103] M. A. M. Anuar, N. A. Amran, and M. S. H. Ruslan: Optimization of Progressive Freezing for Residual Oil Recovery from a Palm Oil-Water Mixture (POME Model), ACS Omega, Vol. 6, No. 4 (2021): 2707–2716.

[104] W. Kang, L. Guo, H. Fan, L. Meng, and Y. Li: Flocculation, Coalescence and Migration of Dispersed Phase Droplets and Oil-water Separation in Heavy Oil Emulsion, J Pet Sci Eng, Vol. 81 (2012): 177–181.

[105] A. M. Schoeler, D. N. Josephides, S. Sajjadi, and P. Mesquida: Controlling the Surface Charge of Water Droplets in Non-polar Oils, Colloids Surf A Physicochem Eng Asp, Vol. 461, No. 1 (2014): 18–21.

[106] M. Hillert, and J. Agren: Effect of Surface Free Energy and Surface Stress on Phase Equilibria, Acta Materialia, Vol. 50 (2002): 2429–2441.

[107] R. G. Dillingham, B. R. Oakley, and D. Gilpin: Wetting Measurements for Identification of Specific Functional Groups Responsible for Adhesion, The Journal of Adhesion, Vol. 84, No. 12 (2008): 1007–1022.

[108] A. N. Gent, and J. Schultz: Effect of Wetting Liquids on the Strength of Adhesion of Viscoelastic Materials, The Journal of Adhesion, Vol. 3, No. 4 (1972): 281–294.

[109] A. Carre, and J. Schultz: Polymer-Aluminium Adhesion II. Role of the Adhesive and Cohesive Properties of the Polymer, The Journal of Adhesion, Vol. 17, No. 2 (1984): 135–155.

[110] H. Wennerström: Adhesion, Entropy and Surface Forces, A: Physicochemical and Engineering Aspects, Vol. 167 (2000): 209–214.

[111] X. Wang, and Q. Zhang: Role of Surface Roughness in the Wettability, Surface Energy and Flotation Kinetics of Calcite, Powder Technol, Vol. 371 (2020): 55–63.

[112] G. Aspenes, S. Høiland, T. Barth, and K. M. Askvik: The Influence of Petroleum Acids and Solid Surface Energy on Pipeline Wettability in Relation to Hydrate Deposition, J Colloid Interface Sci, Vol. 333, No. 2 (2009): 533–539.

[113] Z. Zhang, C. Xu, W. Liu, K. Wang, Y. Rao, C. Jiang, D. Li, Y. Zhang, X. Jiang, X. Chen, and C. Xu: Ultrasonic Assisted Rapid Preparation of Superhydrophobic Stainless Steel Surface and its Application in Oil/water Separation, Ultrason Sonochem, Vol. 81 (2021): 105848.

[114] E. Vazirinasab, R. Jafari, and G. Momen: Application of Superhydrophobic Coatings as a Corrosion Barrier: A review, Surf Coat Technol, Vol. 341, (2018): 40–56.

[115] N. Wang, D. Xiong, Y. Deng, Y. Shi, and K. Wang: Mechanically Robust Superhydrophobic Steel Surface with Anti-icing, UV-durability, and Corrosion Resistance Properties, ACS Appl Mater Interfaces, Vol. 7, No. 11 (2015): 6260–6272.

[116] C. Liu, F. Su, and J. Liang: Facile Fabrication of a Robust and Corrosion Resistant Superhydrophobic Aluminum Alloy Surface by a Novel Method, RSC Advances, Vol. 4, No. 98 (2014): 55556-55564.

[117] C. Li, N. Li, X. Zhang, Z. Dong, H. Chen, and L. Jiang: Uni-Directional Transportation on Peristome-Mimetic Surfaces for Completely Wetting Liquids, Angewandte Chemie, Vol. 128, No. 48 (2016): 15212–15216.

[118] B. Wang, and Z. Guo: Superhydrophobic copper mesh films with rapid oil/water separation properties by electrochemical deposition inspired from butterfly wing, Appl Phys Lett, Vol. 103, No. 6 (2013): 063704.

[119] Q. Chen, A. de Leon, and R. C. Advincula: Inorganic−Organic Thiol-ene Coated Mesh for Oil/water Separation, ACS applied materials & interfaces, Vol. 7, No. 33 (2015): 18566-18573.

[120] J. Zhang and S. Seeger: Polyester Materials with Superwetting Silicone Nanofilaments for Oil/water Separation and Selective Oil Absorption, Adv Funct Mater, Vol. 21, No. 24 (2011): 4699–4704.

[121] A. Deachophon, T. Bovornratanaraks, and S. Poompradub: Modified Silica-based Double-layered Hydrophobic-coated Stainless Steel Mesh and its Application for Oil/seawater Separation, Sci Rep, Vol. 14, No.1 (2024): 731.

[122] B. Li, X. Liu, X. Zhang, and W. Chai: Stainless Steel Mesh Coated with Silica for Oil-water Separation, Eur Polym J, Vol. 73 (2015): 374–379.

[123] H. Kang, Y. Sun, Y. Li, W. Qin, and X. Wu: Mechanically Robust Fish-Scale Microstructured $TiO_2$-Coated Stainless Steel Mesh by Atomic Layer Deposition for Oil-Water Separation, Ind Eng Chem Res, Vol. 59, No. 48 (2020): 21088–21096.

[124] S. Myeong, C. Lim, S. Kim, and Y. S. Lee: High-efficiency Oil/water Separation of Hydrophobic Stainless Steel Mesh Filter Through Carbon and Fluorine Surface Treatment, Korean Journal of Chemical Engineering, Vol. 40, No. 6 (2023): 1418–1424.

[125] Q. Gao, J. Li, R. Ma, Y. Fan, A. Du, M. Yang, X. Zhao, and Y. Bian: Facile Electrodeposition of Corrosion-resistant Superhydrophobic Ni-plated Stainless-steel Mesh for Oil–water Separation, Mater Today Commun, Vol. 37 (2023): 107032.

[126] P. Liu, L. Wu, Y. Guo, X. Huang, and Z. Guo: Rapid Preparation of Ni/Fe-LDH@ Stainless Steel Mesh with Interfacial Emulsion Breaking Effect for Efficient Oil-in-Water Emulsion Separation, Colloids Surf A Physicochem Eng Asp, Vol. 681 (2024): 132792.

[127] Y. Hou, R. Li, and J. Liang: Superhydrophilic Nickel-coated Meshes with Controllable Pore Size Prepared by Electrodeposition from Deep Eutectic Solvent for Efficient Oil/water Separation, Sep Purif Technol, Vol. 192 (2018): 21–29.

[128] X. Zhang, C. Hu, X. Fu, S. Zhang, T. Li, B. Ma, and K. Ren: An Ultra-thin Nickel Electrodeposited Stainless Steel Mesh with Superhydrophobic Property and High Mechanical Durability for Oil-water Separation, J Environ Chem Eng, Vol. 12, No. 1 (2024): 111692.

[129] H. Xu, S. Li, F. Jiang, T. Song, T. Lou, and Z. Xu: Fabrication of a Superhydrophobic Nickel Surface with Superior Corrosion Resistance Using Electrodeposition from Choline Chloride-Ethylene Glycol Deep Eutectic Solvent, J. of Materi Eng and Perform, Vol.34 (2025): 29418–29428.

[130] R. Sreekumar, S. E. Thazhakkuni, and S. S. Suseelamma: Fabrication of a Robust Superhydrophobic Stainless steel Mesh for Efficient Oil/water Separation, Journal of Industrial and Engineering Chemistry, Vol. 135 (2024): 425–433.

[131] H. Hoche, S. Groß, and M. Oechsner: Development of New PVD Coatings for Magnesium Alloys with Improved Corrosion Properties, Surf Coat Technol, Vol. 259 (2014): 102–108.

[132] G. Fox-Rabinovich J. M. Paiva, I. Gershman, M. Aramesh, D. Cavelli, K. Yamamoto, G. Dosbaeva, and S. Veldhuis: Control of Self-organized Criticality Through Adaptive Behavior of Nano-structured Thin Film Coatings, Entropy, Vol. 18, No. 8 (2016): 290.

[133] I. Mrkvica, T. Szotkowski, A. Slaninkova, and T. Jurga: High-Efficiency of PVD Coating Process by Applying an Additional Rotation, Coatings, Vol. 12, No. 6 (2022): 834.

[134] A. Baptista, F. Silva, J. Porteiro, J. Míguez, and G. Pinto: Sputtering Physical Vapour Deposition (PVD) Coatings: A Critical Review on Process Improvement and Market Trend Demands, Coatings, Vol. 8 (2018): 402.

[135] R. P. Martinho, F. J. G. Silva, and A. P. M. Baptista: Cutting Forces and Wear Analysis of $Si_3N_4$ Diamond Coated Tools in High Speed Machining, Vacuum, Vol. 82, No. 12 (2008): 1415–1420.

[136] G. Pinto, F. J. G. Silva, J. Porteiro, J. L. Míguez, A. Baptista, and L. Fernandes: A Critical Review on the Numerical Simulation Related to Physical Vapour Deposition, Procedia Manufacturing, Vol. 17 (2018): 860–869.

[137] F. Silva, R. Martinho, M. Andrade, A. Baptista, and R. Alexandre: Improving the Wear Resistance of Moulds for the Injection of Glass Fibre-reinforced Plastics Using PVD Coatings: A Comparative Study, Coatings, Vol. 7, No. 2 (2017): 28.

[138] L. Somlyai-Sipos, and P. Baumli: Wettability of Metals by Water, Metals, Vol. 12, No. 8 (2022): 1274.

[139] E. H. Abramson: Viscosity of Water Measured to Pressures of 6 GPa and Temperatures of 300 °c, Phys Rev E Stat Nonlin Soft Matter Phys, Vol. 76, No. 5 (2007): 051203.

[140] L. Korson, W. Drost-Hansen, and F. J. Millero: Viscosity of Water at Various Temperatures, The Journal of Physical Chemistry, Vol. 73, No. 1 (1969): 34-39.

[141] A. Han, W. Lu, V. K. Punyamurtula, X. Chen, F. B. Surani, T. Kim, and Y. Qiao: Effective Viscosity of Glycerin in a Nanoporous Silica gel, J Appl Phys, Vol. 104, No. 12 (2008): 124908.

[142] M. R. Riazi, and T. A. A1-Sahhaf: Physical Properties of Heavy Petroleum Fractions and Crude Oils, Vol.117 (1996): 217-224.

[143] J. Y. Wu, C. W. Huang, and P. S. Tsai: Preparation of Poly[3-(Methacryloylamino) Propyl] Trimethylammonium Chloride Coated Mesh for Oil–water Separation, Desalination Water Treat, Vol. 158 (2019): 301–308.

[144] J. S. Buckley, Y. Liu, X. Xie, and N. R. Morrow: Asphaltenes and Crude Oil Wetting - The Effect of Oil Composition, SPE Journal. Vol. 2 (1997): 107-119

[145] Y. Zhang, R. Zhao, M. Sanchez-Sanchez, G. L. Haller, J. Hu, R. Bermejo-Deval, Y. Liu, and J. A. Lercher: Promotion of Protolytic Pentane Conversion on H-MFI Zeolite by Proximity of Extra-framework Aluminum Oxide and BrØnsted Acid Sites, J Catal, Vol. 370 (2019): 424–433.

[146] S. S. Zumdahl, and S. A. Zumdahl: Chemistry: An Atoms First Approach, Handbook, 2nd ed., Cengage Learning, (2014).

[147] K. S. W. Sing, D. H. Everett, R. A. W. Haul, L. Moscou, R. A. Pierotti, J. Rouquerol, and T. Siemieniewska: Reporting Physisorption Data for Gas/solid Systems-with Special Reference to the Determination of Surface Area and Porosity, Pure & Appl. Chem., Vol. 57, No. 4 (1985): 603-619.

[148] A. B. D. Cassie, and S. Baxter: Wettability of Porous Surfaces, Transactions of the Faraday Society, Vol. 40 (1944): 546–551.

[149] A. W. Adamson, and A. P. Gast: Physical Chemistry of Surfaces, A Willy Interscience publishers, Handbook, 6th ed., Vol. 150 (1967).

[150] P. G. de Gennes, F. Brochard-Wyart, and D. Quéré: Capillarity and Wetting Phenomena, Drops, Bubbles, Pearls, Waves, Springer Science & Business Media, (2004).

[151] A. Dabrowski: Adsorption from Theory to Practice, Advances in Colloid and Interface Science, Vol. 93 (2001): 135-224.

[152] VV. A. Parsegian: Van der Waals Forces, A handbook for biologists, chemists, engineers, and physicists. Cambridge University Press, (2005).

[153] V. Beaker: Die Keimbildung bei der Ausscheidung in Metallischen Mischkristallen, Annalen der Physik, Folge 5, Band 32. (1938).

[154] T. Nishizawa, I. Ohnuma, and K. Ishida: Correlation Between Interfacial Energy and Phase Diagram in Ceramic-Metal Systems, Journal of phase equilibria, Vol. 22, No. 3 (2001): 269-275.

[155] C. Kittel, and P. McEuen: Introduction to solid state physics, John Wiley & Sons, 8th ed., (2005).

[156] G. Grosso, G. P. Parravicini: Chapter 3 - The Sommerfeld Free-Electron Theory of Metals, Solid State Physics (Second Edition), Academic Press, (2014): 107-134.

[157] M. V. S. Bonança, P. Nazé, and S. Deffner: Negative entropy production rates in Drude-Sommerfeld metals, American Physical Society, Vol. 103, No. 1 (2021): 012109.

[158] P. N. H. Nakashima, A. E. Smith, J. Etheridge, and B. C. Muddle: The bonding Electron Density in Aluminum, Science, Vol. 331, No. 6024 (2011): 1583-1586

[159] F. Perrot, and M. Rasolt: A New Listing of the Effective $r_s$ Values for Metals, J. Phys. Condens. Journal of Physics: Condensed Matter 6.8 (1994): 1473-1482.

[160] E. L. Houghton, P. W. Carpenter, S. H. Collicott, and D. T. Valentine: Chapter 3: Potential Flow, Aerodynamics for Engineering Students, 6th ed., Butterworth-Heinemann, (2013): 149–207.

[161] G. Mason, and N. R. Morrow: Capillary Behavior of a Perfectly Wetting Liquid in Irregular Triangular Tubes, Journal of Colloid and Interface Science. Vol. 141, No. 1 (1991): 262-274.

[162] O. I. Frette, and J. O. Helland: A Semi-analytical Model for Computation of Capillary Entry Pressures and Fluid Configurations in Uniformly-wet Pore Spaces from 2D rock Images, Adv Water Resour, Vol. 33, No. 8 (2010): 846–866.